

UC Davis

Research reports

Title

Pavement ME Sensitivity Analysis (Version 2.5.3)

Permalink

<https://escholarship.org/uc/item/6bv7d7t6>

Authors

Saboori, Ashkan
Harvey, John
Lea, Jeremy
[et al.](#)

Publication Date

2021-05-01

DOI

10.7922/G25D8Q4H

Pavement ME Sensitivity Analysis (Version 2.5.3)

Authors:

Ashkan Saboori, John Harvey, Jeremy Lea, Jon Lea,
Rongzong Wu, and Angel Mateos

Partnered Pavement Research Center Strategic Plan Element (PPRC SPE) 3.49 (DRISI Task 3199):
Implement Concrete ME Design Tools

PREPARED FOR:

California Department of Transportation
Division of Research, Innovation, and System Information
Office of Materials and Infrastructure

PREPARED BY:

University of California
Pavement Research Center
UC Davis, UC Berkeley




TECHNICAL REPORT DOCUMENTATION PAGE

1. REPORT NUMBER UCPRC-RR-2019-02	2. GOVERNMENT ASSOCIATION NUMBER	3. RECIPIENT'S CATALOG NUMBER
4. TITLE AND SUBTITLE Pavement ME Sensitivity Analysis (Version 2.5.3)		5. REPORT PUBLICATION DATE May 2021
		6. PERFORMING ORGANIZATION CODE
7. AUTHOR(S) Ashkan Saboori (ORCID 0000-0002-8318-3396), John Harvey (ORCID 0000-0002-8924-6212), Jeremy Lea (ORCID 0000-0003-3445-8661), Jon Lea (ORCID 0000-0003-0999-469X), Rongzong Wu (ORCID 0000-0001-7364-7583), and Angel Mateos (ORCID 0000-0002-3614-2858)		8. PERFORMING ORGANIZATION REPORT NO. UCPRC-RR-2019-02 UCD-ITS-RR-21-02
9. PERFORMING ORGANIZATION NAME AND ADDRESS University of California Pavement Research Center Department of Civil and Environmental Engineering, UC Davis 1 Shields Avenue Davis, CA 95616		10. WORK UNIT NUMBER
		11. CONTRACT OR GRANT NUMBER 65A0628
12. SPONSORING AGENCY AND ADDRESS California Department of Transportation Division of Research, Innovation, and System Information P.O. Box 942873 Sacramento, CA 94273-0001		13. TYPE OF REPORT AND PERIOD COVERED Research Report September 2017 to September 2020
		14. SPONSORING AGENCY CODE
15. SUPPLEMENTAL NOTES doi:10.7922/G25D8Q4H		
16. ABSTRACT The Mechanistic-Empirical Pavement Design Guide (MEPDG) is a comprehensive tool developed in 2002 by the American Association of State Highway and Transportation Officials (AASHTO) to analyze and design both flexible and rigid pavements. The models in the MEPDG are implemented in software called Pavement ME, a program calibrated using Long-Term Pavement Performance (LTPP) sections from throughout the United States, including some from California. The MEPDG recommends that nationally calibrated models be validated using local data, and if necessary, recalibrated, which makes sense when considering the climate and materials differences between California and the rest of the nation. The first step in recalibrating Pavement ME is to perform a sensitivity analysis to identify which variables are most important and to look for results that do not match expected performance. The factorial for the sensitivity analysis was designed to identify sensitivity and is not the factorial to be used for the development of design tools. This report presents the results of a sensitivity analysis showing the effects of design input variables controlled by the designer, and those not known to the designer. The sensitivity analysis shows that the overall jointed plain concrete pavements (JPCP) performance prediction by Pavement ME is reasonable. The distresses predicted by Pavement ME did not show any unexpected trends for any of the variables considered in this sensitivity analysis. Over the course of this study, no major issues were identified in running Pavement ME. The next steps are to complete the calibration using California pavement management system data and then to develop the design tool with the calibrated Pavement ME coefficients.		
17. KEY WORDS Pavement ME, jointed plain concrete pavement, sensitivity, pavement design		18. DISTRIBUTION STATEMENT No restrictions. This document is available to the public through the National Technical Information Service, Springfield, VA 22161
19. SECURITY CLASSIFICATION (of this report) Unclassified	20. NUMBER OF PAGES 124	21. PRICE None

Reproduction of completed page authorized

UCPRC ADDITIONAL INFORMATION

1. DRAFT STAGE Final	2. VERSION NUMBER 1				
3. PARTNERED PAVEMENT RESEARCH CENTER STRATEGIC PLAN ELEMENT NUMBER 3.49	4. DRISI TASK NUMBER 3199				
5. CALTRANS TECHNICAL LEAD AND REVIEWER(S) D. Rufino Feldman	6. FHWA NUMBER CA213199A				
7. PROPOSALS FOR IMPLEMENTATION					
8. RELATED DOCUMENTS None					
9. LABORATORY ACCREDITATION The UCPRC laboratory is accredited by AASHTO re:source for the tests listed in this report					
10. SIGNATURES					
Ashkan Saboori FIRST AUTHOR	J.T. Harvey L. Khazanovich TECHNICAL REVIEW	D. Spinner EDITOR	J.T. Harvey PRINCIPAL INVESTIGATOR	D. Rufino Feldman CALTRANS TECH. LEAD	T.J. Holland CALTRANS CONTRACT MANAGER

Reproduction of completed page authorized

TABLE OF CONTENTS

LIST OF FIGURES	v
LIST OF TABLES	vii
PROJECT OBJECTIVES.....	ix
EXECUTIVE SUMMARY.....	xi
LIST OF ABBREVIATIONS.....	xvi
1 INTRODUCTION.....	1
1.1 Previous Calibration and Design Catalog Development.....	1
1.1.1 Earlier Pavement ME Calibration	2
1.2 Overview of Current Calibration and Design Development	3
2 PAVEMENT MANAGEMENT SYSTEM DATA.....	7
2.1 Introduction	7
2.2 JPCP Structural Distress Measures in Caltrans PMS Data	8
2.2.1 Concrete Slab Cracking.....	8
2.2.2 Transverse Joint Faulting	10
2.2.3 International Roughness Index (IRI).....	10
2.3 Pavement Structural As-built, Traffic, and Climate Data in the PMS	10
2.3.1 PCC Slab Thickness	13
2.3.2 PCC Slab Length.....	15
2.3.3 Base Type.....	17
2.3.4 Shoulder Type	20
2.3.5 Climate Region.....	23
2.3.6 WIM Spectrum.....	25
2.3.7 Annual Average Daily Truck Traffic (AADTT).....	26
3 PAVEMENT ME PERFORMANCE PREDICTION MODELS FOR JPCP.....	29
3.1 Introduction	29
3.2 Transverse Cracking.....	29
3.3 Mean Transverse Joint Faulting	30
3.4 International Roughness Index (IRI).....	32
4 SENSITIVITY ANALYSIS.....	35
4.1 Introduction	35
4.2 Pavement Structural and Design Inputs	37
4.2.1 PCC Slab Thickness	37
4.2.2 PCC Slab Length (Transverse Joint Spacing)	40
4.2.3 Load Transfer	43
4.2.4 Friction Loss Duration	45
4.2.5 Base Type.....	47
4.2.6 Shoulder Type (Edge Support).....	50
4.2.7 Subgrade Type	52
4.2.8 Erodibility Index	54
4.3 Pavement Material Inputs.....	56
4.3.1 PCC Compressive Strength.....	57
4.3.2 PCC Coefficient of Thermal Expansion.....	60
4.3.3 PCC Shortwave Absorptivity	62
4.3.4 PCC Heat Capacity.....	64
4.3.5 PCC Thermal Conductivity	66
4.3.6 PCC Built-In Curl-Warp Temperature	68
4.4 Traffic Inputs.....	72
4.4.1 Average Annual Daily Truck Traffic	72

4.4.2	Weigh-in-Motion (WIM) Spectra	74
4.5	Climate	77
5	SUMMARY AND CONCLUSIONS	81
	REFERENCES.....	86
	APPENDIX: PROJECT-SPECIFIC DETAILED MATERIALS DATA	87
	PCC Compressive Strength.....	90
	PCC Estimated Modulus of Elasticity (28-day stiffness).....	93
	PCC Estimated Modulus of Rupture.....	95
	PCC Density.....	97
	PCC Coefficient of Thermal Expansion.....	99
	PCC Shortwave Absorptivity	101
	WIM Spectra	103

LIST OF FIGURES

Figure 2.1: Pavement section length distribution.....	11
Figure 2.2: JPCP project construction year distribution.....	12
Figure 2.3: Pavement age distribution.....	13
Figure 2.4: PCC slab thickness distribution.....	14
Figure 2.5: JPCP first-stage cracking for different PCC slab thicknesses.....	15
Figure 2.6: PCC slab length distribution.....	16
Figure 2.7: PCC slab length pattern history distribution.....	16
Figure 2.8: JPCP first-stage cracking for different PCC slab length patterns.....	17
Figure 2.9: Base type distribution.....	18
Figure 2.10: JPCP first-stage cracking for different base types.....	19
Figure 2.11: Performance model predictions for different base types.....	19
Figure 2.12: Shoulder type distribution.....	20
Figure 2.13: JPCP first-stage cracking for different shoulder types.....	21
Figure 2.14: Performance model predictions for different shoulder types.....	22
Figure 2.15: Distress Type versus Slab Length for WRF Shoulder Type.....	22
Figure 2.16: Climate region distribution.....	23
Figure 2.17: JPCP first-stage cracking for different climate regions.....	24
Figure 2.18: Performance model predictions for different climate regions.....	24
Figure 2.19: WIM spectra distribution.....	25
Figure 2.20: JPCP First-stage cracking for different WIM spectra.....	26
Figure 2.21: AADTT distribution.....	26
Figure 2.22: JPCP first-stage cracking for different AADTTs (thousands of trucks per day per direction per lane).....	27
Figure 4.1: Effect of PCC slab thickness on transverse cracking with 50% reliability.....	38
Figure 4.2: Effects of PCC slab thickness on faulting (while keeping dowel diameter constant) with 50% reliability.....	39
Figure 4.3: Effect of PCC slab thickness on faulting (while changing dowel diameter) with 50% reliability.....	39
Figure 4.4: Effects of PCC slab thickness on IRI with 50% reliability.....	40
Figure 4.5: Effects of PCC slab length on transverse cracking with 50% reliability.....	41
Figure 4.6: Effects of PCC slab length on faulting with 50% reliability.....	42
Figure 4.7: Effects of PCC slab length on IRI with 50% reliability.....	42
Figure 4.8: Effects of load transfer on transverse cracking with 50% reliability.....	43
Figure 4.9: Effects of load transfer on faulting with 50% reliability.....	44
Figure 4.10: Effects of load transfer on IRI with 50% reliability.....	44
Figure 4.11: Effects of friction loss duration on transverse cracking with 50% reliability.....	46
Figure 4.12: Effects of friction loss duration on faulting with 50% reliability.....	46
Figure 4.13: Effects of friction loss duration on IRI with 50% reliability.....	47
Figure 4.14: Effects of base type on transverse cracking with 50% reliability.....	48
Figure 4.15: Effects of base type on faulting with 50% reliability.....	49
Figure 4.16: Effects of base type on IRI with 50% reliability.....	49
Figure 4.17: Effects of shoulder type on transverse cracking with 50% reliability.....	51
Figure 4.18: Effects of shoulder type on faulting with 50% reliability.....	51
Figure 4.19: Effects of shoulder type on IRI with 50% reliability.....	52
Figure 4.20: Effects of subgrade type on transverse cracking with 50% reliability.....	53
Figure 4.21: Effects of subgrade type on faulting with 50% reliability.....	53
Figure 4.22: Effects of subgrade type on IRI with 50% reliability.....	54
Figure 4.23: Effects of erodibility index on transverse cracking with 50% reliability.....	55
Figure 4.24: Effects of erodibility index on faulting with 50% reliability.....	55

Figure 4.25: Effects of erodibility index on IRI with 50% reliability.	56
Figure 4.26: Effects of PCC compressive strength and associated assumptions regarding flexural strength and stiffness on transverse cracking with 50% reliability.	59
Figure 4.27: Effects of PCC compressive strength and associated assumptions regarding flexural strength and stiffness on faulting with 50% reliability.	59
Figure 4.28: Effects of PCC compressive strength and associated assumptions regarding flexural strength, and stiffness on faulting on IRI with 50% reliability.	60
Figure 4.29: Effects of PCC CTE on transverse cracking with 50% reliability.	61
Figure 4.30: Effects of PCC CTE on faulting with 50% reliability.	61
Figure 4.31: Effects of PCC CTE on IRI with 50% reliability.	62
Figure 4.32: Effects of PCC shortwave absorptivity on transverse cracking with 50% reliability.	63
Figure 4.33: Effects of PCC shortwave absorptivity on faulting with 50% reliability.	63
Figure 4.34: Effects of PCC shortwave absorptivity on IRI with 50% reliability.	64
Figure 4.35: Effects of PCC heat capacity on transverse cracking with 50% reliability.	65
Figure 4.36: Effects of PCC heat capacity on faulting with 50% reliability.	65
Figure 4.37: Effects of PCC heat capacity on IRI with 50% reliability.	66
Figure 4.38: Effects of PCC thermal conductivity on transverse cracking with 50% reliability.	67
Figure 4.39: Effects of PCC thermal conductivity on faulting with 50% reliability.	67
Figure 4.40: Effects of PCC thermal conductivity on IRI with 50% reliability.	68
Figure 4.41: Effects of built-in curl-warp temperature on transverse cracking for 8-inch slabs with 50% reliability.	70
Figure 4.42: Effects of built-in curl-warp temperature on faulting with 50% reliability.	70
Figure 4.43: Effects of built-in curl-warp temperature on IRI with 50% reliability.	71
Figure 4.44: Effects of built-in curl-warp temperature on bottom-up, top-down, and total transverse cracking for 8-inch slabs with 50% reliability.	71
Figure 4.45: Effects of AADTT on transverse cracking with 50% reliability.	73
Figure 4.46: Effects of AADTT on faulting with 50% reliability.	73
Figure 4.47: Effects of AADTT on IRI with 50% reliability.	74
Figure 4.48: Effects of WIM spectra on transverse cracking with 50% reliability.	75
Figure 4.49: Effects of WIM spectra on faulting with 50% reliability.	75
Figure 4.50: Effects of WIM spectra on IRI with 50% reliability.	76
Figure 4.51: Equivalent single axle loads associated to WIM spectra.	76
Figure 4.52: Effects of climate on transverse cracking with 50% reliability.	78
Figure 4.53: Effects of climate on faulting with 50% reliability.	79
Figure 4.54: Effects of climate on IRI with 50% reliability.	79
Figure 5.1: Overall sensitivity analysis of the transverse cracking model in Pavement ME.	83
Figure 5.2: Overall sensitivity analysis of the faulting model in Pavement ME.	84
Figure 5.3: Overall sensitivity analysis of the IRI model in Pavement ME.	85
Figure A.1: Distribution map of cores taken across the state (GPR and CaltransDB).	88
Figure A.2: Previous MEPDG calibration pavement sections distribution.	89
Figure A.3: Distribution map of cores taken across the state (ASR).	90
Figure A.4: PCC compressive strength distribution across all projects.	91
Figure A.5: PCC compressive strength cumulative distribution.	92
Figure A.6: PCC compressive strength variability within projects.	92
Figure A.7: PCC estimated 28-day modulus of elasticity distribution across all projects.	93
Figure A.8: PCC estimated modulus of elasticity cumulative distribution.	94
Figure A.9: PCC estimated modulus of elasticity project-level variability.	94
Figure A.10: PCC estimated modulus of rupture distribution across all projects.	96
Figure A.11: PCC estimated modulus of rupture cumulative distribution.	96
Figure A.12: PCC Estimated modulus of rupture project-level variability.	97
Figure A.13: PCC density distribution across all projects.	98

Figure A.14: PCC density cumulative distribution.	98
Figure A.15: PCC density project-level variability.....	99
Figure A.16: PCC coefficient of thermal expansion distribution across all projects.	100
Figure A.17: PCC coefficient of thermal expansion cumulative distribution.	100
Figure A.18: PCC coefficient of thermal expansion project-level variability.....	101
Figure A.19: PCC shortwave absorptivity distribution across all projects.	102
Figure A.20: PCC shortwave absorptivity cumulative distribution.	102
Figure A.21: PCC shortwave absorptivity project-level variability.....	103
Figure A.22: Five WIM spectra in California.	104

LIST OF TABLES

Table 4.1: Input Variables Examined in the Sensitivity Analysis.....	36
Table 4.2: Climate Regions and Corresponding Weather Stations	77

DISCLAIMER

This document is disseminated in the interest of information exchange. The contents of this report reflect the views of the authors who are responsible for the facts and accuracy of the data presented herein. The contents do not necessarily reflect the official views or policies of the State of California or the Federal Highway Administration. This publication does not constitute a standard, specification, or regulation. This report does not constitute an endorsement by the Department of any product described herein.

For individuals with sensory disabilities, this document is available in alternate formats. For information, call (916) 654-8899, TTY 711, or write to California Department of Transportation, Division of Research, Innovation and System Information, MS-83, P.O. Box 942873, Sacramento, CA 94273-0001.

ACKNOWLEDGMENTS

The authors would like to acknowledge the support, assistance, and direction of Dr. Dulce Rufino Feldman and Dr. T. Joseph Holland of Caltrans, and Prof. Lev Khazanovich, who provided advice and technical review. They would also like to acknowledge UCPRC Senior Editor David Spinner's help in producing and publishing this report.

PROJECT OBJECTIVES

The goal of Partnered Pavement Research Center Strategic Plan Element (PPRC SPE) 3.49, titled “Implement Concrete ME Design Tools,” is to calibrate the Pavement ME software for traffic, climate, materials, and construction practices in California and then, based on the calibrated software, update the rigid pavement design catalog in the Caltrans *Highway Design Manual*. An additional goal, if Caltrans decides to pursue it, is to develop a simplified user interface for operating the calibrated version of Pavement ME. The following tasks are to be completed to accomplish these goals, which have been updated based on the results of a meeting with stakeholders in September 2019:

1. Conduct an analysis of the sensitivity of the current version of Pavement ME to design variables
2. Assemble the data needed to calibrate Pavement ME for California traffic and climate conditions, materials, and construction practices
3. Identify any issues with the current version of Pavement ME that will influence local calibration or preparation of the design catalog
4. Calibrate Pavement ME for California conditions and a reliability approach using the results of the calibration
5. Develop a design catalog
6. If Caltrans chooses to have a simplified user interface developed for the catalog, develop a simplified web-based user interface
7. Prepare documentation for the calibration, catalog, and, if developed, the simplified user interface
8. Assist Caltrans in developing design guidance

These results demonstrate the sensitivity of the Pavement ME design software for jointed plain concrete pavements (JPCP) to a set of selected design variable inputs. This analysis considered design variables identified from California pavement sections distributed around the state. The work presented was also used to identify potential issues in the Pavement ME software that should be considered in calibration and development of the design catalog.

(This page intentionally blank)

EXECUTIVE SUMMARY

The *Mechanistic-Empirical Pavement Design Guide* (MEPDG) is a comprehensive tool released in 2004 by the American Association of State Highway and Transportation Officials (AASHTO) to analyze and design both flexible and rigid pavements, and it has been updated several times in the succeeding years. The models in the MEPDG are implemented in a software program called Pavement ME that was calibrated using Long-Term Pavement Performance (LTPP) sections from around the United States, including some from California. The MEPDG recommends that nationally calibrated models be validated using local data and then recalibrated if necessary. This makes sense for California because of differences between the state's climate and those of the other states where sections were used for the national calibration. The recalibration would also account for any differences in traffic, materials, and construction practices.

The first step in the recalibration process is to perform a sensitivity analysis study to check the reasonableness of the models' predictions, to identify potential software issues, and to help identify and understand the inputs that significantly affect the models' outputs. The factorial of cases and the variable factor levels used for the sensitivity analysis are intended to evaluate the trends and sensitivity of the models in the Pavement ME software. However, the factorial variables and their levels used in the sensitivity analysis will differ from the ones that will be used after calibration of the models to create the design catalog.

In 2006, the University of California Pavement Research Center (UCPRC) performed a research study that included an initial sensitivity analysis of jointed plain concrete pavement (JPCP) distress prediction models in the MEPDG. That study identified the most important variables affecting predicted performance, and studied a design variable that was found to be the most important for the predicted performance of JPCP pavements in California—the time to loss of bonding between the concrete and the base. After that calibration, the software was used to produce a preliminary design catalog for the Caltrans *Highway Design Manual* (HDM); Caltrans adjusted that catalog further to produce the one in the current *HDM*.

In 2010, Caltrans developed a capacity for Automated Pavement Condition Survey (APCS) data collection from the state highway network, and as a result a much larger and more reliable pavement condition database is now available in the pavement management system (PMS). Due to a considerable effort on the part of Caltrans, the database now includes as-built data such as pavement structure, base type, shoulder type, slab length, and construction year, items that were scarce in the previous study but are now available for almost every project built since 1990, and many built prior to that year. These data provide the capability to validate and calibrate Pavement ME using thousands of performance data observations and to use the explanatory data in the as-built database. In addition to the data in the PMS, the UCPRC has collected detailed data for Caltrans for more than 100 projects, sampled in the early 2000s and 2010s. Those data are for variables not in the as-built database in the PMS, such as the properties of the concrete and the stiffnesses of underlying layers.

Updates in Pavement ME and improvements, combined with the increased amount and higher quality of data now in the Caltrans PMS, have created the opportunity to perform a new JPCP prediction model sensitivity analysis and calibration specifically for California. This study used version of Pavement ME (v.2.5.3), the latest version available at the time.

The traditional approach for validating and calibrating mechanistic-empirical (ME) design methods is to collect all input data, including performance, as-built, and detailed materials data from tens of sections within a state, and to compare the predicted and measured performance for those few sections. For the national calibration of Pavement ME, this was done on the scale of several hundred LTPP sections across the US. The next Pavement ME calibration for California will take advantage of a combination of hundreds of times more performance and as-built data from the Caltrans PMS, as well as detailed materials data collected from tens of sections in the state. This will provide a much different and much larger database than has been used to date for the national and several state calibrations of Pavement ME using the traditional approach.

A new approach will be used for the calibration process, whose results will be checked further using the data for the tens of sections in the state that have complete sets of detailed data. This new approach recognizes that in the design-bid-build (low-bid) contracting environment used in California, a designer does not actually know in detail the properties of the materials that will be used when the design is built. Therefore, the calibration will use detailed median statewide values of the materials' properties to calibrate the models using the large performance database, and to calculate the variability of performance caused by differences between the contractors' as-built materials and the statewide median values. The calibration will use the detailed information available from the PMS regarding layer types, thicknesses, slab dimensions, shoulder types, dates of construction, and performance data, along with detailed climate and traffic data, to find the coefficients in Pavement ME that on average produce the best match between predicted performance and observed performance. The distribution of differences between the predicted and observed performance also provide information needed for introducing reliability into the future design tools.

As noted above, before the models can be calibrated, a sensitivity analysis must first be performed to check the reasonableness of the models' predictions, to identify potential software issues, and to help identify and understand the inputs that significantly affect the models' outputs. That sensitivity analysis is the subject of this report. It should be noted that the ranges of variables considered in this study were selected based on the historical data available in the PMS database for design variables (known to the designer, e.g., portland cement concrete [PCC] slab thickness, PCC slab length, base type, shoulder type, etc.), and the UCPRC material database for non-design variables (not known to the designer, e.g., PCC compressive strength, PCC coefficient of thermal expansion [CTE], PCC shortwave absorptivity, etc.). Therefore, the range selected for each variable reflects past construction practices in California while checking the sensitivity of the models' performance to the variable's change. These

variables and the ranges selected for them for the sensitivity analysis factorial are not the same as those that will be used for either calibration or design catalog development. In the calibration process, the selected range for each variable will include all the values ever used for JPCP construction in California, based on the PMS database. The design catalog development will both include selected values from the calibration for use in future designs and additional values intended to reflect future ranges for the design variables in California. Pavement ME calibration and design catalog development will be explained in detail in the next report produced by this project.

This sensitivity analysis included the Pavement ME models for transverse cracking, mean transverse joint faulting, and smoothness index (International Roughness Index [IRI]). The Caltrans pavement management system manages JPCP based on third-stage cracking rather than on transverse cracking. An earlier California calibration of Pavement ME attempted to calibrate transverse cracking by estimating historical transverse cracking; that attempt used the historical first-stage and third-stage cracking data collected in the PMS. The calibration effort also used a very limited set of transverse cracking observations for the tens of sections included in that calibration. However, combining these data resulted in added uncertainty to the calibration. Soon after, Caltrans asked for a transfer function that could predict third-stage cracking from predictions of transverse cracking; this function was developed and used in the creation of the preliminary design tables that served as the basis for the design tables included in the 2007 HDM.

Following this sensitivity analysis, Pavement ME will be calibrated to transverse cracking rather than first- or third-stage cracking. That calibration process will use a much more extensive database of simultaneous transverse and longitudinal cracking observations, and first-stage (first crack, either transverse or longitudinal) and third-stage cracking observations from two years of statewide APCS data. These data will be used to create a model to estimate transverse cracking in the entire historical PMS data, which otherwise consists only of first- and third-stage cracking observations. While they are still limited to only two years of simultaneous data collection for the different types of cracking, these efforts will produce hundreds of times more observations that can be used to create a model that translates first-stage cracking into transverse cracking throughout the entire PMS database. The amount and scope of the data used in these efforts will also enable considerations about the influence that climate, shoulder type, and other variables have on the propensity of a pavement to first form either a longitudinal or transverse crack. The transverse cracking newly translated from first-stage cracking will then be added to the already-known third-stage cracking in the database, because any third-stage crack has at least one transverse crack in it. The new, combined results will then be used in the Pavement ME calibration.

In this study, the sensitivity analysis performed on these models considered various design and non-design variables: portland cement concrete (PCC) slab thickness, PCC slab length, load transfer, friction loss duration, base type, shoulder type, subgrade type, erodibility index, PCC compressive strength, PCC coefficient of thermal expansion (CTE), PCC shortwave absorptivity, PCC heat capacity, PCC thermal conductivity, traffic inputs,

average annual daily truck traffic (AADTT), weigh-in-motion (WIM) spectra, and climate. These variables were found to have different effects on the three performance prediction models, with the items listed below having the greatest influence ranked from most to least for the variable ranges (factor levels) used:

- Transverse cracking
 - PCC slab thickness
 - Built-in curl-warp temperature
 - PCC coefficient of thermal expansion (CTE)
 - PCC shortwave absorptivity
 - PCC compressive strength, which was used with American Concrete Institute (ACI) equations implemented in Pavement ME to predict PCC flexural strength and modulus of elasticity
 - Shoulder type
- Mean transverse joint faulting
 - Load transfer (use of dowels)
 - Built-in curl-warp temperature
 - Shoulder type
 - Climate
 - AADTT
 - PCC coefficient of thermal expansion
 - PCC thickness
 - Subgrade type
- Smoothness index
 - Load transfer (use of dowels)
 - Shoulder type
 - Coefficient of thermal expansion
 - PCC shortwave absorptivity
 - Built-in curl-warp temperature
 - AADTT
 - PCC thermal conductivity
 - PCC thickness

As noted, these rankings are based on the scenarios and ranges of variables run in this analysis using Pavement ME, and it is certain that these rankings would change if the ranges of variables were changed.

The sensitivity analysis shows that the overall JPCP performance predictions by Pavement ME are reasonable. The Pavement ME–predicted distresses followed trends expected for the variables considered in the analysis.

Further, over the course of the study, the Pavement ME software ran without the occurrence of any major issues, such as unreasonable results that could be attributed to software bugs. Based on these results, the next steps are calibration of Pavement ME according to California conditions and development of the design tools.

LIST OF ABBREVIATIONS

AADTT	Average Annual Daily Truck Traffic
AASHTO	American Association of State Highway and Transportation Officials
AB	Aggregate base
APCS	Automated Pavement Condition Survey
ASR	Alkali-silica reaction
BVS	Blind Verification Sections
CTB	Cement-treated base
CTE	Coefficient of Thermal Expansion
EICM	Enhanced Integrated Climate Model
FHWA	Federal Highway Administration
GPR	Ground-penetrating radar
HDM	Highway Design Manual
HMA	Hot mix asphalt
IRI	International Roughness Index
JPCP	Jointed plain concrete pavements
LTE	Load transfer efficiency
LTPP	Long-Term Pavement Performance
ME design	Mechanistic-Empirical design
MEPDG	Mechanistic-Empirical Pavement Design Guide
MR	Modulus of Rupture
PMS	Pavement management system
PCC	Portland cement concrete
PPRC	Partnered Pavement Research Center
SHS	State highway system
UCPRC	University of California Pavement Research Center
WIM	Weigh-in-Motion

SI* (MODERN METRIC) CONVERSION FACTORS

APPROXIMATE CONVERSIONS TO SI UNITS				
Symbol	When You Know	Multiply By	To Find	Symbol
LENGTH				
in.	inches	25.40	millimeters	mm
ft.	feet	0.3048	meters	m
yd.	yards	0.9144	meters	m
mi.	miles	1.609	kilometers	km
AREA				
in ²	square inches	645.2	square millimeters	mm ²
ft ²	square feet	0.09290	square meters	m ²
yd ²	square yards	0.8361	square meters	m ²
ac.	acres	0.4047	hectares	ha
mi ²	square miles	2.590	square kilometers	km ²
VOLUME				
fl. oz.	fluid ounces	29.57	milliliters	mL
gal.	gallons	3.785	liters	L
ft ³	cubic feet	0.02832	cubic meters	m ³
yd ³	cubic yards	0.7646	cubic meters	m ³
MASS				
oz.	ounces	28.35	grams	g
lb.	pounds	0.4536	kilograms	kg
T	short tons (2000 pounds)	0.9072	metric tons	t
TEMPERATURE (exact degrees)				
°F	Fahrenheit	(F-32)/1.8	Celsius	°C
FORCE and PRESSURE or STRESS				
lbf	pound-force	4.448	newtons	N
lbf/in ²	pound-force per square inch	6.895	kilopascals	kPa
APPROXIMATE CONVERSIONS FROM SI UNITS				
Symbol	When You Know	Multiply By	To Find	Symbol
LENGTH				
mm	millimeters	0.03937	inches	in.
m	meters	3.281	feet	ft.
m	meters	1.094	yards	yd.
km	kilometers	0.6214	miles	mi.
AREA				
mm ²	square millimeters	0.001550	square inches	in ²
m ²	square meters	10.76	square feet	ft ²
m ²	square meters	1.196	square yards	yd ²
ha	hectares	2.471	acres	ac.
km ²	square kilometers	0.3861	square miles	mi ²
VOLUME				
mL	milliliters	0.03381	fluid ounces	fl. oz.
L	liters	0.2642	gallons	gal.
m ³	cubic meters	35.31	cubic feet	ft ³
m ³	cubic meters	1.308	cubic yards	yd ³
MASS				
g	grams	0.03527	ounces	oz.
kg	kilograms	2.205	pounds	lb.
t	metric tons	1.102	short tons (2000 pounds)	T
TEMPERATURE (exact degrees)				
°C	Celsius	1.8C + 32	Fahrenheit	°F
FORCE and PRESSURE or STRESS				
N	newtons	0.2248	pound-force	lbf
kPa	kilopascals	0.1450	pound-force per square inch	lbf/in ²

*SI is the abbreviation for the International System of Units. Appropriate rounding should be made to comply with Section 4 of ASTM E380. (Revised April 2021)

1 INTRODUCTION

1.1 Previous Calibration and Design Catalog Development

The American Association of State Highway and Transportation Officials (AASHTO) 2002 *Mechanistic-Empirical Pavement Design Guide* (MEPDG) was calibrated using Long-Term Pavement Performance (LTPP) sections throughout the United States, including some from California (1). However, the MEPDG recommends that nationally calibrated models be validated using local data and, if necessary, recalibrated. This makes sense for California because nearly all of the state's climate zones are drier and warmer than the climates of most of the sections in the national calibration set. It also makes sense because much of the national data set pertains to concrete with limestone aggregates, while the aggregates used in California's concrete are primarily of igneous origin, and these igneous aggregates often have greater coefficients of thermal expansion (CTE) than limestone aggregates. The dry climate and igneous aggregates would tend, respectively, to increase the drying shrinkage gradients and the effects of thermal gradients, increasing the tensile stresses that cause cracking. Further, California has neither the prolonged freezing nor thawing prevalent in the national calibration, which characterize the climatic conditions of a significant portion of the country.

Therefore, to use the MEPDG for pavement design in California, it became necessary to validate the models in the MEPDG based on the performance of the state's pavements, and to recalibrate the models if needed. In addition, the reliability approach used in the software program Pavement ME, which implements the MEPDG models, is based on the national calibration and does not explicitly address the typical localized variability of important variables. Therefore, once the models have been calibrated to account for local conditions, updated design tools based on the calibrated software must be developed. The first step in this process is to perform a sensitivity analysis to check the reasonableness of the models' predictions, to identify potential software issues, and to help identify and understand the inputs that significantly affect the models' outputs.

In 2006, the University of California Pavement Research Center (UCPRC) performed a research study that included an initial sensitivity analysis of jointed plain concrete pavement (JPCP) distress prediction models in the MEPDG (2). That study identified the most important variables affecting predicted performance, and studied a design variable that was found to be the most important one for predicting the performance of JPCP pavements in California (3)—the time to loss of bonding between the concrete and the base. After that study, the software was used to produce a preliminary design catalog for the Caltrans *Highway Design Manual* (HDM); Caltrans further adjusted that catalog to produce the one in the current HDM. The assumptions and results for that preliminary design catalog are documented in Reference (4).

As noted, Pavement ME, the current software program developed from the MEPDG models, uses those models to predict IRI, faulting, and transverse cracking. (*Note: in this report the design guide is referred to as MEPDG and the software is referred to as Pavement ME.*)

The Caltrans pavement management system (PMS) bases its management of JPCP on third-stage cracking, as opposed to first-stage cracking or transverse cracking. *First-stage cracking* is defined as cracking state where the first crack divides a slab into two pieces. A first-stage crack can be a transverse crack, the only type of cracking modeled by Pavement ME, or a longitudinal crack, which also occurs on Caltrans JPCP (5). *Third-stage cracking* is defined as a state of cracking that divides a slab into three or more pieces. In California, a transverse crack is one of the crack types that commonly creates a third-stage crack when it combines with a longitudinal crack—although, less frequently, third-stage cracking is also created by two transverse cracks, or two longitudinal cracks.

1.1.1 Earlier Pavement ME Calibration

The traditional approach taken for validating and calibrating mechanistic-empirical (ME) design methods is to collect all input data—including performance, as-built, and detailed materials data—for tens of sections within a state, and to then compare the predicted and measured performance of those sections. For the national calibration of Pavement ME, data was collected on several hundred Long-Term Pavement Performance (LTPP) sections across the US.

The California-focused calibration of an early version of Pavement ME (3) followed the traditional approach, and included just 52 JPCP and 43 crack, seat, and overlay sections. At the time they were cored, the sections' first-stage transverse and longitudinal cracking and third-stage cracking were measured, and deflection testing was performed on areas of the sections that had not been overlaid with asphalt. To develop better transverse cracking histories of all the sections, and to learn whether the measured third-stage cracks had begun as a first-stage transverse or a longitudinal crack, it was necessary to produce an estimated transverse cracking history for each section, starting at the time of its construction. But because there was insufficient data and because the section did not come from enough areas of the state to be truly representative of conditions everywhere, it was not possible to develop a model for predicting whether a third-stage crack had originated as a transverse crack or a longitudinal one. To account for these specifics, a range of potential transverse cracking histories was produced for each section; in these histories, the maximum of the range assumed that all third-stage cracks began as transverse cracks while the minimum of the range assumed that all third-stage cracks began as longitudinal cracks. Although this provided a means for dealing with the lack of data, it also added uncertainty to the calibration performed.

Soon after that calibration, Caltrans requested development of a transfer function that could predict third-stage cracking from transverse cracking predictions; this function was developed and used in the creation of the preliminary design tables that served as the basis for the design tables included in the 2007 HDM. (No documentation of the transfer function's development has been published.) The calibration of Pavement ME that follows this sensitivity study will be to transverse cracking, but it will use a model that is better at separating the first-stage cracking histories in the PMS performance data into estimates of transverse and longitudinal cracking. This is now possible using the much larger and better database that is now available.

1.2 Overview of Current Calibration and Design Development

In 2010, Caltrans developed the capacity to collect Automated Pavement Condition Survey (APCS) data from the state highway network, and as a result a much larger and more reliable pavement condition database is now available in the pavement management system (PMS). After a considerable effort by Caltrans to update the database, it now includes as-built data such as pavement structure, base type, shoulder type, slab length, and construction year. Items that were mostly unavailable for the previous study are now accessible for almost every project built since 1990, and many built prior to that year. These data provide the capability to validate and calibrate Pavement ME using thousands of performance data observations and to use the explanatory data in the as-built database. Further, in addition to the new data in the PMS, there are also more detailed data collected for Caltrans by the UCPRC on more than 100 projects sampled in the early 2000s and 2010s. These are data for variables not in the PMS as-built database, such as the properties of concrete materials and the stiffnesses of underlying layers.

Pavement ME has continued to evolve since the earlier study, and since 2006 AASHTO has released several new versions that include improvements to both the models and the implementation of the software.

Having an updated, improved version of Pavement ME and more, higher quality data in the Caltrans PMS gave Caltrans and the UCPRC the opportunity to perform a new JPCP cracking model sensitivity analysis and a California-specific calibration whose results can be used to produce updated design tools. This current study undertook those tasks using the latest version of Pavement ME available at the time, version v.2.5.3. And, more importantly, the study followed a new approach to the calibration process.

This new calibration process approach recognizes that in California's design-bid-build (low-bid) contracting environment, a designer does not actually know in detail the properties of the materials that will be used when the design is built. Therefore, the calibration will use detailed median statewide values of the materials' properties to calibrate the models using the large performance database, and to calculate the variability of performance caused

by differences between the contractors' as-built materials and the statewide median values. The calibration will use the details from the PMS regarding layer types, thicknesses, slab dimensions, shoulder types, dates of construction, and performance data, along with detailed climate and traffic data, to find the coefficients in Pavement ME that on average produce the best match between predicted and observed performance. The distribution of differences between the predicted and the observed performance also provide information needed for introducing reliability into the future design tools.

This project will calibrate Pavement ME to the transverse cracking estimates that result from adding the transverse cracking estimated from first-stage cracking to third-stage cracking. To achieve this result, the study will develop a new model that yields the probability that a first-stage crack is longitudinal or transverse. This effort will use the 2011/2012 APCS data, which accurately separated transverse and longitudinal cracking on all of the JPC pavements across the state, thereby providing sufficient data to produce the model. This model will then be used to predict the rate of transverse and longitudinal cracking development independently for all of the JPCP performance data in the PMS database, including consideration of explanatory variables such as shoulder type, climate region, thickness, and slab dimensions, among others.

The model will also be able to relate the development of transverse cracking to the subsequent development of third-stage cracking. Data about this relationship can be used to set transverse cracking failure levels for the development of design tools, and to relate predicted transverse cracking from Pavement ME to the third-stage cracking used in the PMS.

The calibration of the Pavement ME empirical model transverse cracking coefficients C_4 and C_5 will be made using the predicted portion of transverse cracking from the observed first-stage cracking. The model will also be able to identify situations where longitudinal cracking is expected, and associated design guidance will be developed to help designers limit the possibility of early failure from this cracking mode. Pavement ME was not developed to predict longitudinal cracking because this type of cracking seldom occurs outside of the dry climate regions that are predominant in California and in some other Western states.

As a first step in the validation and calibration process, a sensitivity analysis was performed on the Pavement ME models for JPCP. This step is the subject of this report. As noted in Section 1.1, the sensitivity analysis was performed to check the reasonableness of the models' predictions, to identify potential software issues, and to help identify and understand the inputs that significantly affect the models' outputs. The sensitivity analysis included the development of detailed materials properties distributions, followed by an evaluation of the sensitivity of Pavement ME performance predictions to both the variables known to the designer and the distributions of the unknown detailed materials variables.

It should be noted that the ranges of variables considered in this study were selected based on the historical data available in the PMS database for design variables (known to the designer, e.g., portland cement concrete [PCC] slab thickness, PCC slab length, base type, shoulder type, etc.) and the UCPRC material database for non-design variables (not known to the designer, e.g., PCC compressive strength, PCC coefficient of thermal expansion [CTE], PCC shortwave absorptivity, etc.). Therefore, the range selected for each variable reflects past construction practices in California while testing the sensitivity of the models' performance with the variables' changes.

The variables and their ranges used in the sensitivity analysis factorial are different from those that will be used for either calibration or design catalog development. In the calibration process, the range selected for each variable will include all the values ever used for JPCP construction in California, based on the PMS database. The design catalog development will both include selected values from the calibration and additional values intended to reflect future ranges for the design variables in California. The Pavement ME calibration and design catalog development will be explained in detail in the next report produced by this project.

The sensitivity analysis included the models for transverse cracking, mean transverse joint faulting, and smoothness index (International Roughness Index [IRI]).

The results presented in this report demonstrate the sensitivity of the results of the Pavement ME design software to the various inputs based on an assessment of the distributions of design variables. In addition, the work presented was also used to identify potential issues with the Pavement ME software and to provide a practical assessment of how best to use Pavement ME for design.

In Chapter 2, Pavement ME performance prediction models for transverse cracking, mean transverse joint faulting, and smoothness index are summarized. In Chapter 3, the sensitivity analysis results are presented. Chapter 4 presents the sensitivity analysis study's conclusions. The appendix provides information about the distributions of the detailed materials data available for calibration obtained from various earlier UCPRC projects, including the range, mean, and standard deviations for each variable, and a short description of weigh-in-motion (WIM) groups in California.

2 PAVEMENT MANAGEMENT SYSTEM DATA

2.1 Introduction

Pavement management is the process of using available financial resources as efficiently as possible to ensure the highest overall functional performance of a road network, both spatially and with time, while maintaining the structural condition of the pavements to protect the initial investment in construction. To perform pavement management, it is necessary to capture the current functional and structural condition of the network and predict the future condition for different management scenarios. Historically, a team of Caltrans pavement raters conducted a manual pavement condition survey at various locations along the state highway system (SHS) once a year. The pavement raters visually inspected the outside highway lanes for both directions of travel using systematic sampling techniques. Pavement condition assessments were extrapolated for each section of the entire SHS based on sample locations within each section.

The boundaries of pavement management sections across the network changed annually, as did the locations where surveys occurred. This made building performance histories difficult for the 2006 Pavement ME calibration because the same location was not sampled each year. The changing of section boundaries from year to year also meant that a given pavement's location could be included in a different pavement section in any given year. Typically, jointed plain concrete pavements (JPCPs) sections were approximately one mile long.

Between 2011 and 2012, Caltrans began testing and transitioning to the Automated Pavement Condition Survey (APCS). The APCS can efficiently collect, evaluate, and analyze pavement conditions for all lanes on the SHS. It utilizes vehicles equipped with an array of on-board high-definition cameras, laser sensors, Global Positioning System trackers, and other measurement devices that quickly collect pavement data at highway speeds. The information collected includes geographical locations of the highways, downward-looking pavement surface images, forward right-of-way images, and pavement surface profiles. The data are collected in segments referred to as *elements*, which are 26.4-foot sections. This is true for both asphalt pavement and continually reinforced concrete pavement (CRCP). The same is done on every concrete slab for a JPC pavement. These data are then aggregated to calculate a weighted average of the pavement condition for each 0.1-mile segment.

Because evaluating condition, especially functional condition, can be subjective, agencies have generally settled on trying to identify and quantify specific distresses. A distress is a measurable phenomenon on the surface of a pavement, such as observable cracking, changes in ride quality (smoothness/roughness), or rutting. Distress is the result of internal deterioration within the pavement, such as bottom-up fatigue cracking or plastic deformation of materials. Deterioration, in turn is the result of internal damage within the materials, which is not observable. This might include particle movement, breaking of bonds, or other atomic/microscopic changes.

These damage processes also take place at different rates at different locations in the pavement because of variability in the materials and construction of the pavement. As a result, distress is observed to accumulate at different rates along the road surface, even within a section that is nominally uniform with regard to construction, traffic, and climate.

This chapter outlines the pavement structural, climate, and traffic variables along with distress measures available in California's pavement management system (called *PaveM*) database. It also briefly discusses in qualitative terms the effects of different variables on the performance of the JPCP over the service life observed in the data. These same data were used to develop empirical performance models for the Caltrans PMS, which were in turn used to calibrate Pavement ME.

A statistical performance model is developed using data obtained through pavement condition surveys. The model predicts the future performance (condition) of the pavement—in this study, the model predicted performance in terms of cracking as a percent of slabs cracked, ride quality as measured by the International Roughness Index (IRI), and faulting. As explanatory variables, the model used both pavement structural variables such as slab thickness, PCC slab length, base type, shoulder type, and load transfer efficiency (doweled/undoweled), as well as nonstructural variables such as climate and traffic loads. This report is not intended to cover the development of performance models; however, the results of the performance models for first- and third-stage JPCP cracking developed for the PMS were used to investigate the effects of different variables on the performance of JPCP. Detailed descriptions of the *PaveM* performance models will be provided in a separate report.

2.2 JPCP Structural Distress Measures in Caltrans PMS Data

2.2.1 Concrete Slab Cracking

Cracking is a typical type of distress that occurs in jointed plain concrete due to traffic loading and environmental conditions. Each traffic loading pass applies damage-inducing stress and strain in the concrete slabs, with the minor damage from each load accumulating over thousands to hundreds of millions of load passes until it eventually results in failure in the form of fatigue cracking. Environmental conditions such as the curling caused by differential temperatures in the slab and the warping caused by differential shrinkage also create stress in the concrete that contributes to the damage in the concrete slab.

Cracking in concrete slabs can be categorized into three main types: transverse cracking, longitudinal cracking, and corner cracking. The typical type of cracking in concrete slabs in California is transverse cracking. Transverse cracks appear perpendicular to the pavement centerline and extend across the entire slab from one longitudinal

edge to the other. Longitudinal cracks appear parallel to the pavement centerline and extend along the entire slab from one transverse joint to the other. Corner cracks occur in one quadrant of a slab, and have one endpoint on a longitudinal joint and the other on a transverse joint.

Typically, a combination of repeated loads combined with thermal and shrinkage stresses causes transverse cracking in concrete slabs. The initiation and progression of transverse cracking generally occur in two patterns: *bottom-up cracking* and *top-down cracking*. In the case of bottom-up cracking, when truck axles are near the longitudinal edge of the slab, midway between the transverse joints, a critical tensile stress occurs at the bottom of the slab with its maximum vector in the longitudinal direction. The presence of a high positive vertical temperature gradient (the top of the slab is warmer than the bottom of the slab) through the slab thickness causes additional tensile stress at the bottom of the concrete slab that contributes to bottom-up cracking.

In contrast, heavy trucks with shorter axle spacings load the opposite ends of a slab simultaneously. The result is that higher tensile stresses occur at the top of the slab than the bottom, and consequently transverse fatigue cracking begins at the top of the slab. Top-down transverse cracking is accelerated by high negative temperature gradients (the top of the slab is cooler than the bottom of the slab) that cause tensile stress at the top of the slab.

Longitudinal cracking in California is primarily caused by high differential drying shrinkage that causes high tensile stresses at the top of the slab, which combined with truck axle loading near the edge of the slab results in top-down cracking. Corner cracking is also caused by a top-down mechanism, where load repetitions at the corner of the slab combined with poor joint and shoulder load transfer, loss of support in the base, and curling and warping stresses cause cracks at the corner of the slab. The lack of support and poor load transfer may be due to the pumping of underlayer material or a loss of load transfer between adjacent concrete slabs, such as an undoweled concrete pavement that does not have tied concrete shoulders.

Caltrans has also categorized the cracking in JPCP in terms of its severity into two main groups: *first-stage cracking* and *third-stage cracking*. In Caltrans's official definition, a first-stage crack is a crack that breaks the concrete slab into two pieces; this crack can be a transverse, longitudinal, or diagonal crack. A third-stage crack is a set of two or more intersecting cracks, longitudinal or transverse, that divide the concrete slab into two or more pieces. However, despite these specific definitions, Caltrans raters have long used simpler definitions: a slab has first-stage cracking if it is divided into two pieces, and it has third-stage cracking if it is divided into three or more pieces. It should be noted that corner cracking is not considered in these two categories and is defined and measured separately.

Caltrans measures cracking as the percent of cracked slabs in a pavement section. Caltrans historically has collected first- and third-stage cracking data only, without defining whether the first-stage cracking is transverse or longitudinal. However, as part of the APCS data collection in 2011 to 2012 and in 2018, Caltrans also collected transverse and longitudinal cracking as individual measures. Therefore, the amount of transverse and longitudinal cracking data in the database comes only from these years, and the amount of data with transverse and longitudinal cracks defined is much smaller than the amount of first- and third-stage cracking data.

2.2.2 Transverse Joint Faulting

Faulting is the difference in elevation across a transverse joint between two adjacent concrete slabs or across a transverse crack. It is primarily caused by poor load transfer and is therefore usually an issue with undoweled JPCP.

The main mechanism that causes faulting is movement of fine material, from under the leave concrete slab to under the approach slab, caused by large differences in deflection between the loaded slab and the unloaded slab. These differences in deflection reverse as a wheel travels across a joint, creating a pumping action. Dowel bars significantly decrease relative deflections across transverse joints under load, thus reducing faulting development and further deterioration of joints and corner cracks.

Caltrans quantifies faulting as the percentage of transverse joints in a pavement section with faults greater than a threshold value.

2.2.3 International Roughness Index (IRI)

Pavement roughness is generally defined as an expression of pavement-surface irregularities that adversely affect ride quality for vehicles and for users. Roughness is an important pavement characteristic because it affects not only ride quality but also vehicle maintenance costs and fuel consumption. In Pavem, roughness data are quantified using the International Roughness Index (IRI). IRI is used to define a characteristic of the longitudinal profile of a traveled wheel track and constitutes a standardized roughness measurement. In Pavem, IRI is measured in units of inches/mile.

2.3 Pavement Structural As-built, Traffic, and Climate Data in the PMS

Caltrans records new JPCP projects as “Lane Replacement” in the PMS database.

The Caltrans condition survey database contains about 260,000 observations of first- and third-stage cracking performance data collected from 30,000 JPCP sections, totaling about 4,300 lane-miles built on 302 lane replacement projects completed between 1947 and 2017. The database’s performance data were obtained from manual pavement condition surveys (PCS) conducted from 1978 to 2013 and from the automated pavement condition surveys conducted from 2011 to 2012 and in 2018. Each observation in the condition survey data corresponds to the performance condition of a pavement section in the highway network at the time the survey was done.

These data were divided into approximately uniform subsections as part of the performance modeling effort, with section boundaries kept constant through time and defined as having the same pavement structure from the last construction project, the same traffic loading, and the same climate condition. Figure 2.1 shows the variability in the resulting lengths of these sections in the dataset.

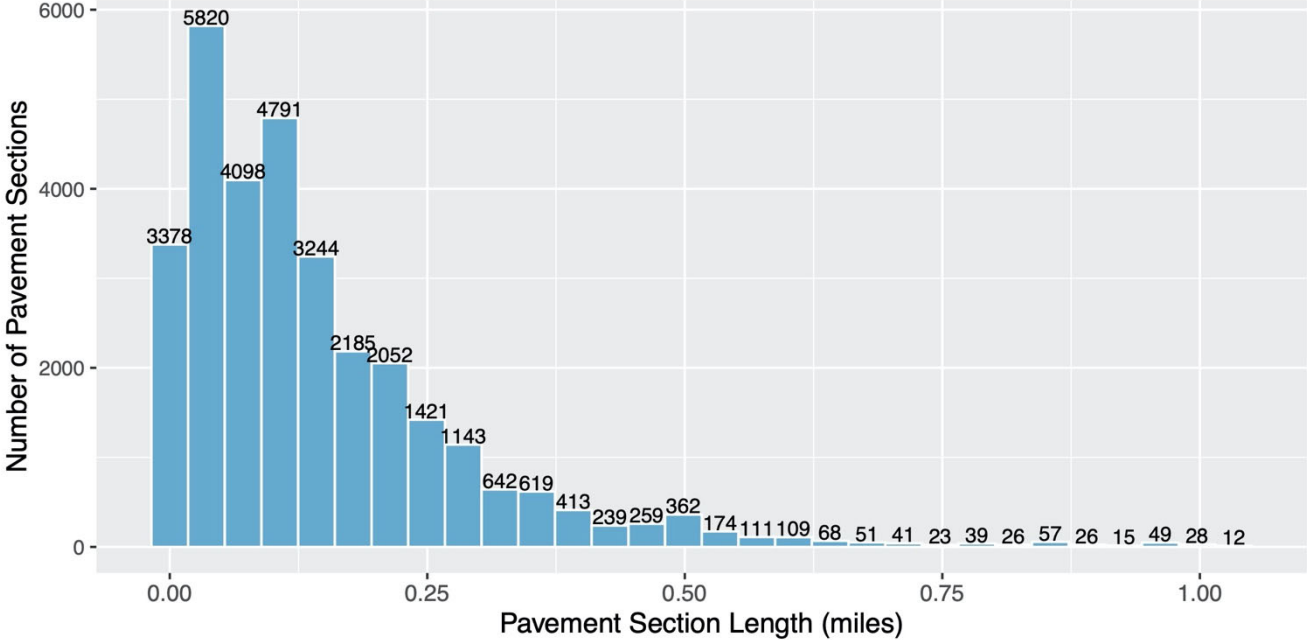


Figure 2.1: Pavement section length distribution.

Figure 2.2 shows the JPCP construction year distribution. Construction years in the figure range between 1947 and 2017. Condition survey data were first collected in 1978, thus the oldest JPCP performance histories began in that year.

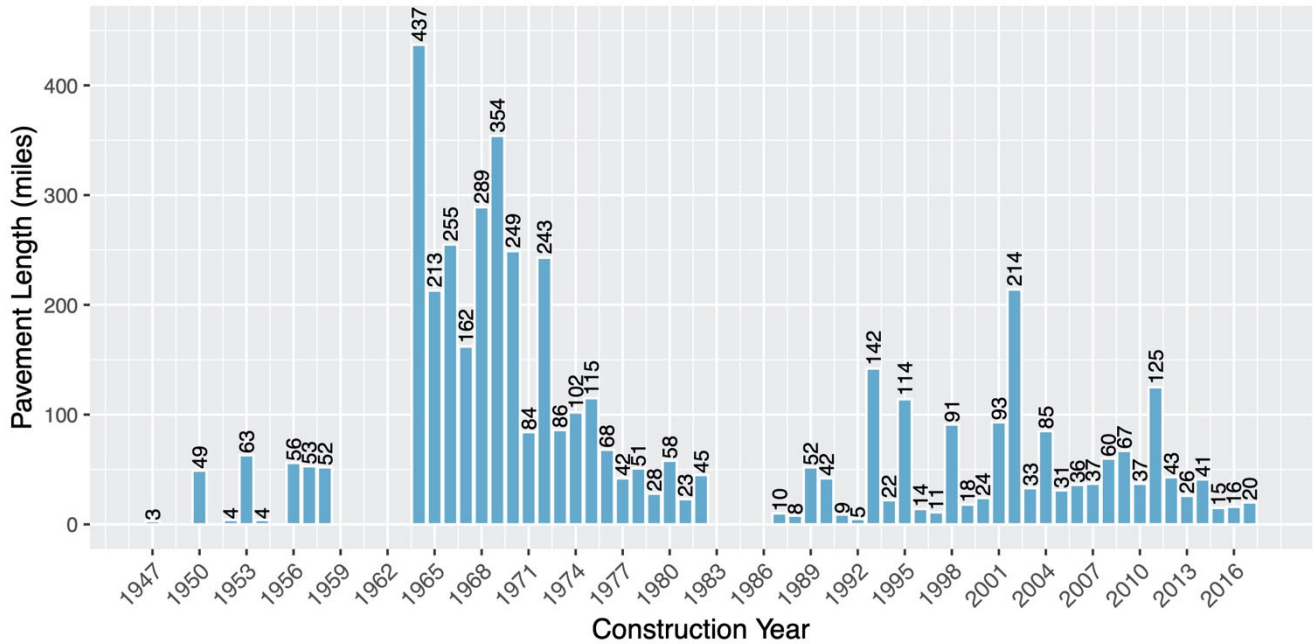


Figure 2.2: JPCP project construction year distribution.

Figure 2.3 shows the pavement age distribution for condition survey observations. Each pavement section’s age was determined by calculating the difference between its construction date and the date of the pavement condition survey. Most of the pavement condition observations were taken on pavements that are less than 40 years old in the condition survey data set.

The as-built database includes information on PCC slab thickness, PCC slab length, base type, and shoulder type. The as-built database does not record whether JPCP projects are doweled, and no other sources were found to obtain that information. Projects with completion dates after about the year 2000 are highly likely to be doweled JPCP because in 1998 Caltrans standard plans mandated the use of dowels in JPCP projects; consequently, this study made the assumption that they are doweled. In Section 2.3.1 through Section 2.3.7 of this report, the distribution of each of the as-built variables and a qualitative evaluation of their effects on the measured cracking performance of JPCP are discussed.

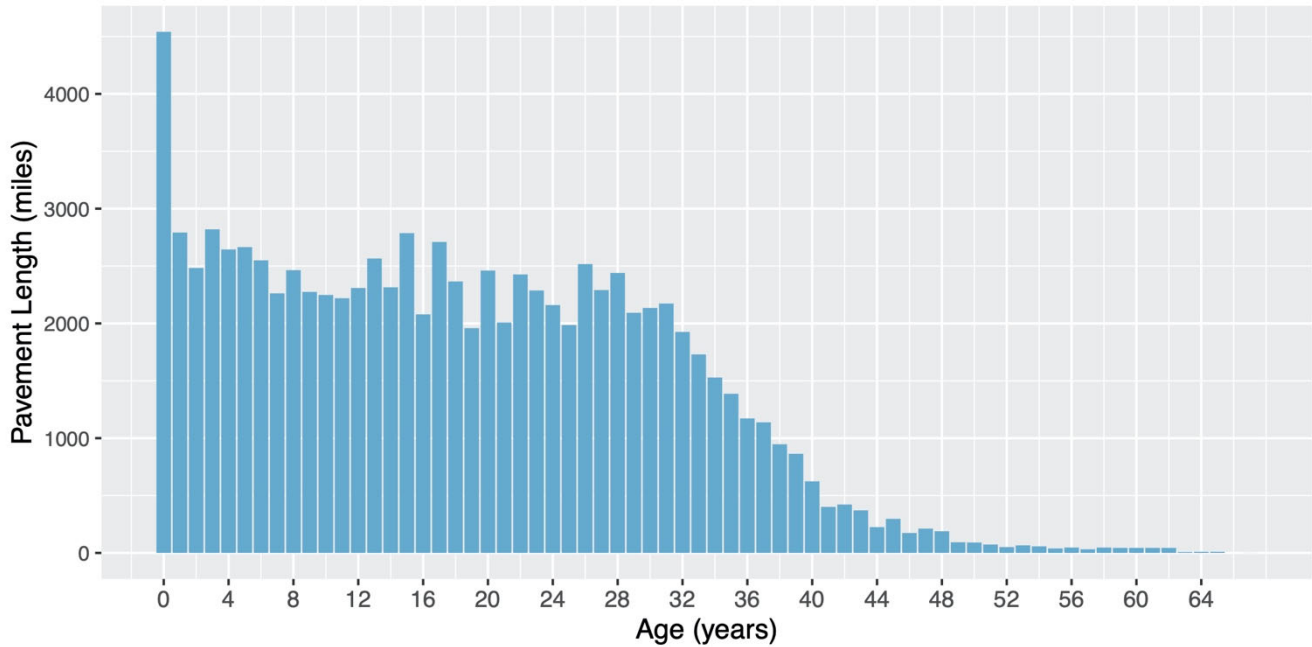


Figure 2.3: Pavement age distribution.

This large pavement performance database will be used to calibrate the Pavement ME performance models in the next step of this research. Prior to that step, however, a sensitivity analysis study had to be performed to check the reasonableness of the models in Pavement ME as well as their sensitivity to different input variables. That analysis is the subject of the rest of this report. The values chosen for each input variable in Chapter 4 are based on the historical distributions of the design variables (variables controlled by the designer) shown in this chapter, along with the distributions of the variables not controlled by the designer, shown in the Appendix. It should be noted that the values chosen for the sensitivity analysis are not necessarily those that will be used for Pavement ME calibration, and they will definitely not be the values used for developing catalogs for future designs.

2.3.1 PCC Slab Thickness

Figure 2.4 shows the distribution of PCC slab thickness in the PMS database. The PCC slab thickness was categorized into bins with a 0.1-ft. interval. It can be seen that the majority of PCC slabs were constructed with thicknesses between 0.6 ft. and 0.9 ft.

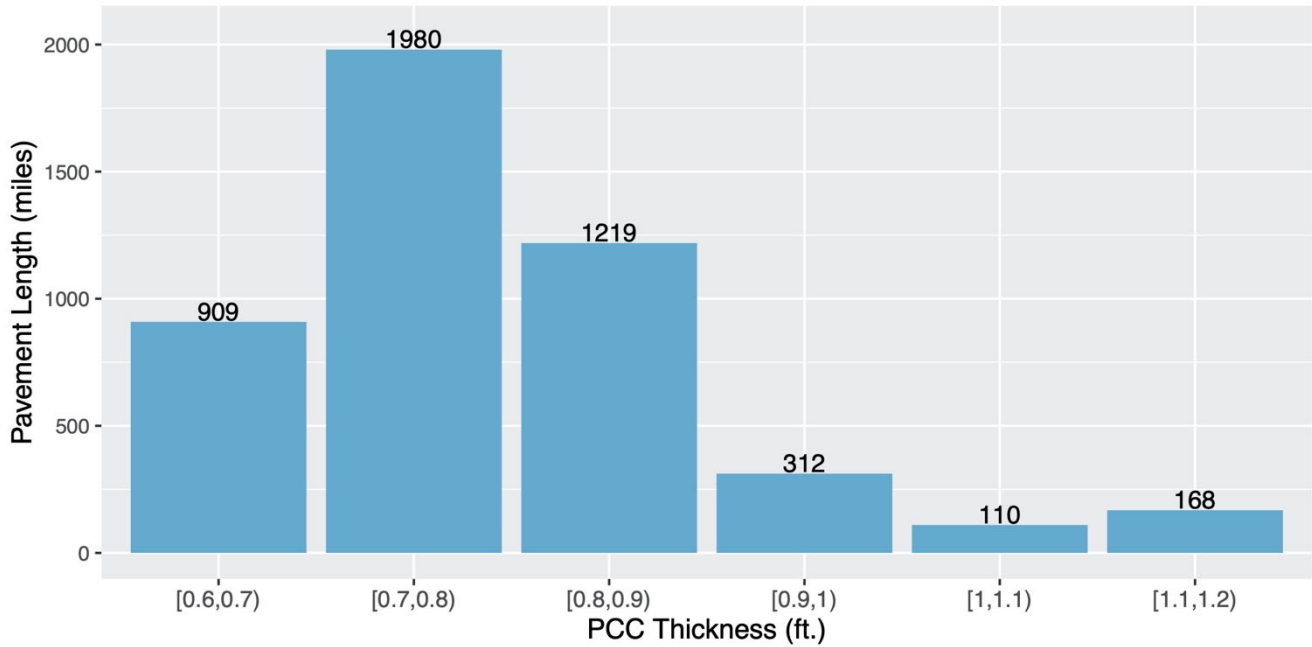


Figure 2.4: PCC slab thickness distribution.

Figure 2.5 shows the cracking performance of the JPCP with different thicknesses over the years. The Y-axis represents the first-stage cracking percentage, the X-axis represents the age of the pavement, and each panel corresponds to a PCC slab thickness. The black points in each plot are the observations of cracking in each thickness range, with the size of each point representing the amount of data in lane-miles; for reference, all the data in the complete data set are shown with gray-shaded points. It can be seen from Figure 2.5 that thicker slabs perform better, with less first-stage cracking than thinner ones, despite the fact that truck traffic is not controlled in the plot. This indicates that despite the intention of previous Caltrans design methods to account for traffic in a manner that results in similar functional lives, the result has been that locations with thinner slabs fail faster than those with thicker slabs. It is uncertain how much of the difference is due to under- or overestimation of truck traffic, or of the design method not doing a good job of accounting for traffic. There may also be interactions with other variables, such as slab length, base type, and shoulder type that are causing differences in performance because of unequal distributions of those variables' factor levels within each thickness category.

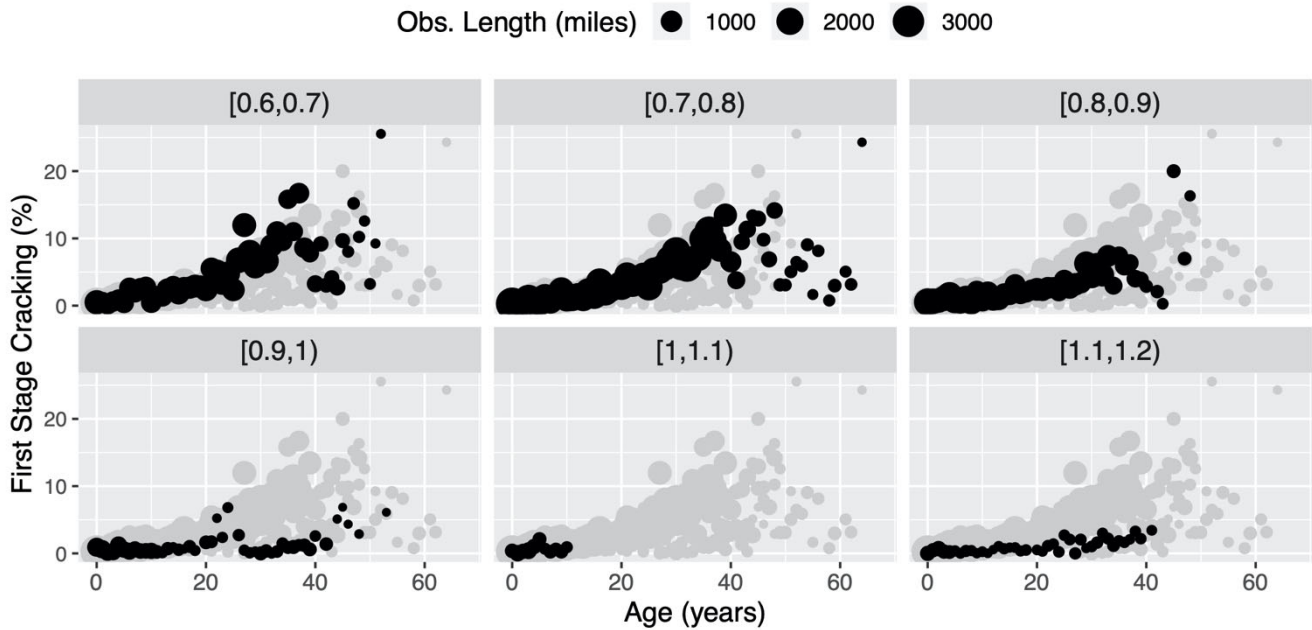


Figure 2.5: JPCP first-stage cracking for different PCC slab thicknesses.

2.3.2 PCC Slab Length

Figure 2.6 shows the slab length patterns for JPCP constructed in California. Three slab length patterns—12,13,14,15 ft.; 12,13,18,19 ft.; and 15 ft.—are the common patterns that have been constructed in different time intervals over the years in California. Figure 2.7 shows the history of slab length pattern construction over the years. Each panel in the figure corresponds to a 10-year interval of construction years. Before about 1990, the 12,13,18,19 ft. slab length pattern was more common, whereas after 1990 the 12,13,14,15 ft. slab length pattern became the dominant length pattern. The slab length patterns were categorized into two groups for the calibration, with 12,13,14,15 ft. being the short pattern, and 12,13,18,19 ft. being the long pattern.

Figure 2.8 shows that the longer slab pattern had a higher rate of first-stage cracking over the years. However, the difference in performance between different slab length patterns is not as significant as was expected.

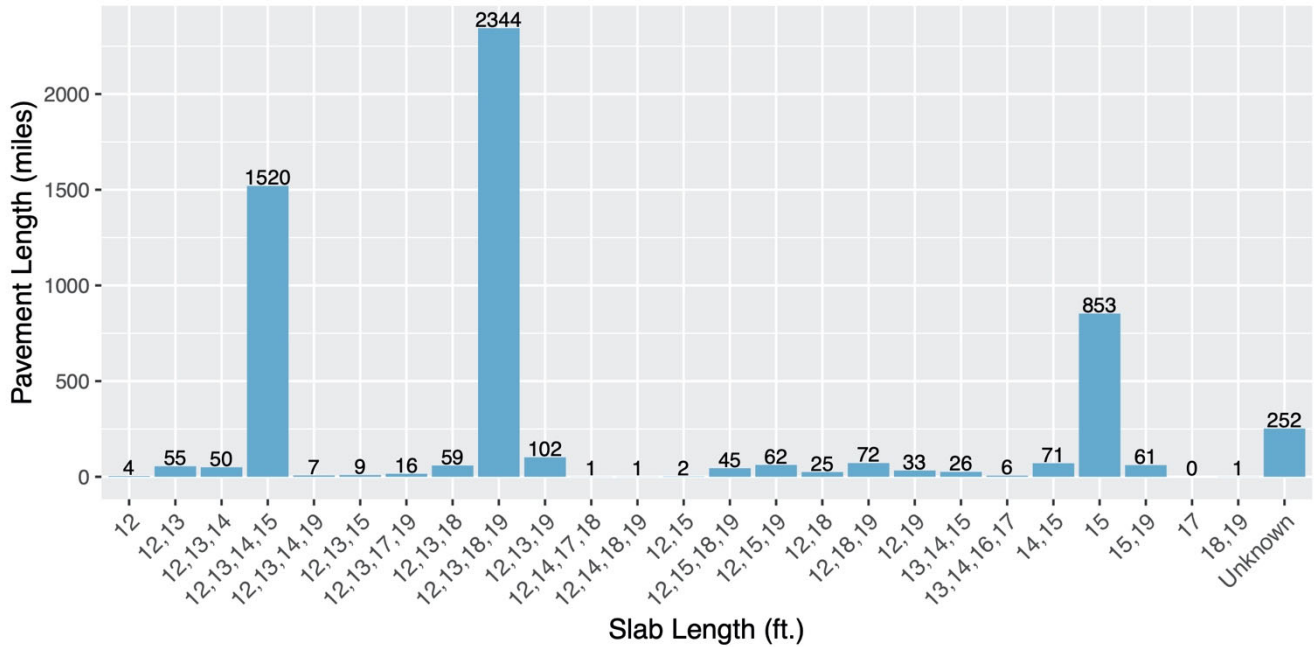


Figure 2.6: PCC slab length distribution.

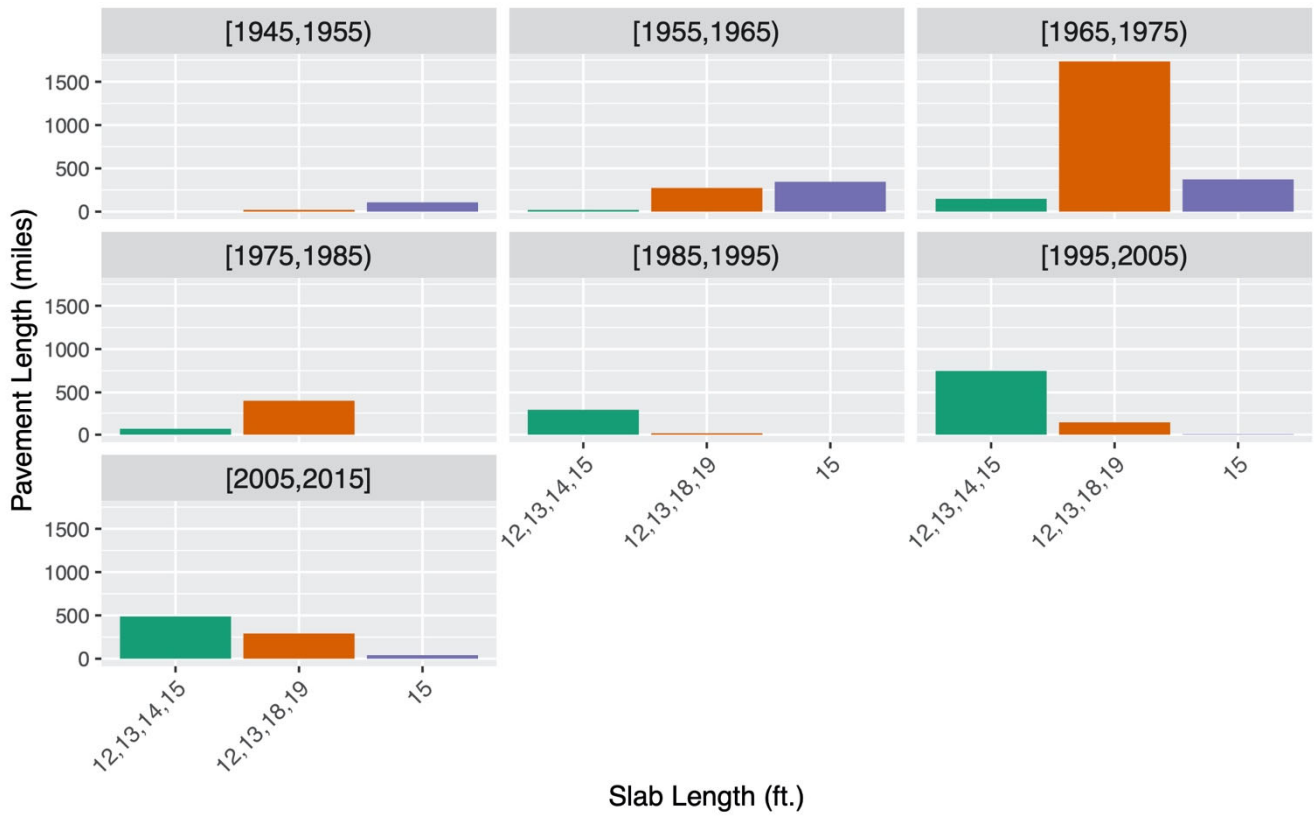


Figure 2.7: PCC slab length pattern history distribution.

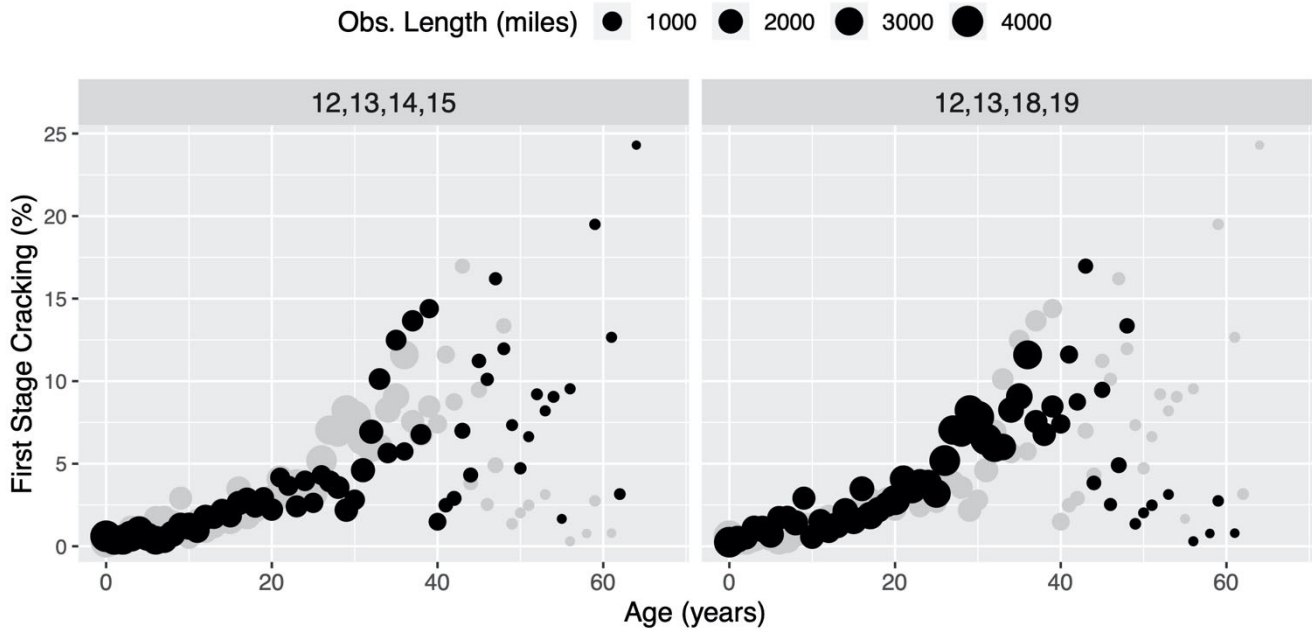


Figure 2.8: JPCP first-stage cracking for different PCC slab length patterns.

2.3.3 Base Type

Five different base types are in the Caltrans pavement management system performance database: aggregate base (AB), asphalt-treated permeable base (ATPB), cement-treated base (CTB), asphalt base (HMA), and lean concrete base (LCB). Based on Figure 2.9, it can be seen that the majority of JPCP was constructed with CTB, and that ATPB was used the least.

From a first glance at Figure 2.10, one can infer that CTB has the worst performance among the other base types. However, this is not necessarily a correct conclusion, since Figure 2.10 considers only one variable (base type) affecting the performance of the JPCP and does not account for other variables such as PCC slab thickness, PCC slab length, shoulder type, traffic, and climate.

To consider all the variables and their simultaneous interactions on the cracking performance of JPCP, a statistical model based on the performance data was developed. In making its predictions, this model considers the variables *PCC slab thickness*, *PCC slab length pattern*, *base type*, *shoulder type*, *climate*, and *Average Annual Daily Truck Traffic (AADTT)*. Predictions from this statistical model are shown in a number of figures that follow, but details of the model will be provided in a separate report.

Figure 2.11 shows the effects of base type on the performance of the JPCP while keeping the other variables constant and using the predictions of the statistical performance model. The results are for 0.9-ft. PCC slab thickness, flexible shoulder type, 7,000 AADTT, and the Inland Valley climate region. Each panel in the figure corresponds to a different base type and slab length pattern. The green shaded area represents the probability of the pavement being undamaged, the yellow area represents the probability of first-stage cracking, and the red represents the probability of third-stage cracking versus years in service. It can be seen that LCB and ATPB show poorer performance than the rest of the base types, and that AB and CTB show better performance.

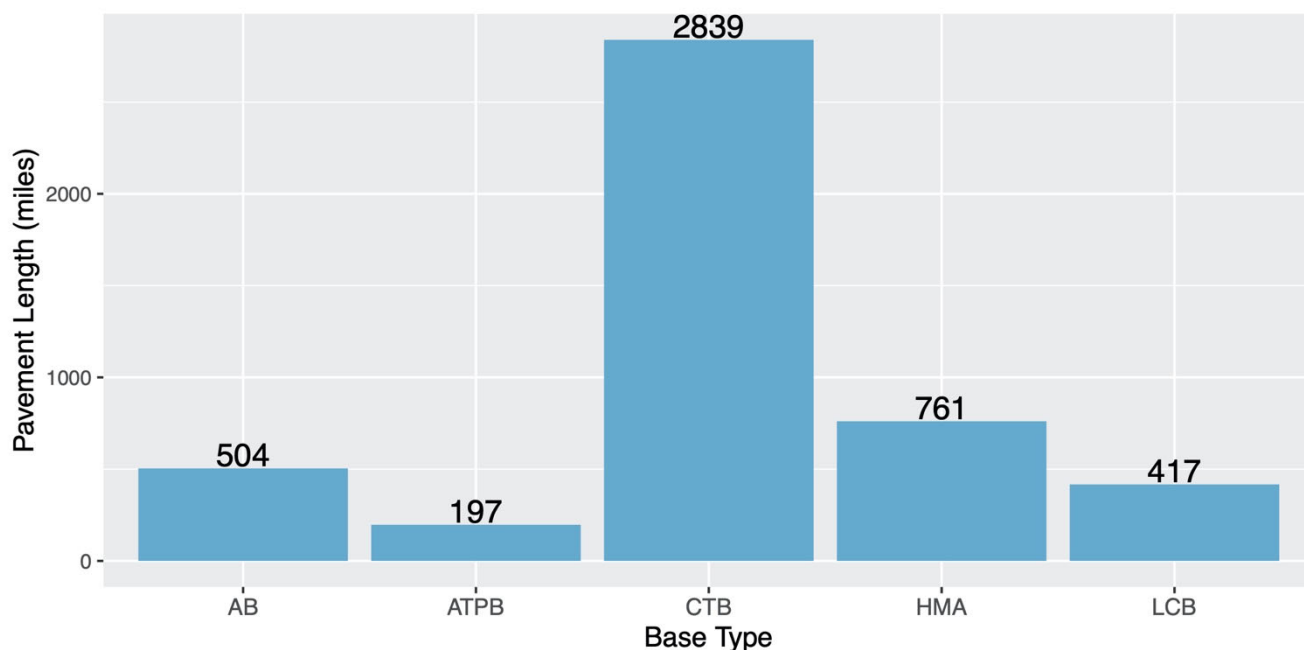


Figure 2.9: Base type distribution.

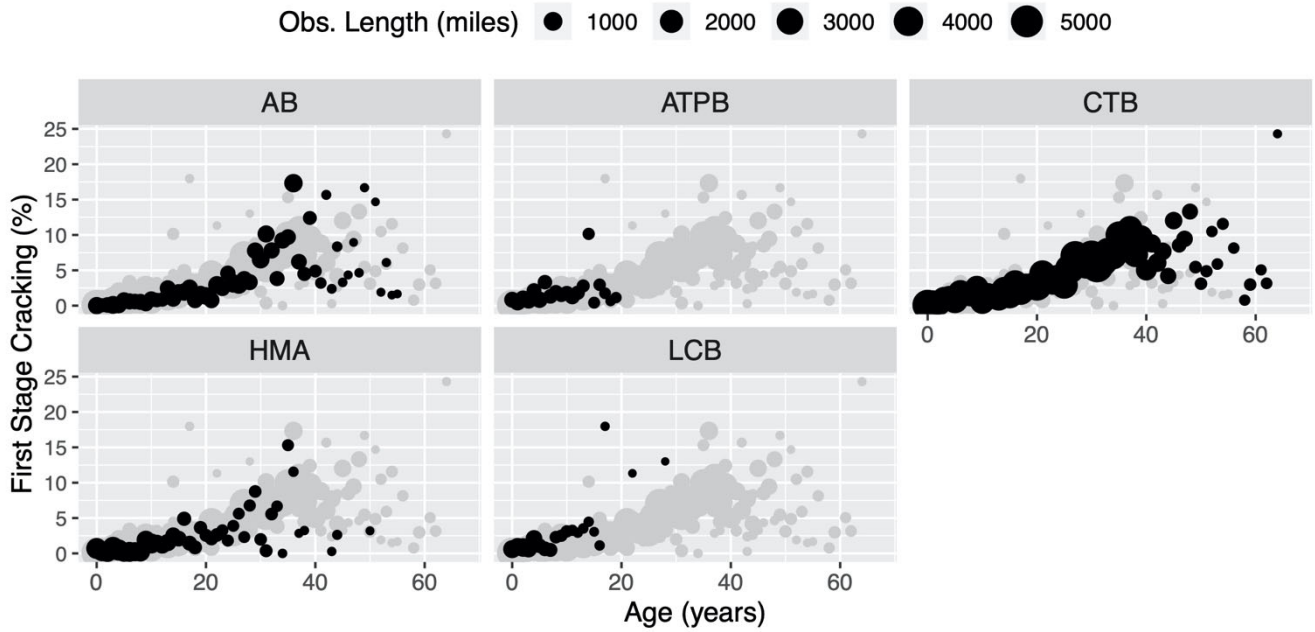


Figure 2.10: JPCP first-stage cracking for different base types.

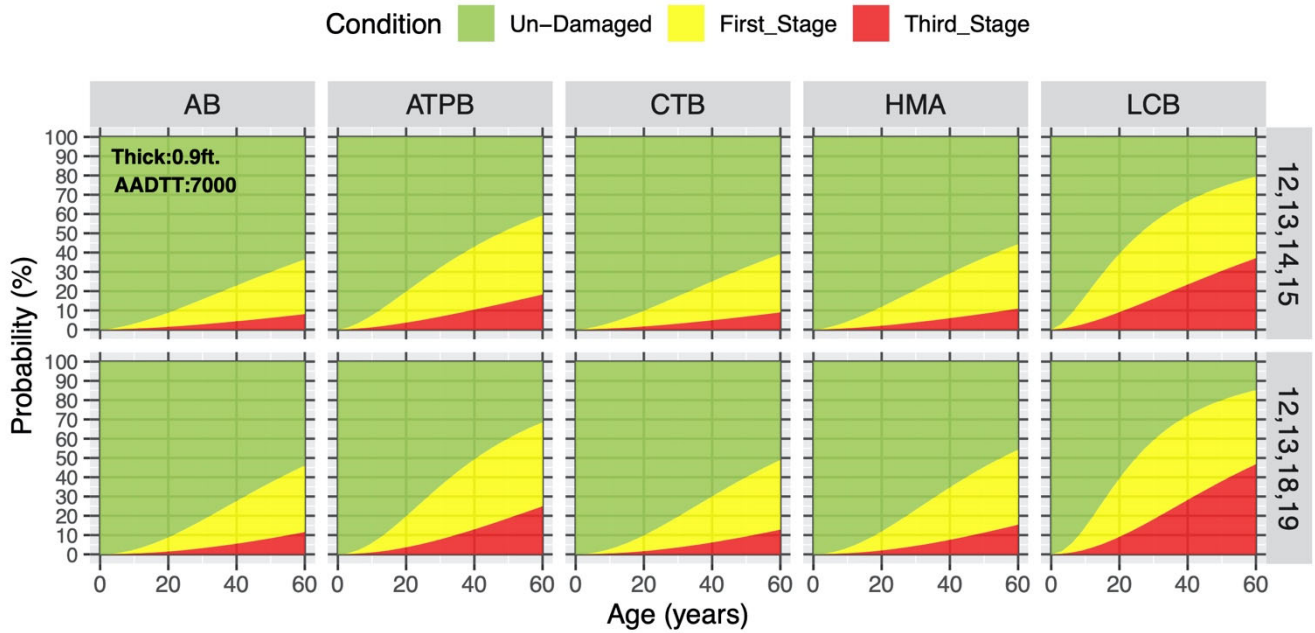


Figure 2.11: Performance model predictions for different base types.

2.3.4 Shoulder Type

Four different shoulder types are defined in the database: not applicable (NAP) for interior lanes without a shoulder, untied flexible (FLX) shoulder, tied concrete (RIG) shoulder, and widened (WRF) lane. It should be noted that the WRF lane type represented in the database is a 2-ft.-wide shoulder. Figure 2.12 shows the distribution of each of these shoulder types in the database. WRF has the fewest constructed lane-miles of all the shoulder types in the database.

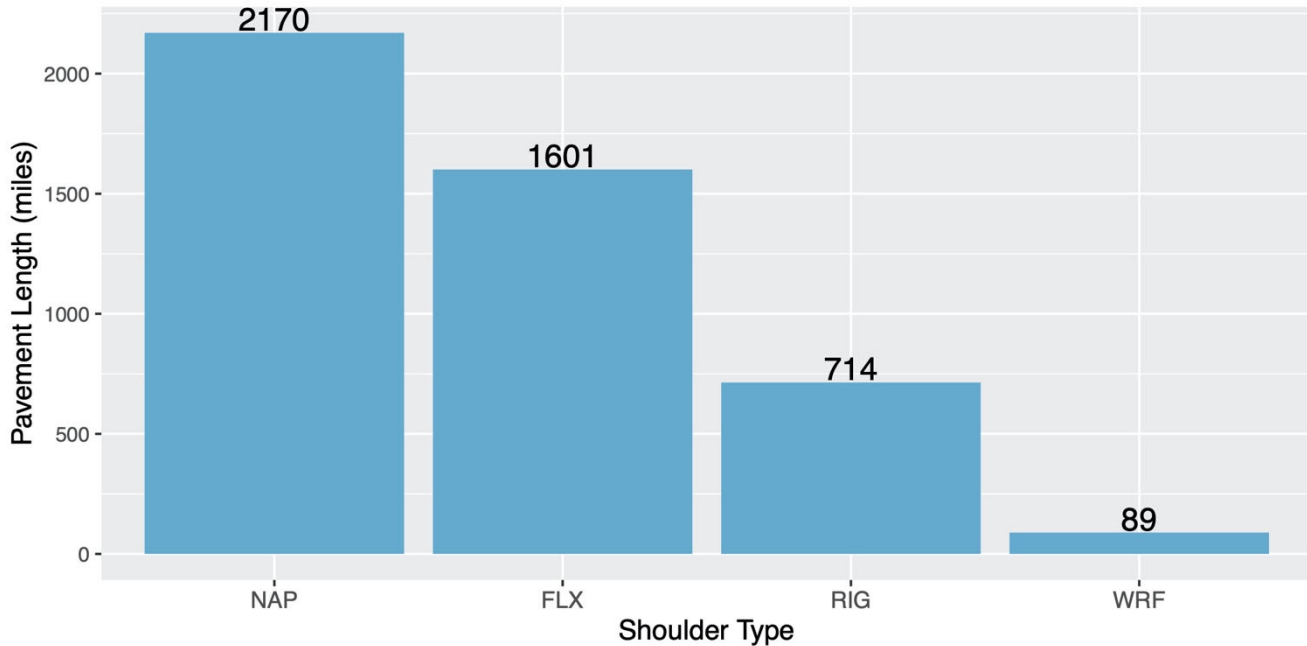


Figure 2.12: Shoulder type distribution.

(Note: NAP: not applicable for interior lanes without a shoulder; FLX: untied flexible shoulder; RIG: tied concrete shoulder; WRF: widened lane.)

Looking at Figure 2.13, one might conclude that the flexible shoulder type (FLX) has the poorest performance of all the shoulder types. This is not necessarily a correct conclusion as other pavement structural, traffic, and climate variables were not accounted for in this plot. Figure 2.14 shows the results of the statistical performance model for shoulder type performance while holding all other variables constant. It can be seen that widened lane (WRF) had the most first- and third-stage cracking, followed by the untied flexible (FLX) shoulder type. The tied concrete shoulder (RIG) type had the best performance among all the shoulder types.

To investigate the reason for the poor performance of the widened lanes (WRF), the per-slab performance data from the 2011 – 2012 APCS data were studied. Figure 2.15 shows the amount of cracking for JPCP, with the WRF shoulder type categorized into panels with different base types and PCC slab thicknesses. The panels show

the model results for the percentage of slabs with no cracking in green, first-stage cracking in yellow, and third-stage cracking in red versus years in service, with different panels for combinations of shoulder type and PCC slab length. It can be seen by looking at the middle two bottom panels that WRF mitigates the transverse cracking problem for longer slabs. However, it can also be seen that shorter slabs, those less than 16 ft., with widened slabs show increased longitudinal cracking. This susceptibility to longitudinal cracking for shorter slabs explains the poor performance of the WRF shoulder type. Again, it should be noted that the propensity for longitudinal cracking of the widened lanes in the database is for 2-ft. extra-wide lanes. It is expected that better longitudinal cracking performance may be obtained with a 1-ft widened lane; however, it is suggested that the reduction in risk of longitudinal cracking be further investigated through modeling.

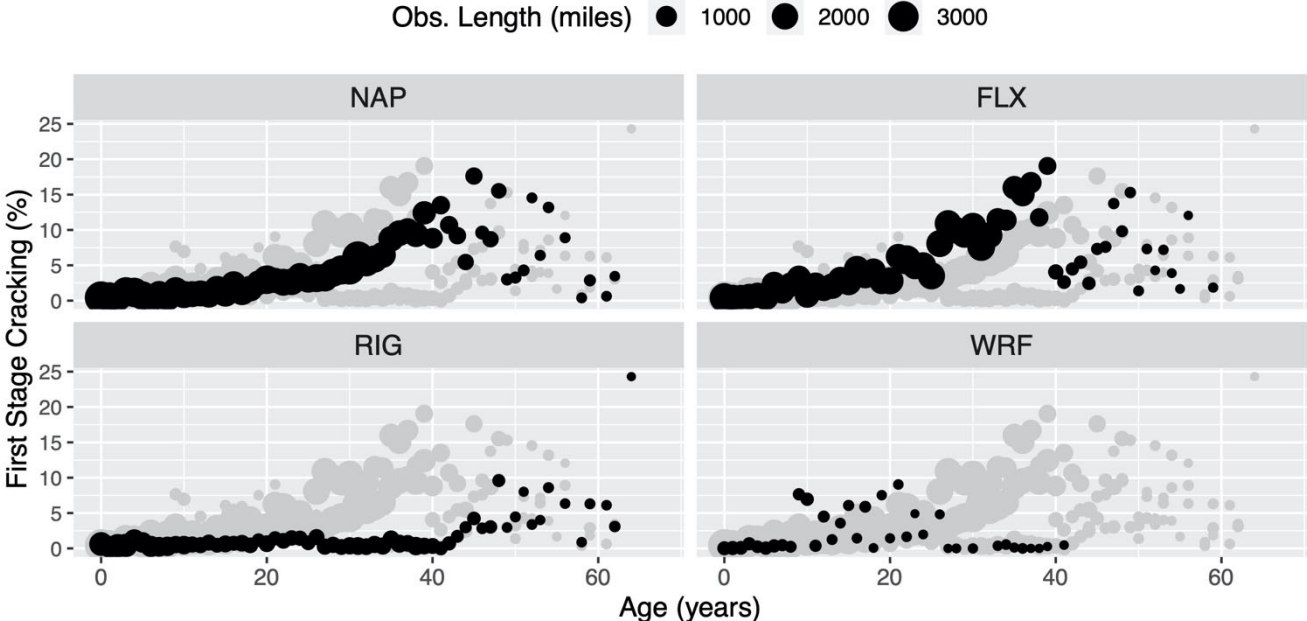


Figure 2.13: JPCP first-stage cracking for different shoulder types.

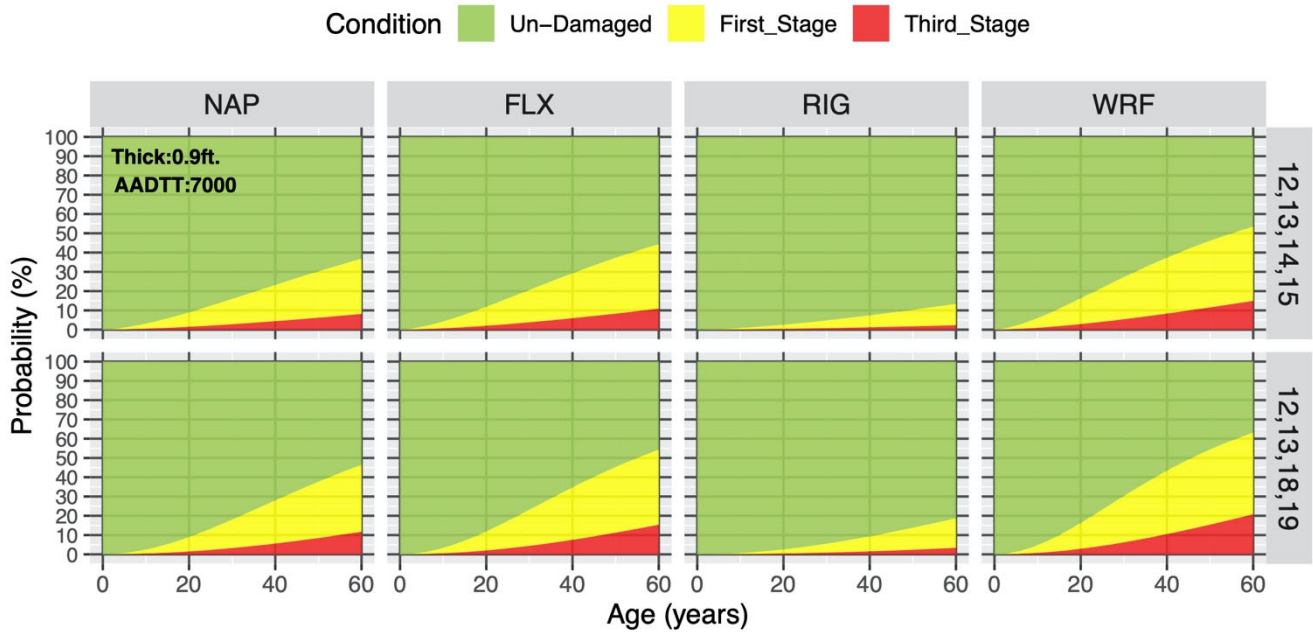


Figure 2.14: Performance model predictions for different shoulder types.

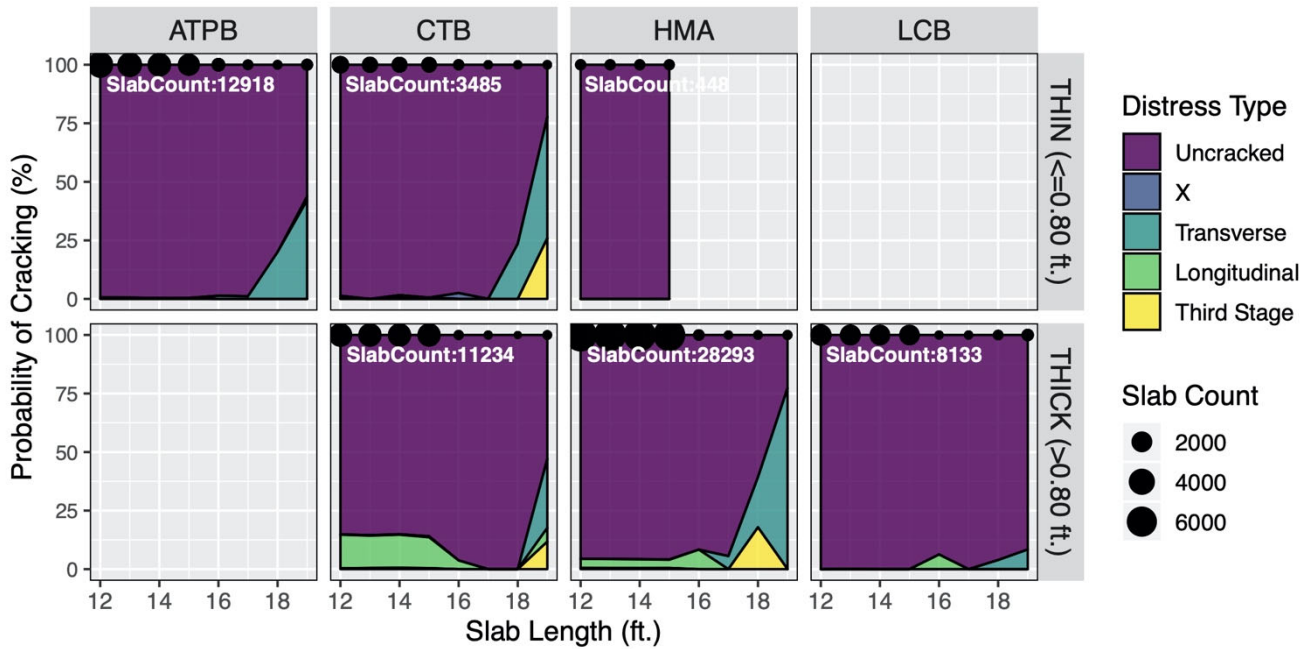


Figure 2.15: Distress Type versus Slab Length for WRF Shoulder Type.

2.3.5 Climate Region

Figure 2.16 shows the Caltrans climate region distribution. Most of the JPCP is located in the Inland Valley and South Coast, while the High Desert and Low Mountain climate regions have the fewest lane-miles of JPCP.

Figure 2.17 shows the JPCP performance in different climate regions. The High Desert (small amount of data), Inland Valley, Low Mountain (small amount of data), and South Mountain climate regions have poorer performance than the others. The lane-miles of JPCP in the South Coast region appear to have excellent performance. The statistical performance model captures observations from the raw data as shown in Figure 2.18.

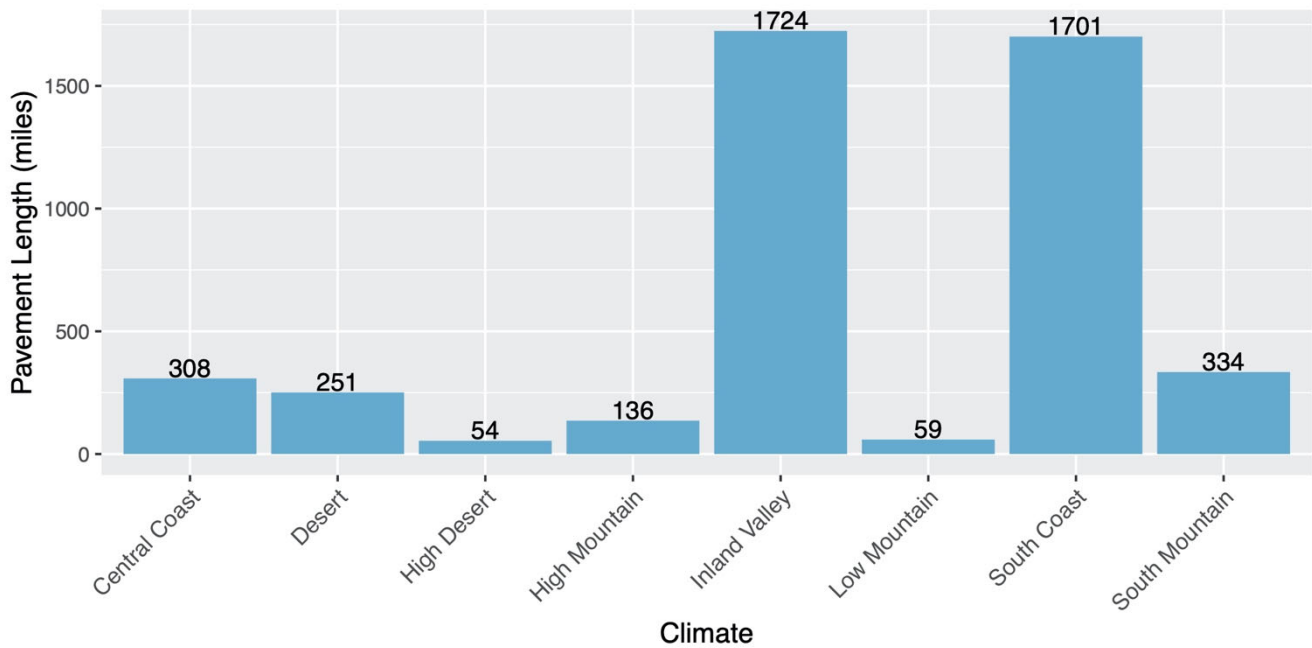


Figure 2.16: Climate region distribution.

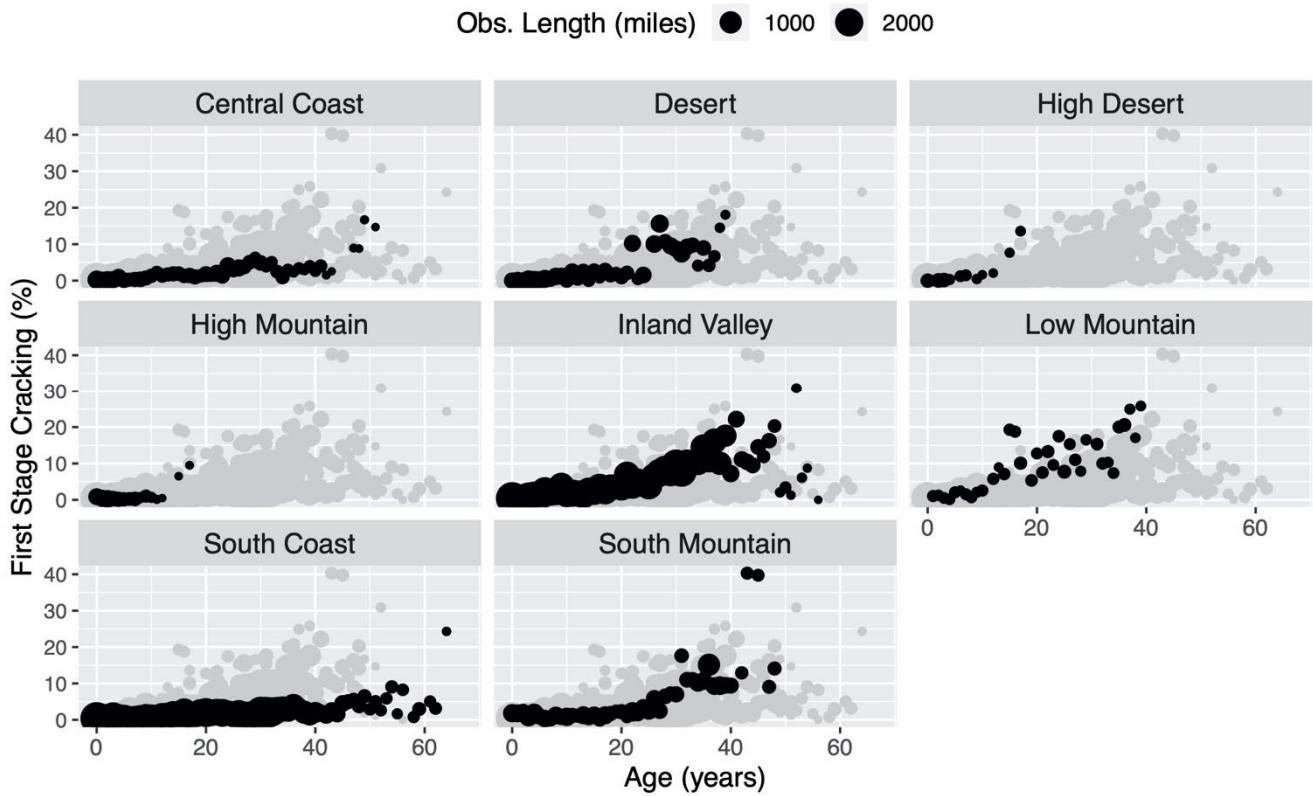


Figure 2.17: JPCP first-stage cracking for different climate regions.

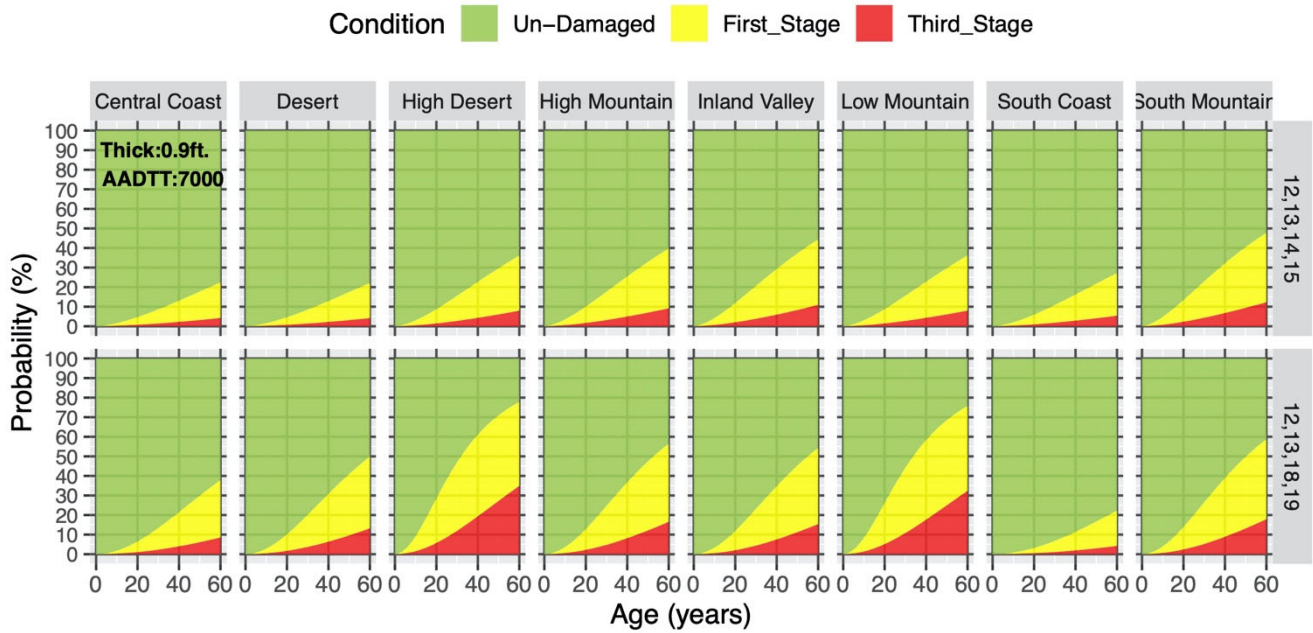


Figure 2.18: Performance model predictions for different climate regions.

2.3.6 WIM Spectrum

Figure 2.19 shows the distribution of the lane-miles with for the five WIM spectra in the database. Higher WIM spectrum numbers correspond to heavier truck traffic loads. It can be seen that most of the JPC pavement has WIM spectra 1 and 2. This is certainly weighted by the lane-miles of inner lanes that have fewer trucks, and the trucks in those lanes tend to be smaller and lighter.

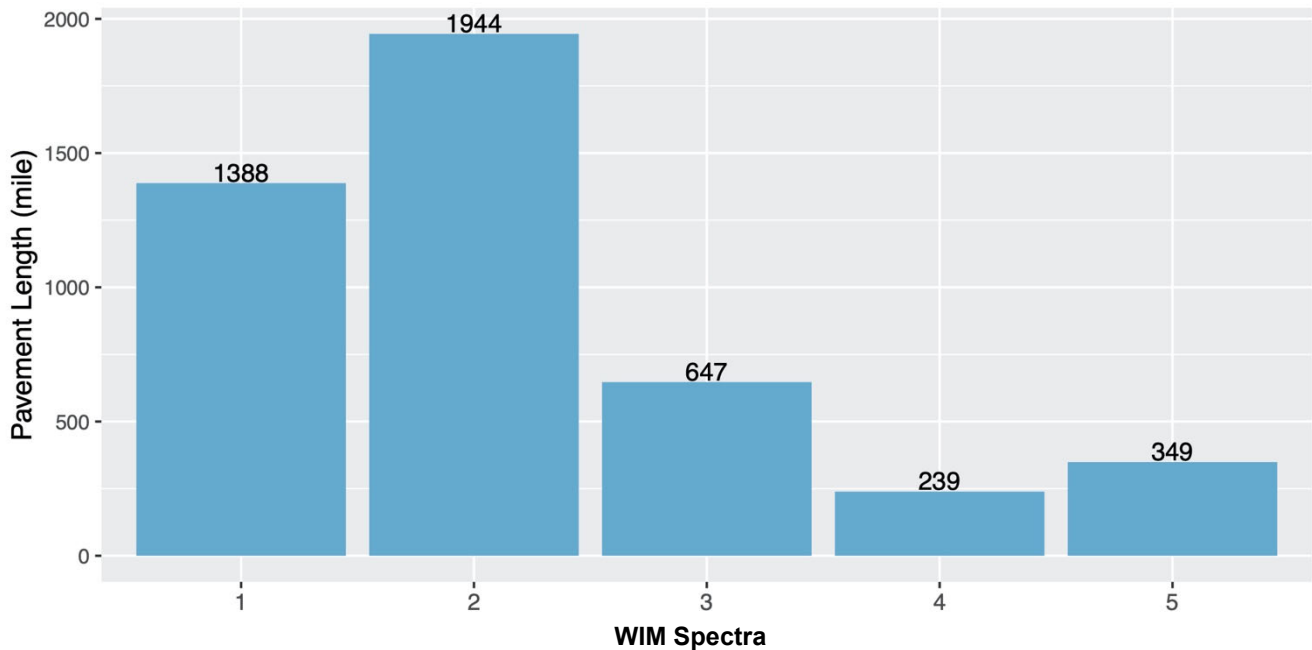


Figure 2.19: WIM spectra distribution.

Figure 2.20 shows the JPCP performance for the different WIM spectra. As the WIM spectrum increases from 1 to 3, the amount of first-stage cracking increases, as expected. However, this is not the case for the heavier WIM Spectra 4 and 5, which have similar performance. Similarly, the statistical performance model did not show a consistent increase in cracking as the WIM spectrum increased, which was an unexpected outcome. The same trend was noted while developing the statistical model, and, therefore, it was decided to not include the WIM spectra variable in the cracking statistical performance model.

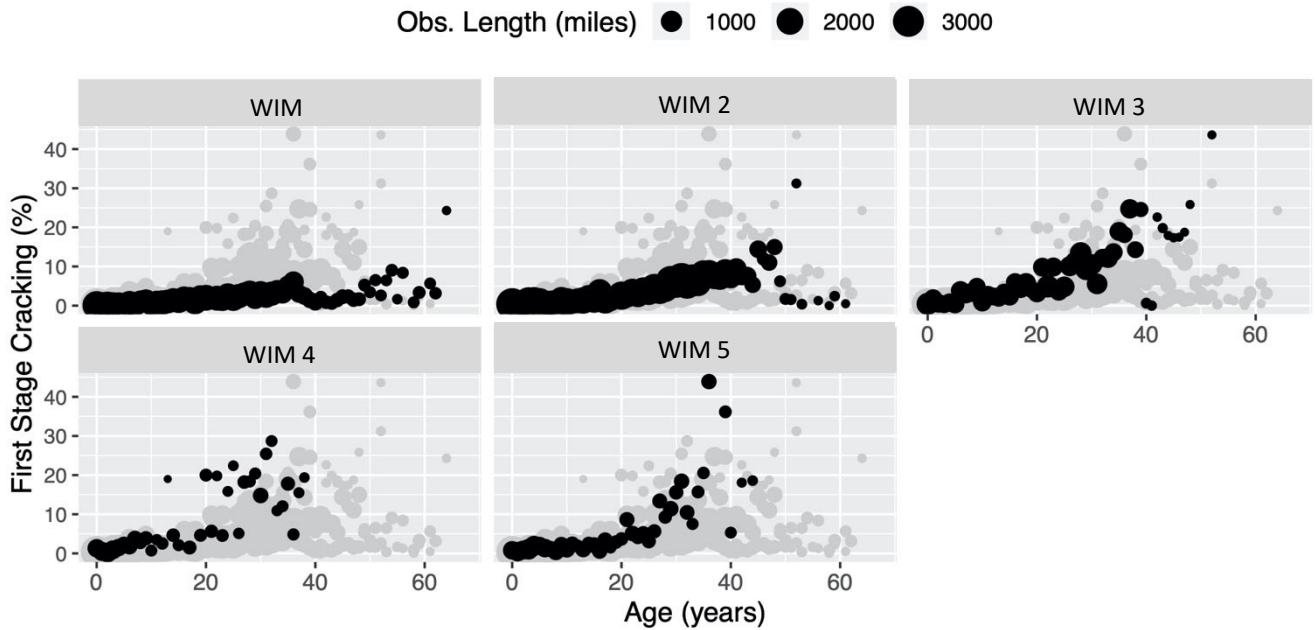


Figure 2.20: JPCP First-stage cracking for different WIM spectra.

2.3.7 Annual Average Daily Truck Traffic (AADTT)

Figure 2.21 shows the distribution of uni-directional per lane AADTT. The X-axis shows the AADTT in thousands of trucks in 300 truck-per-day increments.

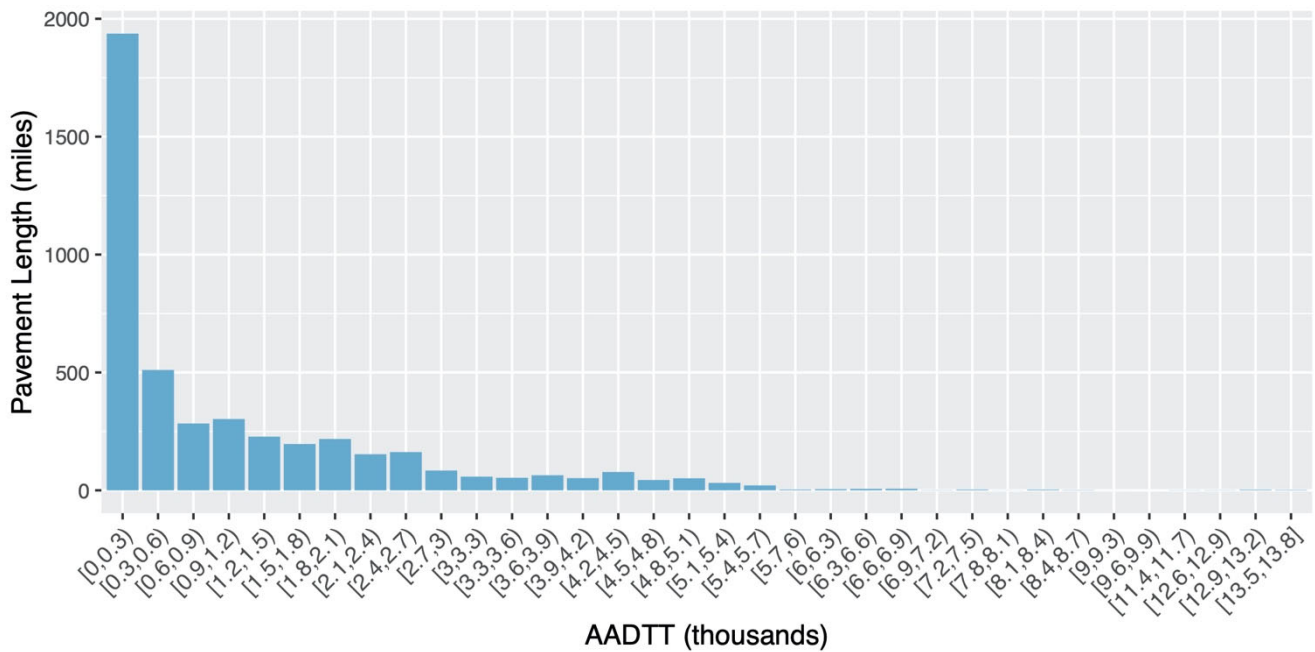


Figure 2.21: AADTT distribution.

Figure 2.22 shows the performance of JPCP for different AADTTs. Each panel corresponds to a range of AADTT in thousands. As shown in the figure, as truck traffic increases, the amount of first-stage cracking increases. The last four panels have sparse data and drawing conclusions from them is not advised. However, predictions by the performance model support the visual observation in the data that greater AADTT causes more cracking, which was expected.

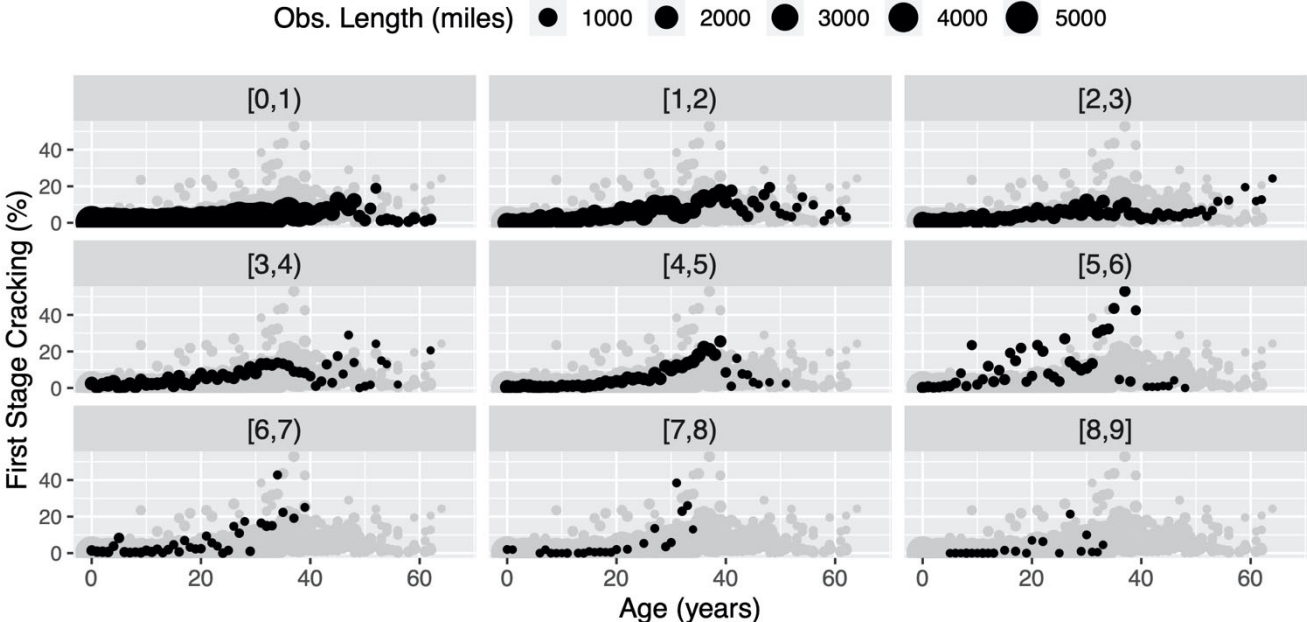


Figure 2.22: JPCP first-stage cracking for different AADTTs (thousands of trucks per day per direction per lane).

3 PAVEMENT ME PERFORMANCE PREDICTION MODELS FOR JPCP

3.1 Introduction

The following three distress models are used in Pavement ME for analyzing and designing jointed plain concrete pavement (JPCP):

- Transverse cracking
- Mean transverse joint faulting
- Smoothness index (IRI)

The transverse cracking and mean transverse joint faulting models are stand-alone developed based on mechanics and statistical modeling principles. However, the IRI model was developed solely by relating the output of the transverse cracking and faulting models to IRI using statistical techniques. Each of these models is discussed further below.

3.2 Transverse Cracking

In Pavement ME, the structural responses of JPCP such as stress, strain, and deflection are computed using neural networks developed from a large factorial of finite element analysis results. Through the Miner's law fatigue equation, these structural responses are related to the accumulated damage in the pavement caused by environmental conditions and traffic loadings. The general expression for fatigue damage accumulation that considers all the critical factors for JPCP transverse cracking is as follows:

$$FD = \sum \frac{n_{i,j,k,l,m,n}}{N_{(i,j,k,l,m,n)}} \quad (3.1)$$

where FD is the total fatigue damage (top-down and bottom-up), $n_{i,j,k,l,m,n}$ is the applied number of load applications at condition i, j, k, l, m, n , and $N_{(i,j,k,l,m,n)}$ is the allowable number of load applications at condition i, j, k, l, m, n . Each subscript represents different conditions, such as age, month, axle type, load level, temperature difference, traffic path, etc. The allowable number of load applications is the number of load cycles at which fatigue failure is expected (corresponding to 50 percent of slabs with transverse cracking) and is a function of the applied stress and the strength of the portland cement concrete (PCC). The allowable number of load applications is determined using the following field-calibrated fatigue model:

$$\log(N_{i,j,k,l,m,n}) = C_1 \left(\frac{MR}{\sigma} \right)^{C_2} \quad (3.2)$$

where $N_{i,j,k,l,m,n}$ is the allowable number of load applications, MR is the PCC modulus of rupture in psi , σ is the applied stress in psi , and C_1 and C_2 are equation constants that should not be changed because they have been calibrated by previous researchers and new data are not available to calibrate them.

The amount of transverse cracking observed in a JPCP section is calculated using the fatigue damage calculated by Equation (3.1) as follows:

$$CRK = \frac{100}{1 + C_4(FD)^{C_5}} \quad (3.3)$$

where CRK is the percentage of bottom-up or top-down transverse cracking appearing on the surface, FD is the fatigue damage index calculated using Equation (3.1), and C_4 and C_5 are the equation constants calibrated using field data. It should be noted that in Pavement ME, it is assumed that both top-down and bottom-up cracking can occur. Damage is calculated at the top and bottom of the slab, and the results are used to determine top-down and bottom-up transverse cracking, respectively. Finally, top-down and bottom-up transverse cracking are regarded as two independent phenomena and are used to estimate the total transverse cracking probability:

$$CRK = CRK_{top_down} + CRK_{bottom_up} - CRK_{top_down} * CRK_{bottom_up} \quad (3.4)$$

3.3 Mean Transverse Joint Faulting

Faulting is the result of slab edge and corner deflections that cause erosion and pumping of fine materials from beneath a loaded leave concrete slab to under the approach slab that has just been unloaded. These factors result in faulting:

- Significant adjacent-slab differential deflections that impart energy to underlying pavement materials
- Erodible underlying pavement materials
- Free water in the pavement structure

The faulting progression rate in JPCP increases due to poor load transfer across a joint or crack; heavy axle loads that result in increased differential deflections; and free moisture and high fines content in the layers beneath the concrete that lead to erosion and fines pumping of the base, subbase, and subgrade materials under the pavement. According to the MEPDG (1), traffic loading, slab thickness, PCC modulus of elasticity, modulus of subgrade reaction (k-value), base type, shoulder type, transverse joint spacing, and dowel diameter are among the design factors that affect transverse joint faulting.

Pavement ME uses an incremental approach to calculate faulting in JPCP. A faulting increment is determined at each month, and the current faulting level affects the magnitude of the increment. The following model—shown

as Equations (3.5), (3.6), (3.7), and (3.8)—determines monthly faulting by summing the incremental faulting over the pavement life since opening to traffic:

$$Fault_m = \sum_{i=1}^m \Delta Fault_i \quad (3.5)$$

$$\Delta Fault_i = C_{34} (FaultMax_{i-1} - Fault_{i-1})^2 * DE_i \quad (3.6)$$

$$FaultMax_i = FaultMax_0 + C_7 * \sum_{j=1}^m DE_j * \log(1 + C_5 * 5^{Erod})^{C_6} \quad (3.7)$$

$$FaultMax_0 = C_{12} * \delta_{curling} * [\log(1 + C_5 * 5^{Erod}) * \log\left(P_{200} * \frac{WetDays}{P_s}\right)]^{C_6} \quad (3.8)$$

where $Fault_m$ is the mean joint faulting at the end of month m in inches, $\Delta Fault_i$ is the incremental change in mean joint faulting on a monthly basis (during month i) in inches, DE_i is the differential deflection energy density of subgrade deformation for month i in $\frac{lb}{in}$, $FaultMax_i$ is the maximum mean transverse joint faulting in month i in inches, $FaultMax_0$ is the initial maximum mean transverse joint faulting in inches, $Erod$ is a base/subbase erodibility factor, $\delta_{curling}$ is the maximum mean monthly PCC slab corner upward deflection due to temperature curling and moisture warping, P_s is the overburden on subgrade in lbs, P_{200} is the percent subgrade material passing #200 sieve, and $WetDays$ is the average annual number of wet days (greater than 0.1 inches of rainfall). The constants C_{12} and C_{34} are defined as follows:

$$C_{12} = C_1 + C_2 * (FR)^{0.25} \quad (3.9)$$

$$C_{34} = C_3 + C_4 * (FR)^{0.25} \quad (3.10)$$

where FR is base freezing index defined as the percentage of time the temperature at the top of the base is below freezing. C_1 through C_7 in Equations (3.6) through (3.9) are the mean transverse joint faulting model constants that are calibrated against field data.

The model's functional form reflects the hypothesis that faulting potential depends on the amount of PCC slab curling, base erodibility, and the presence of fines and free water in the subgrade. Faulting potential decreases with an increase of overburden pressure on the subgrade. The faulting development rate depends on the faulting level and decreases as the cumulative faulting increases until it stabilizes to a certain level.

The process of calculating mean transverse joint faulting in Pavement ME can be summarized in the following steps:

- Process the traffic data to calculate the equivalent number of single, tandem, and tridem axles.
- Process the pavement temperature profile data to convert the hourly pavement temperature profile generated by the *Enhanced Integrated Climate Model* (EICM) to effective nighttime differences.
- Process the monthly relative humidity to take into account the effect of seasonal changes in moisture conditions on differential shrinkage in terms of monthly deviations in slab warping expressed in terms of equivalent temperature differential.
- Calculate initial maximum faulting.
- Evaluate joint load transfer efficiency (LTE).
- Calculate current maximum faulting.
- Determine critical pavement responses for the increment.
- Evaluate the loss of shear capacity and dowel damage.
- Calculate the faulting increment.
- Calculate cumulative faulting.

3.4 International Roughness Index (IRI)

According to the MEPDG (1), for a given rigid pavement with an initial smoothness, several factors combine to contribute to smoothness loss over time. The occurrence and progression of visible distresses in JPCP was found to be the main factor decreasing a pavement’s smoothness after construction. JPCP smoothness decreases as the quantity and severity of distresses such as transverse cracking, mean transverse joint faulting, and joint spalling increase. The initiation and progression of such distresses result from application of traffic loads, environmental loads, loss of foundation support, and the effect of aging on the pavement materials. As shown previously, these variables’ effects on the occurrence of distresses in JPCP—such as transverse cracking and mean transverse joint faulting—were taken into account using mechanistic-empirical (ME) approaches. The results from these models will be used as input data for the Pavement ME smoothness model.

In Pavement ME, smoothness is predicted as a function of the initial as-constructed profile of the pavement and any change in the longitudinal profile over time due to traffic. The following is the smoothness (IRI) model developed and used in Pavement ME:

$$IRI = IRI_0 + C_1 * CRK + C_2 * SPALL + C_3 * TFAULT + C_4 * SF \quad (3.11)$$

where IRI is the predicted roughness index in $\frac{in.}{mi.}$, IRI_0 is the initial smoothness in $\frac{in.}{mi.}$, CRK is the percent of slabs with transverse cracking, $SPALL$ is the percentage of joints with spalling, $TFAULT$ is the cumulative transverse joint faulting per mile in inches, SF is the site factor, and C_1 through C_4 are the equation constants that should be calibrated using field data.

Transverse cracking and faulting are calculated with the models explained earlier. The site factor is defined as the following:

$$SF = AGE * (1 + 0.556 * FR) * (1 + P_{200}) * 10^{-6} \quad (3.12)$$

where AGE is the pavement age in years, FR is the freezing index, and P_{200} is the percentage of subgrade materials passing the #200 sieve.

Transverse joint spalling is determined using the following equation:

$$SPALL = \left[\frac{AGE}{AGE + 0.01} \right] \left[\frac{100}{1 + 1.005^{-12 * AGE + SCF}} \right] \quad (3.13)$$

where $SPALL$ is the percentage of spalled joints, AGE is the pavement age in years, and SCF is scaling factor based on site, design, and climate. The equation for SCF is:

$$SCF = -1400 + 350 AC_{PCC} * (0.5 + PREFORM) + 43.4 * f'_c{}^{0.4} - 0.2 * (FT_{cycle} * AGE) + 43 * HPCC - 536 WC_{PCC} \quad (3.14)$$

where AC_{PCC} is PCC air content in percent; AGE is the age of the pavement in years, $PREFORM$ is 1 if preformed sealant is present, otherwise 0, f'_c is PCC compressive strength in psi,; FT_{cycle} is average annual number of freeze-thaw cycles; $HPCC$ is PCC slab thickness in inches; and WC_{PCC} is the PCC water-cement ratio.

4 SENSITIVITY ANALYSIS

4.1 Introduction

The main goal of this project, Partnered Pavement Center Project Strategic Plan Element (PPRC SPE) 3.49 is to calibrate the distress prediction models in Pavement ME for JPCP design in California. However, prior to calibration, it is necessary to review the ranges of values for input variables and then to evaluate the sensitivity to those ranges to determine which have the most significant effect on the results. The results of the sensitivity analysis identify which variables should get more attention in the design method. These variables will be used to check the reasonableness of the model predictions, to identify problems in the software, and to understand the level of difficulty involved in obtaining the inputs.

The inputs considered for the JPCP sensitivity analysis were categorized into four groups, and a range of values for each input was selected (see Table 4.1). *(Note: the values appearing in boldface in Table 4.1 are those used for the baseline model. In the rest of this chapter, the Pavement ME results for all cases show the predicted performance range for the range of inputs relative to the baseline model.)* The input value ranges selected for the analysis are different than the ranges that will need consideration when developing design tools for Caltrans. In particular, the slab thicknesses needed to cover the range of designs for Caltrans conditions will include thinner and thicker slabs.

The ranges for the variables considered in this study were selected based on the historical data available in the Caltrans PMS database for variables controlled by the designer (e.g., PCC slab thickness, PCC slab length, base type, shoulder type, etc., discussed in Chapter 2) and the UCPRC material database for variables the designer either has some or no control over (e.g., PCC compressive strength, PCC CTE, PCC shortwave absorptivity, etc. discussed in the appendix). Therefore, the range selected for each variable reflects the common construction practice in California and validates the sensitivity of the models' performance to the variable's change. These values were selected for the analysis to identify the reasonableness of the results from the models based on California experience, to identify which variables are most sensitive, and to identify variables for which the results are non-monotonic (that is, an increase in the input variable may result in an increase or decrease in the predicted performance depending on the input variable value). In many cases, identifying a variable's sensitivity requires the range used to check for sensitivity to be much larger than the range expected in the field.

These ranges will not be used for either calibration or design catalog development. In the calibration process, the range selected for each variable will include all the values ever used for JPCP construction in California, based on the PMS database. Development of the design catalog will use both the values used in the calibration and

additional ones that would reflect future design in California. Therefore, the ranges studied in this report are a subset of those that will be used for both the Pavement ME calibration and the design catalog development that will be explained in future reports.

As noted, the variables can be divided into those that a pavement designer can determine and others that the designer cannot control. More specifically, first group of variables, the ones determined by the designer, are the structural design variables of the pavement. The second group of variables are the material inputs, which are unknown to a designer in a design-bid-build project delivery environment—although some materials variables are partly constrained by specifications and some are not (e.g., strength is constrained by specifications but CTE is not). The third and fourth groups, traffic and climate, are generally known to the designer but they cannot be controlled. Of course, there are many other input variables that need to be defined as part of Pavement ME runs. However, some variables that the designer cannot know, such as shrinkage, were not considered because data for them were lacking. These variables’ effects were not considered in this project, and their default values were used in the Pavement ME runs.

Table 4.1: Input Variables Examined in the Sensitivity Analysis

Input Category	Variable
Pavement structural design	PCC slab thickness: (7, 8 , 9) in inches
	PCC slab length: (12-13-14-15, 15 , 12-13-18-19) in feet
	Load transfer: (Doweled , Undoweled)
	Friction loss duration: (No Friction, 120 , 240) in months
	Base type: (Aggregate Base (AB), Hot-Mix Asphalt (HMA) , Cement-treated Base (CTB), Lean concrete base (LCB))
	Shoulder type (edge support): (Not-Tied, Tied , Widened)
	Subgrade type: (Gravel&Sand (A-1a) , Sand (A-3), Clay (A-5))
	Erodibility index: (ExtremelyErosionResistant (1), FairlyErodible (4) , VeryErodible (5))
Pavement material	PCC compressive strength: (4,730, 5,730 , 6,730) in psi
	PCC Coefficient of Thermal Expansion (CTE): (4, 5 , 6) in $10^{-6}F^{-1}$
	PCC shortwave absorptivity: (0.65, 0.7 , 0.8, 0.9)
	PCC heat capacity: (0.2 , 0.24, 0.28) in BTU.lb.°F
	PCC thermal conductivity: (1.0, 1.15, 1.25 , 1.5) in BTU.hr.ft.°F
	Built-in curl-warp temperature: (-15, -10 , -5, 0) in °F
Traffic	Average annual daily truck traffic for two lanes (AADTT): (7,000, 12,000, 14,000 , 16,000, 20,000)
	WIM spectra: (1, 3 , 5)
Climate	Climate region: (Desert, High Desert, South Mountain, Low Mountain , High Mountain, Inland Valley, Central Coast, South Coast)

Notes:

The units used in the Pavement ME software are presented, although they are not necessarily the units used by Caltrans in design; Caltrans units and metric units [rounded to nearest 15 mm] are shown in parentheses in the initial discussion of each variable.

The values appearing in boldface were used for the baseline model.

To perform a sensitivity analysis of the distress prediction models for JPCP in Pavement ME, a baseline model was defined with a reference set of input values. The values were selected to investigate the effects of variation of input variables on the results of the Pavement ME models. The baseline model was defined as a pavement structure with an 8-inch (200 mm, 0.67 ft) PCC slab, a 4-inch (105 mm, 0.33 ft) HMA base, a 6-inch (150 mm, 0.5 ft) aggregate subbase, and a well-graded gravel and sand (A-1a) subgrade.

4.2 Pavement Structural and Design Inputs

4.2.1 PCC Slab Thickness

According to the *Mechanistic-Empirical Pavement Design Guide (1)*, PCC slab thickness is one of the most critical design features from the standpoints of both performance and cost. In general, as slab thickness increases, critical bending stresses and deflections decrease, with a consequent reduction in cracking and faulting.

This sensitivity analysis considered three PCC thicknesses: 7, 8, and 9 inches (0.58, 0.67, 0.75 ft [175, 200, 230 mm]). These thicknesses were selected because most of the performance data used for the calibration came from projects with 8- to 10-inch slabs, and because of a desire to consider slabs somewhat less than 8 inches, the current minimum in the HDM, which may be used on routes with lower truck traffic volumes.

The significant effect that PCC slab thickness has on JPCP transverse cracking performance can be observed in Figure 4.1. It can be seen from the figure that in this particular scenario, decreasing slab thickness from 9 inches to 7 inches resulted in an unacceptable design in terms of transverse fatigue cracking.

Note: in all the following figures, the shaded area shows the change in JPCP performance illustrated in Figure 4.1. The shaded area is shown as a reference for comparing the effects that result from adjusting other variables. In this example, the strategy was used to compare the sensitivity of Pavement ME cracking predictions that include the rest of the variables with changes in PCC slab thickness.

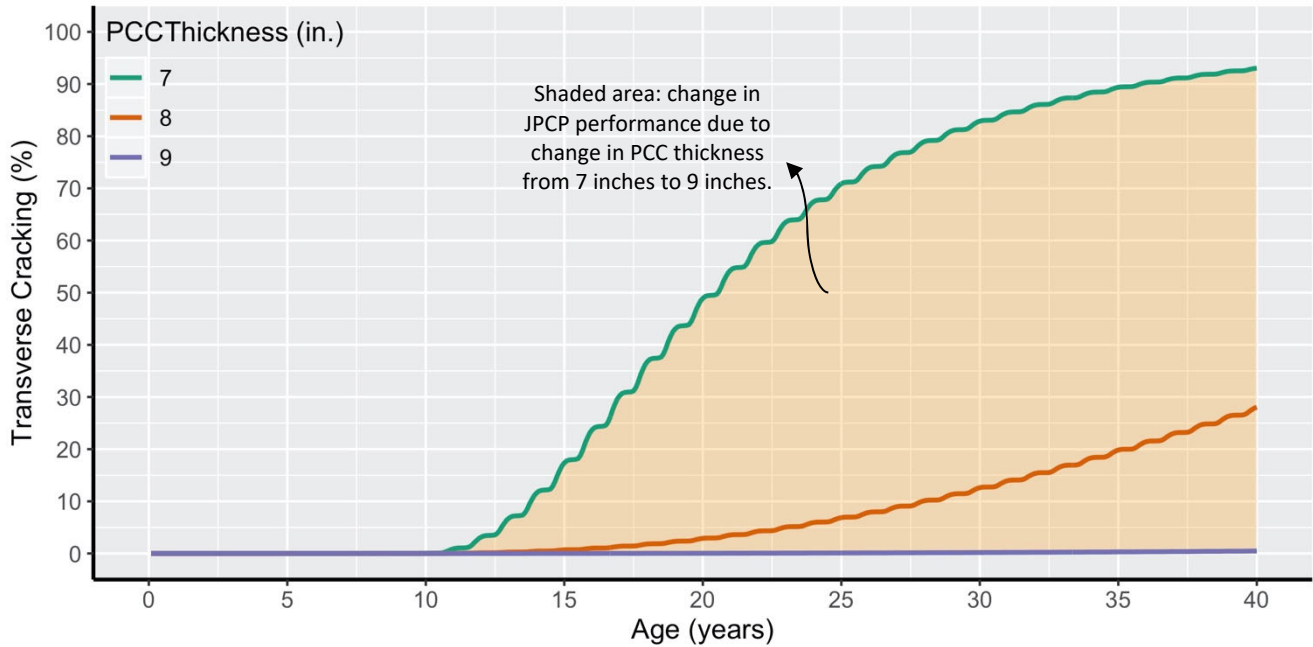


Figure 4.1: Effect of PCC slab thickness on transverse cracking with 50% reliability.

Figure 4.2 shows the effect of PCC slab thickness on the JPCP faulting. These results do not match the stated expectation that thicker PCC slabs would have less faulting. Instead, this figure shows that 7-inch thick slabs have less faulting than thicker slabs. This outcome is believed to be related to the fact that dowel bar diameter was kept constant for all the PCC slab thicknesses (1.25 in.). Maintaining the same dowel diameter while increasing slab thickness results in a reduction in nondimensional dowel stiffness (JD), which is the ratio of cross-sectional steel area to total cross-sectional slab area. This in turn reduces LTE, which increases the differential energy of subgrade deformation, thus resulting in increased cumulative faulting. Therefore, a designer should increase dowel bar size with thicker PCC slabs. As shown in Figure 4.3, Pavement ME predicted faulting decreases versus slab thickness if the dowel diameter is adjusted for each slab thickness (1.0, 1.25, and 1.5 in. dowel diameter, respectively, for 7, 8, and 9 in. slab thickness). In any case, as long as a JPCP has an adequate dowel bar size at the transverse joints according to Caltrans guidelines, faulting should not be the critical path distress for long-term JPCP performance.

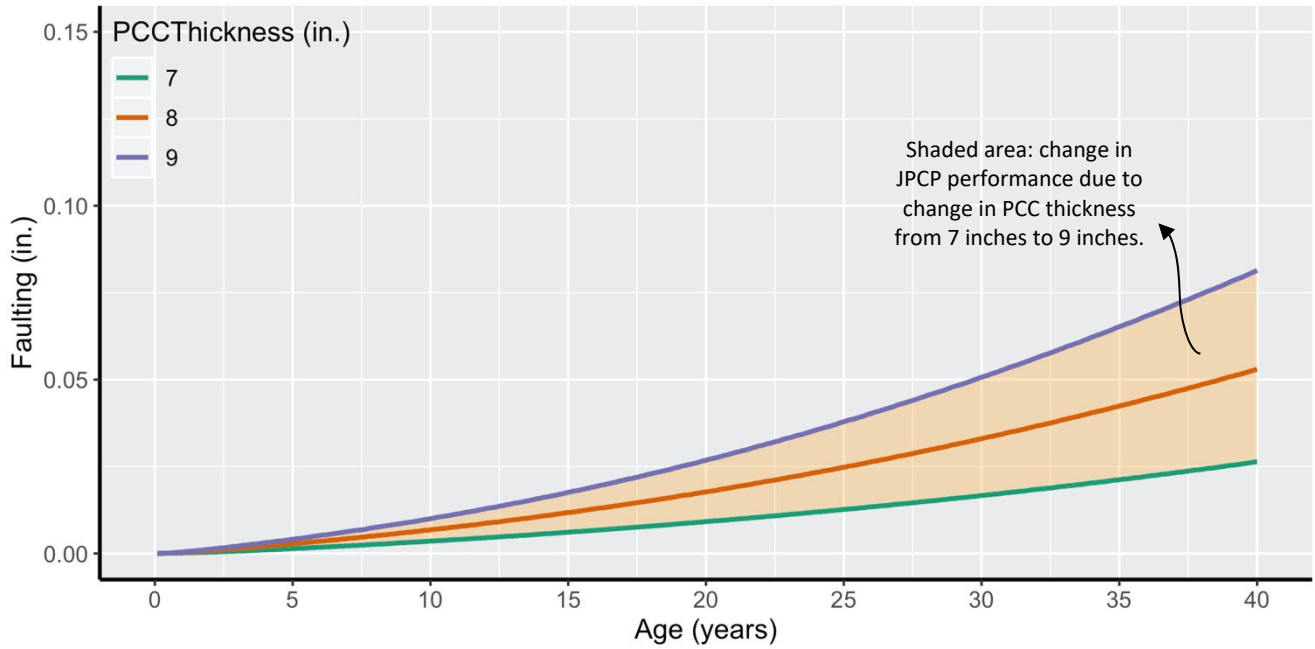


Figure 4.2: Effects of PCC slab thickness on faulting (while keeping dowel diameter constant) with 50% reliability.

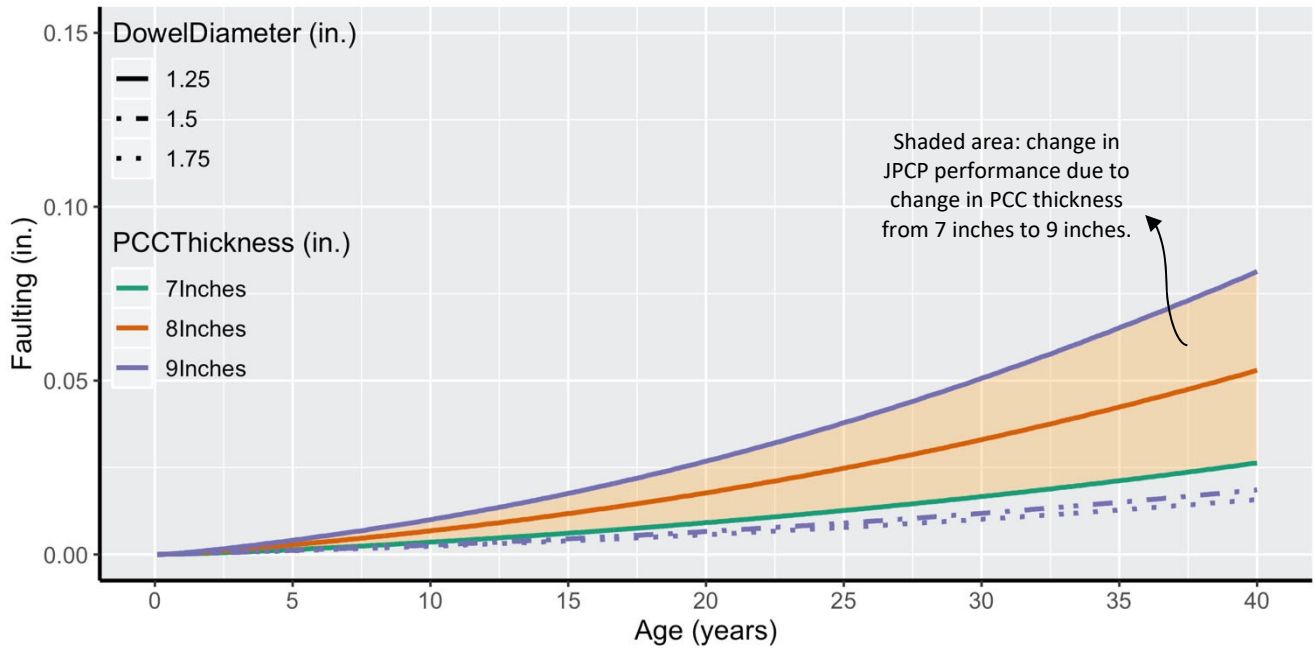


Figure 4.3: Effect of PCC slab thickness on faulting (while changing dowel diameter) with 50% reliability.

The change in IRI is shown in Figure 4.4. Pavement ME determines IRI as a function of initial IRI, site conditions, transverse cracking, faulting, and spalling. Dowel diameter was adjusted for each slab thickness (1.0-, 1.25-, and 1.5-inch dowel diameters, respectively, for 7-, 8-, and 9-inch slab thicknesses) to produce the data shown in the figure. As expected, IRI decreased as slab thickness increased.

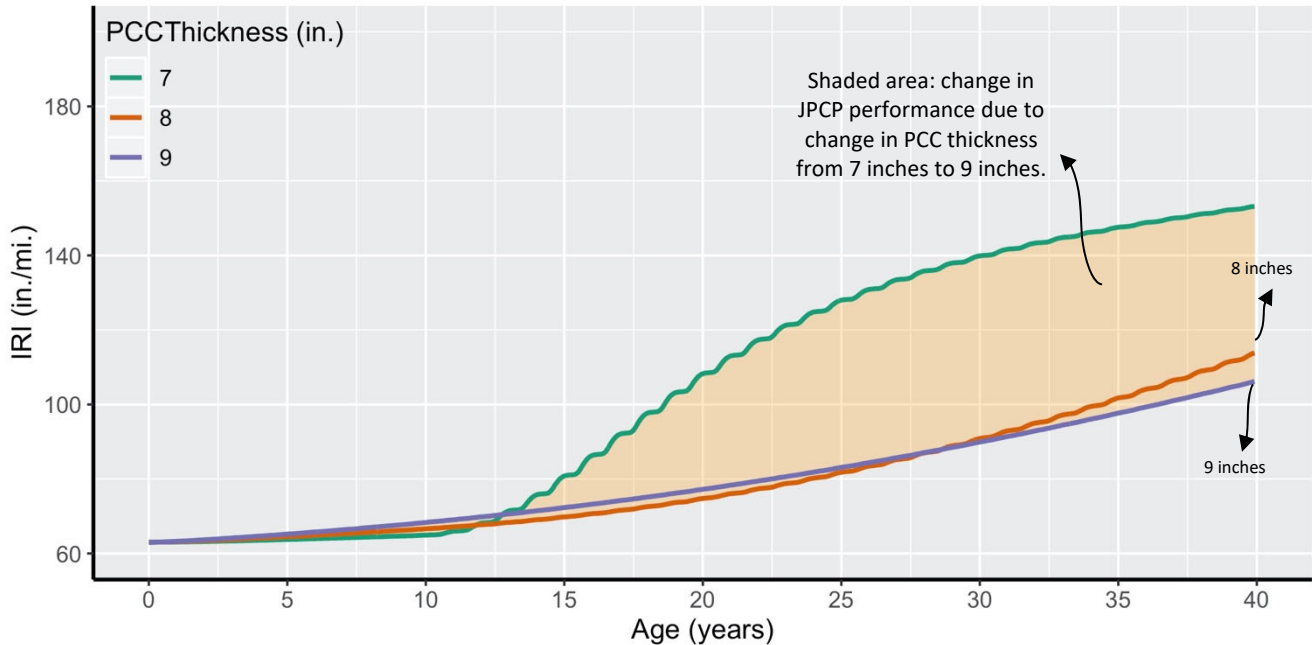


Figure 4.4: Effects of PCC slab thickness on IRI with 50% reliability.

4.2.2 PCC Slab Length (Transverse Joint Spacing)

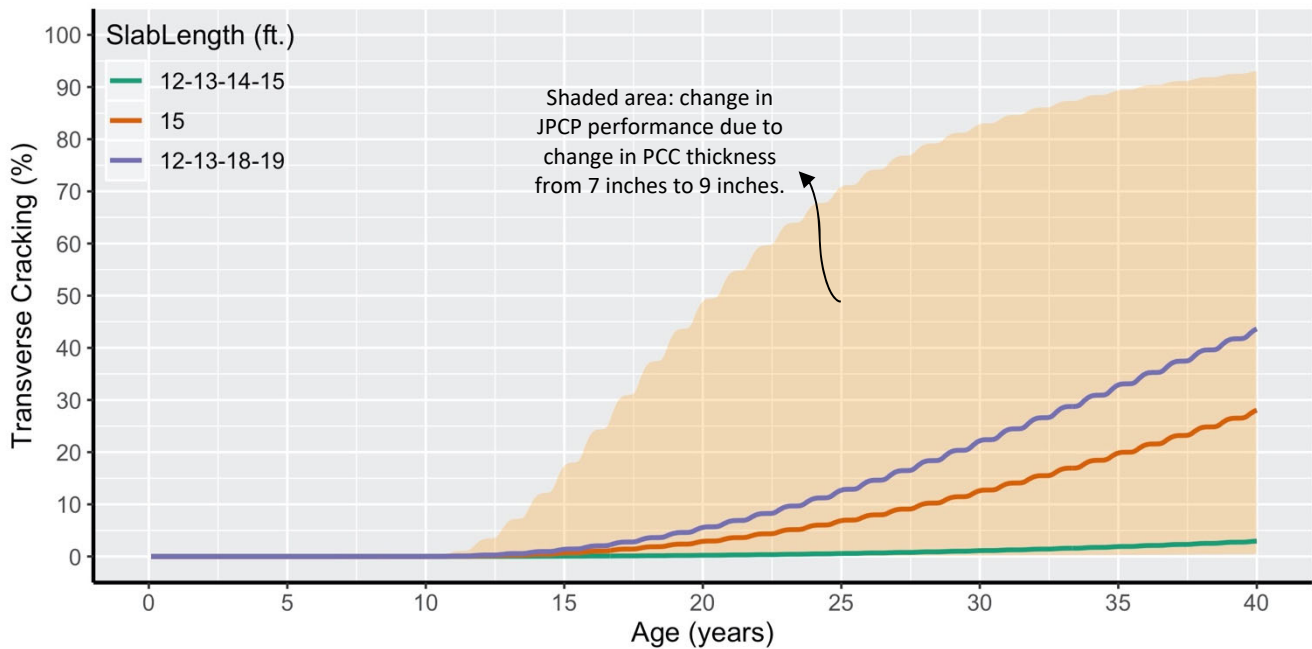
The MEPDG (1) states that transverse joint spacing affects transverse cracking, and to a lesser degree it also affects joint faulting. The MEPDG also states that field studies have shown that JPCPs with longer transverse joint spacing tend to be more susceptible to transverse cracking, and that therefore transverse joint spacing should be chosen within the context of JPCP design features such as PCC slab thickness, PCC slab width, PCC material properties, base type, and shoulder type.

Three different PCC slab length sets, 15 ft., (12,13,14,15 ft.), and (12,13,18,19 ft.) are considered in this study. These slab lengths are (or were) the ones most commonly constructed in California, and designers who are adding or reconstructing lanes must either match the joint spacing in the adjacent lane or place an isolation joint between lanes if they are using joint spacings in the new lanes that do not match those in the existing lanes. The current version of Pavement ME cannot model random slab length. When the option “random joint spacing” is selected

in the software, the mean slab length is used in cracking and faulting calculations; something similar applies to IRI. Consequently, the three slab length sets are modeled by Pavement ME as single slab lengths of 15, 13.5, and 15.5 ft. respectively.

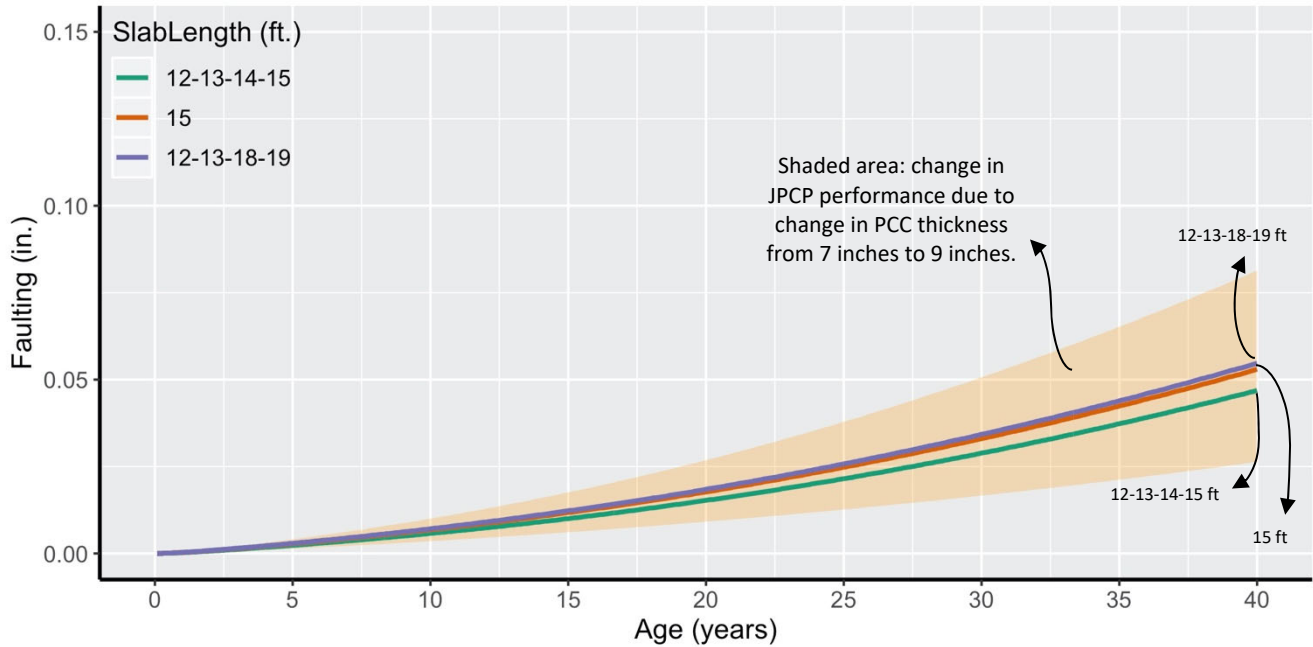
Figure 4.5 shows the effect of transverse joint spacing on JPCP transverse cracking performance. This figure shows that longer PCC slabs have more transverse cracking than shorter ones. These results indicate that a 1-inch slab thickness change from 8 to 9 inches increases the percentage of transverse cracking as much as a change from a joint length set of (12,13,14,15 ft.) to one with only 15 ft. joint spacing.

Figure 4.6 shows the effect of transverse joint spacing on JPCP faulting. As stated in the Pavement ME documentation, slab length is not a major factor affecting JPCP faulting. In this figure, it can be seen that over a 40-year service life, the difference in faulting is insignificant for different PCC slab lengths. The effect of transverse joint spacing is more important for IRI (Figure 4.7) than for faulting because the Pavement ME IRI model considers transverse cracking, which is sensitive to slab length.



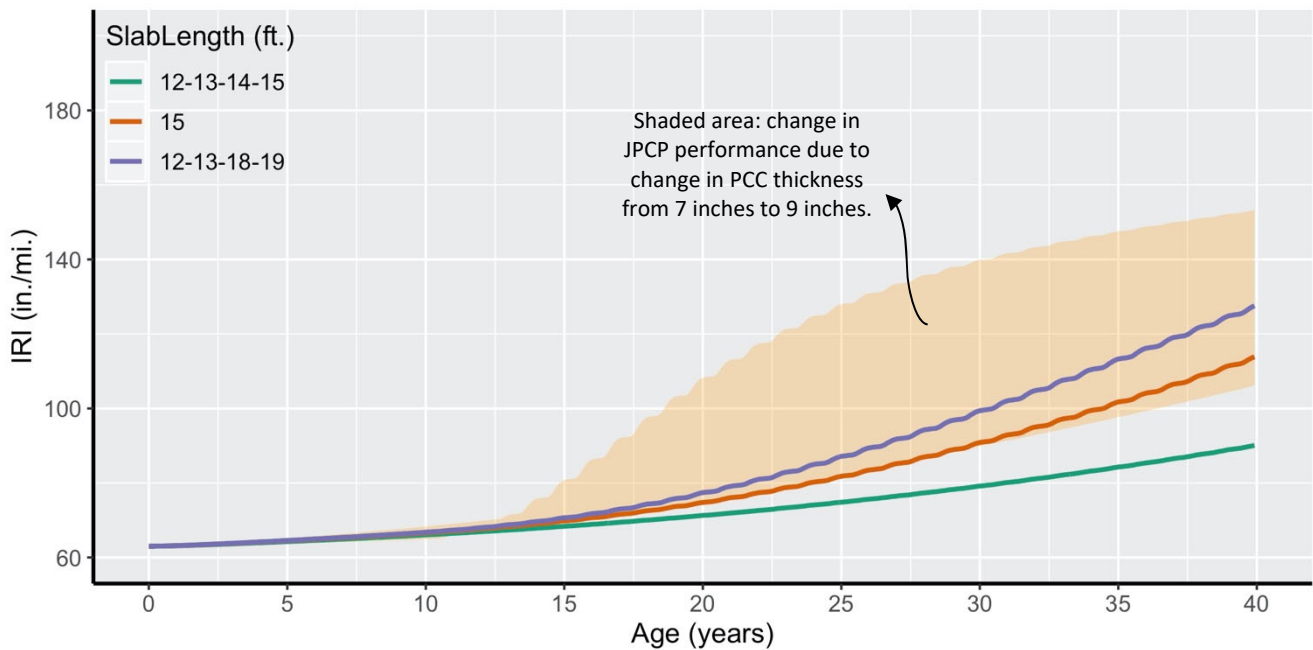
Note: Pavement ME models random joint spacing by using the average slab length: 13.5 ft for (12,13,14,15) ft and 15.5 ft for (12,13,18,19).

Figure 4.5: Effects of PCC slab length on transverse cracking with 50% reliability.



Note: Pavement ME models random joint spacing by using the average slab length: 13.5 ft for (12,13,14,15) and 15.5 ft for (12,13,18,19).

Figure 4.6: Effects of PCC slab length on faulting with 50% reliability.



Note: Pavement ME models random joint spacing by using the average slab length 13.5 ft for (12,13,14,15) and 15.5 ft for (12,13,18,19).

Figure 4.7: Effects of PCC slab length on IRI with 50% reliability.

4.2.3 Load Transfer

According to the Pavement ME documentation, load transfer across transverse joints is the most critical factor controlling JPCP joint faulting and, subsequently, smoothness. The documentation also states that load transfer affects JPCP top-down cracking, and that field studies have shown that use of mechanical devices (dowels) greatly decreases the potential for transverse joint faulting, with the dowel diameter being an important factor affecting JPCP faulting. Small-diameter dowels (1 inch or less) are relatively ineffective in preventing joint faulting, but large-diameter dowels (e.g., 1.5 inch) are highly effective. This size difference matters because the larger the dowel embedded in the concrete, the more it will spread and, therefore, reduce the compressive stresses on the concrete around it. The lower those stresses are, the better the concrete can maintain a tight fit around the dowel—and for a longer time.

Figure 4.8 shows the effect of using dowels on JPCP transverse cracking. This figure shows that the Pavement ME transverse cracking model is unaffected by the use of dowels. However, as expected, Figure 4.9 and Figure 4.10 show the significant effect dowels have on the faulting and smoothness performance of JPCP. These figures show that undoweled JPCP will fail the faulting and smoothness criteria within almost the first five years of service life. Therefore, constructing doweled JPCP is an essential practice for having a long-lasting smooth pavement for heavier traffic.

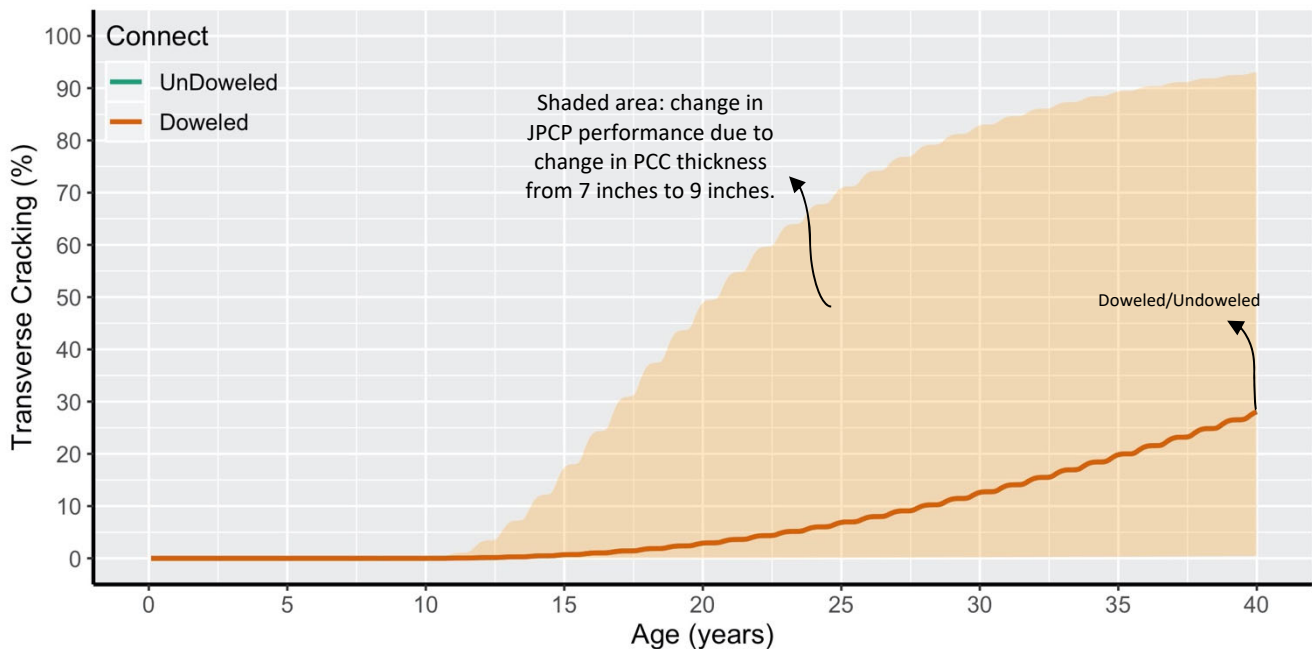


Figure 4.8: Effects of load transfer on transverse cracking with 50% reliability.

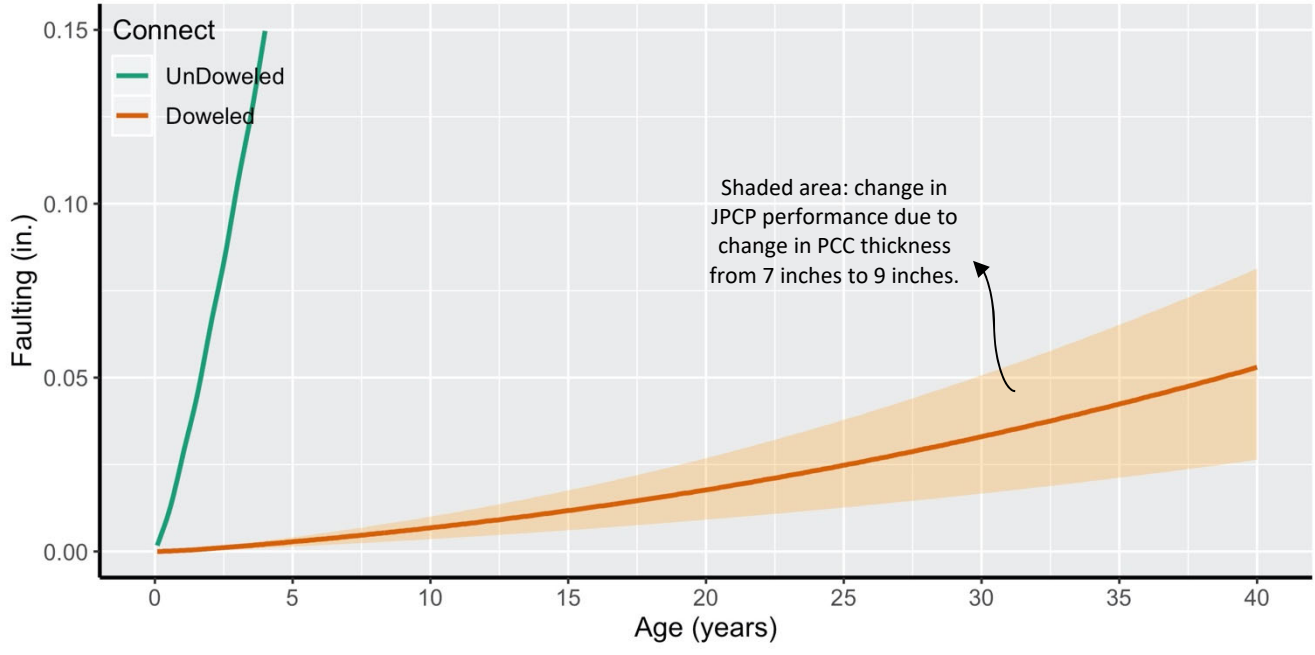


Figure 4.9: Effects of load transfer on faulting with 50% reliability.

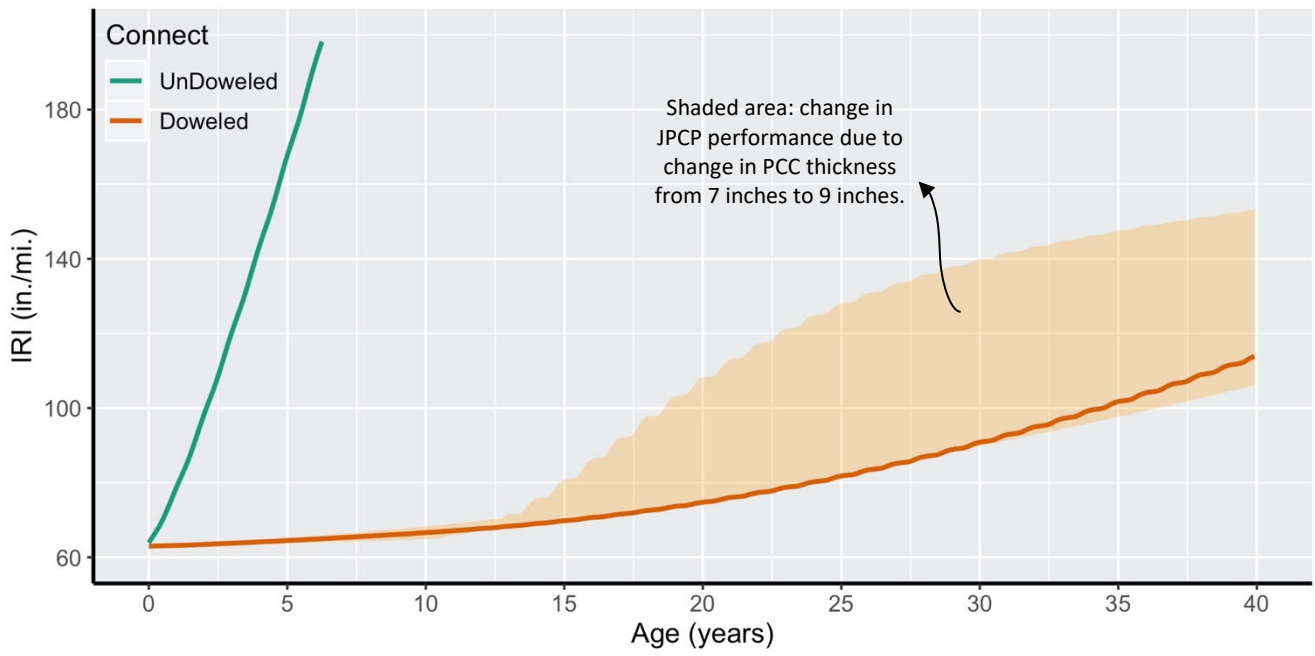


Figure 4.10: Effects of load transfer on IRI with 50% reliability.

4.2.4 Friction Loss Duration

Base friction is an important property affecting the formation and distribution of JPCP transverse cracking. Based on the Pavement ME documentation, the interface between a stabilized base and a PCC slab can be modeled only as being either completely bonded or completely unbonded for JPCP design. The documentation also notes that the structural contribution of a stabilized base is significant if the base is fully bonded to the slab, and much less significant if there is no bonding, with the extent of the contribution depending on the relative thicknesses of the stabilized base and PCC. Even if it is bonded, a very thin stabilized base will not contribute much to structural capacity because it will not substantially shift the neutral axis in the PCC slab downward and reduce the tensile stress in the PCC. Full bonding is stated to be the typical condition, especially for asphalt-stabilized bases, based on an analysis of deflection testing results conducted at slab interiors. The documentation also notes that over time the effects of environmental and traffic loading tend to weaken this bond around the edges. The assumption of full bonding over the entire design period is therefore often un-conservative compared to the actual condition over the full design period.

If the initial condition is bonded, both the starting condition (bonded or unbonded) and the pavement age (month) when the debonding will occur can be input. The slab-base interface is assumed to be fully bonded up to the age when debonding occurs; after the debonding age, the interface is assumed to be fully unbonded. In this study, three different durations of loss of bonding (referred to by the software as *friction*) were considered: no base friction (0-month base friction), 120-month base friction, and 240-month base friction. It should be noted that all these cases shown are on an HMA base, and the results may change for a different kind of base type.

Figure 4.11 shows the effect of friction loss duration on transverse cracking for a pavement with an HMA base type. In the plot, it can be seen that the pavement shows no signs of transverse cracking before the friction loss period. Once the pavement age has passed that point, it starts showing signs of deterioration and transverse cracking. Therefore, the longer that full bonding is modeled between the PCC slab and the base, the less transverse cracking that the model will predict in the pavement during its service life.

Figure 4.12 shows that friction loss duration has no effect on JPCP faulting and that no matter what value is chosen for this variable, the pavement will have the same faulting performance during its service life. As shown in Figure 4.13, this is not the case for IRI, as IRI depends on both faulting and transverse cracking and, as a result, the longer the time to debonding, the less transverse cracking, and hence, less IRI.



Figure 4.11: Effects of friction loss duration on transverse cracking with 50% reliability.

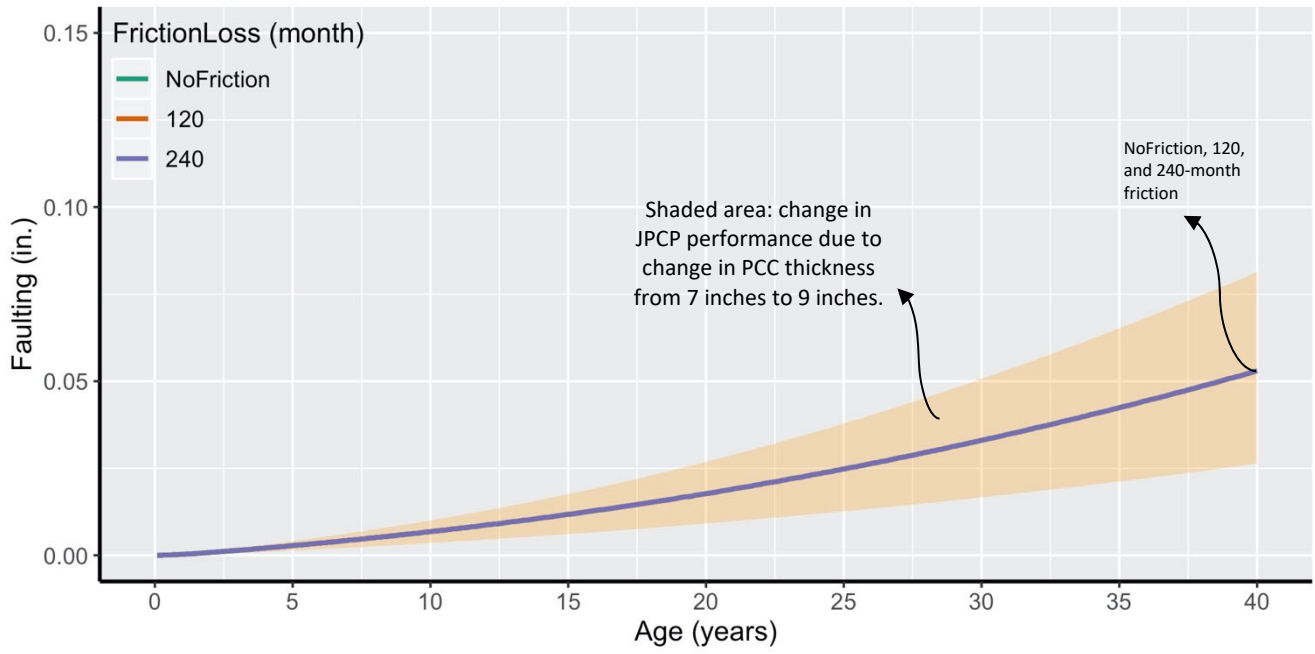


Figure 4.12: Effects of friction loss duration on faulting with 50% reliability.

(Note: the figure has three nearly identical lines that are hard to distinguish—one each for NoFriction, 120, and 240-month friction.)

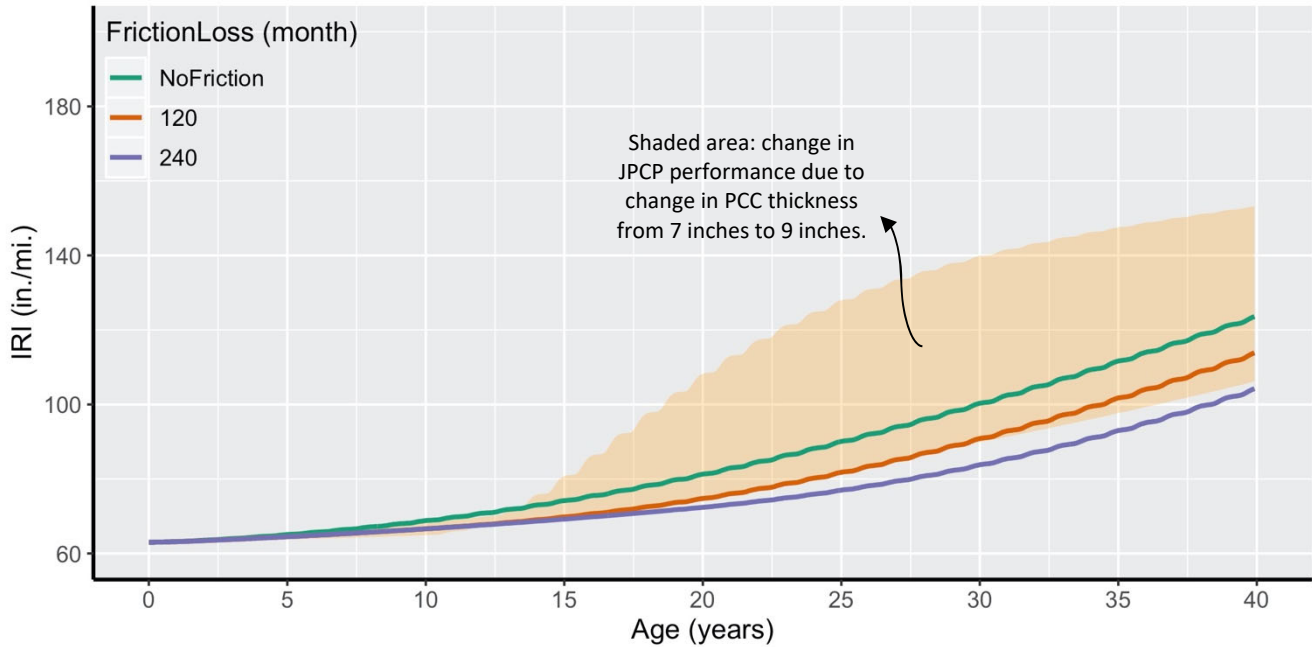


Figure 4.13: Effects of friction loss duration on IRI with 50% reliability.

4.2.5 Base Type

According to the Pavement ME documentation, base type has been shown to affect joint faulting, smoothness, and slab cracking. A stiff stabilized base's structural contribution can be very significant if the base is bonded to the slab. However, the main purpose of providing a base course in JPCP is to provide uniform support and erosion resistance, which are critical for avoiding localized failures and faulting. The documentation states that for structural capacity, there are several other design factors (e.g., slab thickness, PCC strength, and edge support) that have a more direct and far greater impact than a stabilized base. In this study four different base types were considered: aggregate base (AB), cement-treated base (CTB), lean concrete base (LCB), and hot mix asphalt (HMA). The erodibility index was kept constant for the different base types since the erodibility index effects are specifically evaluated in Section 3.2.8.

Figure 4.14 shows the effects of these base types on JPCP transverse cracking. It should be noted that the bonding period (friction loss) for AB is zero months, as AB does not bond with the PCC slabs, and therefore the transverse cracking predicted in the pavement starts at the initial stage of service life. On the other hand, HMA, CTB, and LCB start to show transverse cracking after 12 years (*120-month friction loss* is the defined value for friction loss in the model). Eventually, as expected, the HMA base shows the best transverse cracking performance of the four base types, a result that aligns with the pavement condition survey data from California's state highway network.

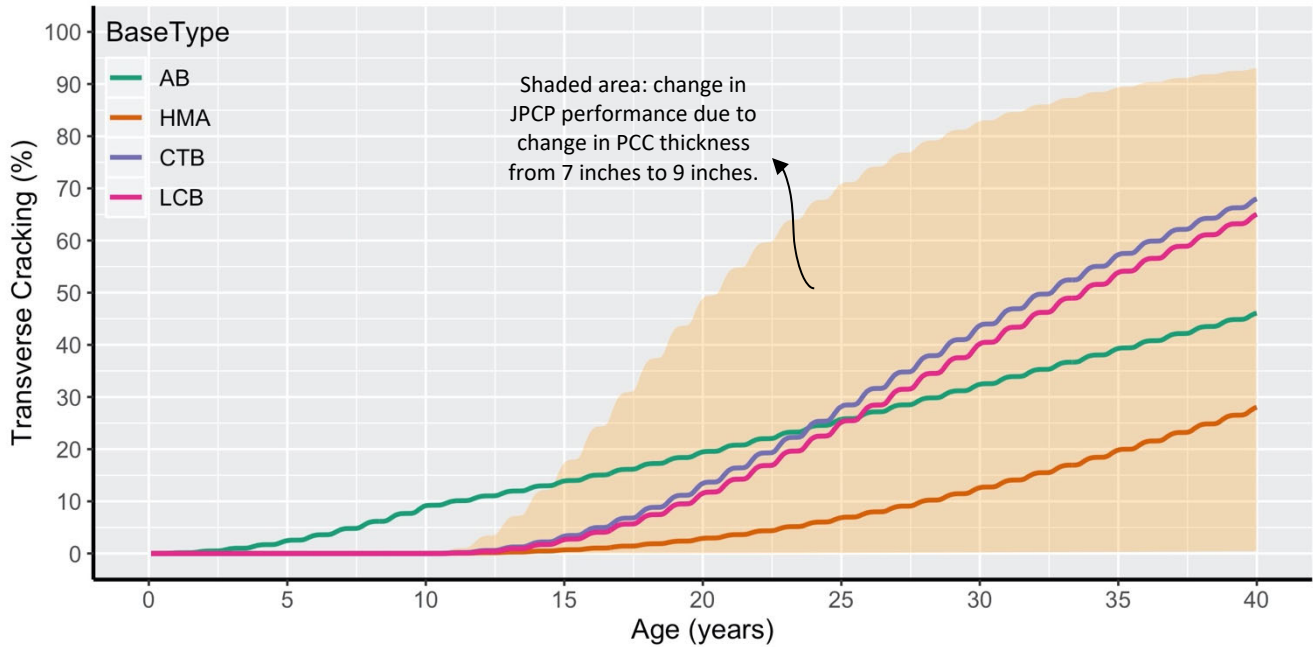


Figure 4.14: Effects of base type on transverse cracking with 50% reliability.

Figure 4.15 shows that base type did not affect faulting performance as much as it affected transverse cracking performance. This figure shows that CTB and LCB have the best faulting performance, as they provide stiffer support compared to other alternatives. The differences between the different base types would have been larger if the erodibility index had been adjusted for each material. LCB and HMA can provide an erodibility index of 1 (extremely erosion resistant) and HMA can provide an index value of 2 (very erosion resistant), while an erodibility index of 4 (fairly erodible) can be expected from a crushed aggregate base. Figure 4.16 shows that HMA provided the best smoothness performance among the base types studied in this report because it had less transverse cracking than the others.

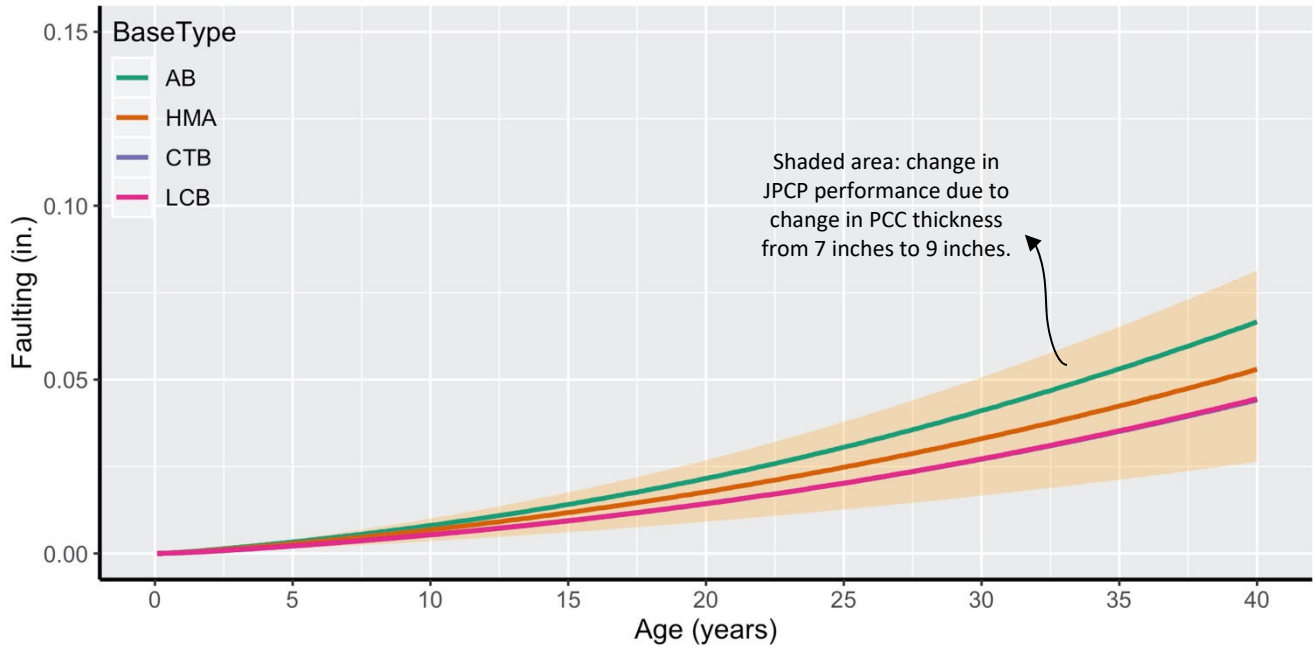


Figure 4.15: Effects of base type on faulting with 50% reliability.

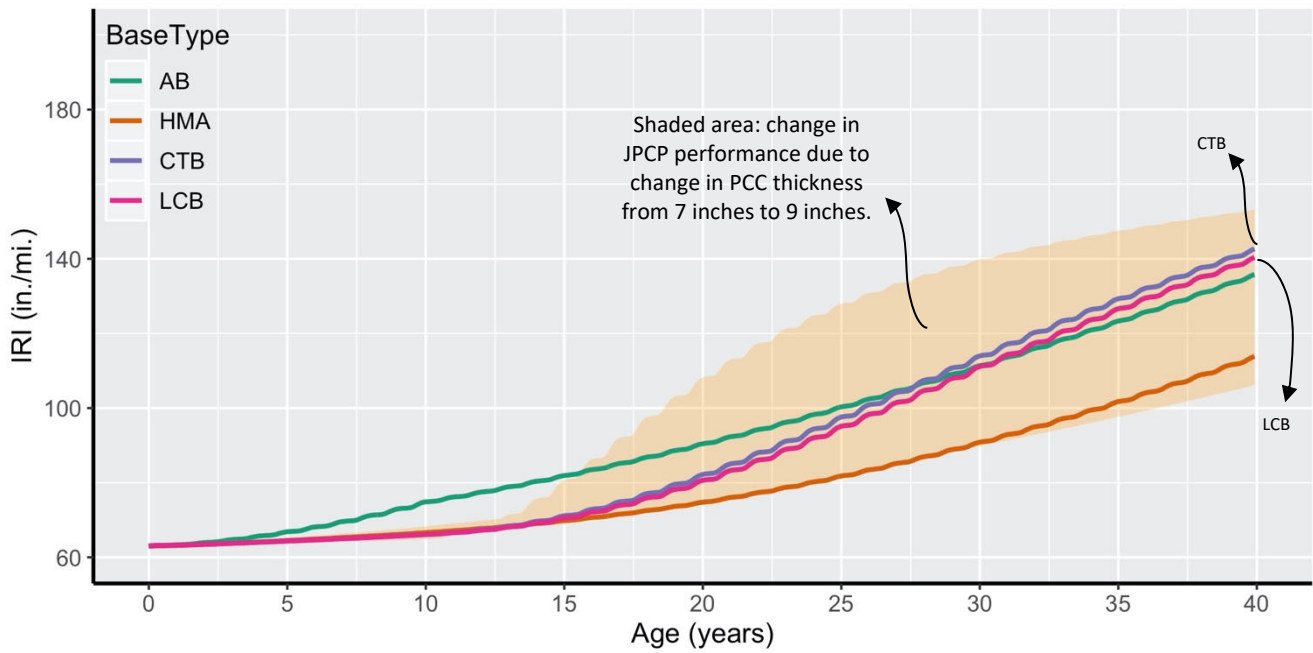


Figure 4.16: Effects of base type on IRI with 50% reliability.

4.2.6 Shoulder Type (Edge Support)

According to the Pavement ME documentation, tied PCC shoulders and widened slabs can significantly improve JPCP performance by reducing critical deflections and stresses along the edge. Shoulder type also affects the amount of moisture infiltrating the pavement structure. The effects of moisture infiltration are considered in determining the unbound layers' seasonal moduli values. In this analysis, three shoulder types (edge supports) are considered: not-tied, tied, and widened. Not-tied JPCP, where there is an asphalt or gravel shoulder, does not support any load transfer between the PCC slabs and shoulder.

When a tied PCC shoulder is built, the PCC slabs are tied to the concrete shoulders. In models for these types of shoulders, the long-term load transfer efficiency (LTE) between the lane and the shoulder is an input value, which in this study was assumed to be the default value of 50 percent. *LTE* is defined as the ratio of deflections of the unloaded and loaded slabs. The higher the LTE, the greater the support provided by the shoulder to reduce critical responses of the mainline slabs.

Widened slabs improve JPCP performance by effectively moving the mean wheelpath away from the pavement edges where the critical loadings occur, and thereby reduce the risk of transverse cracking. The design input for widened slab is *slab width*, which can range from 12 to 14 ft. This study assumed the default value of 14 ft.

Figure 4.17 shows the effectiveness of edge support (shoulder type) on the JPCP's transverse cracking performance. As stated earlier, and as shown in the figure, the widened slabs and tied-shoulder slab types have better performance than the not-tied shoulder type. Similar trends can be observed in Figure 4.18 and Figure 4.19 for faulting and IRI, respectively.

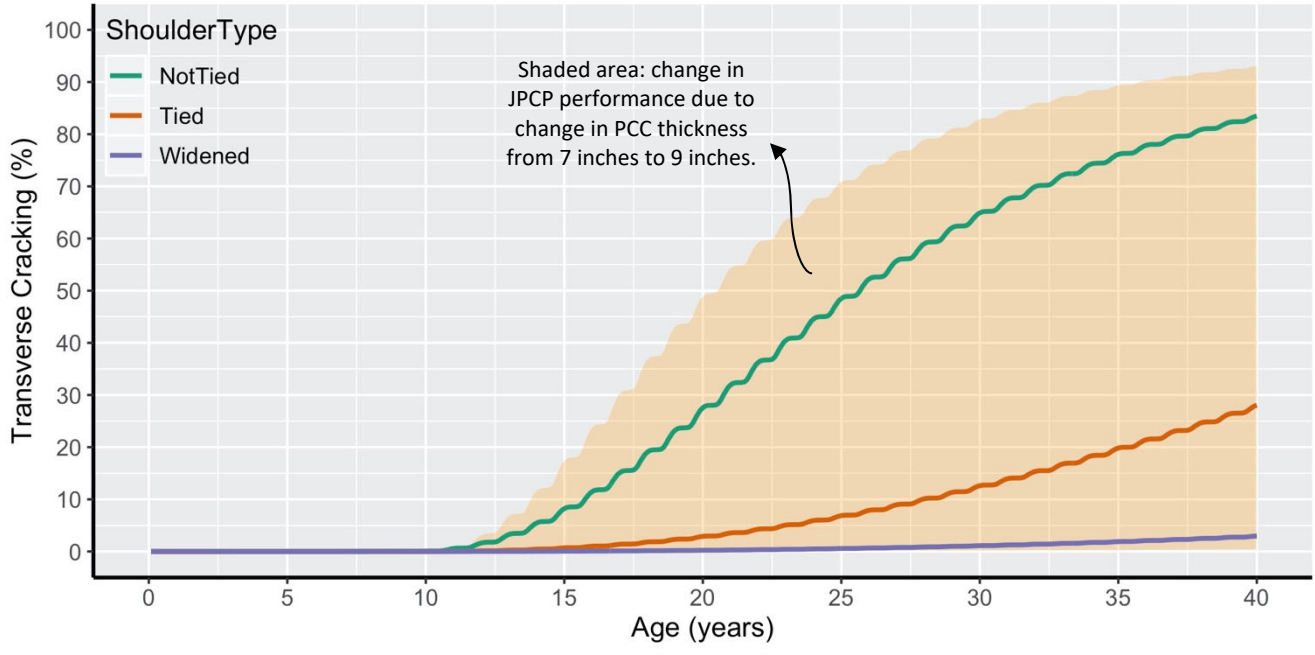


Figure 4.17: Effects of shoulder type on transverse cracking with 50% reliability.

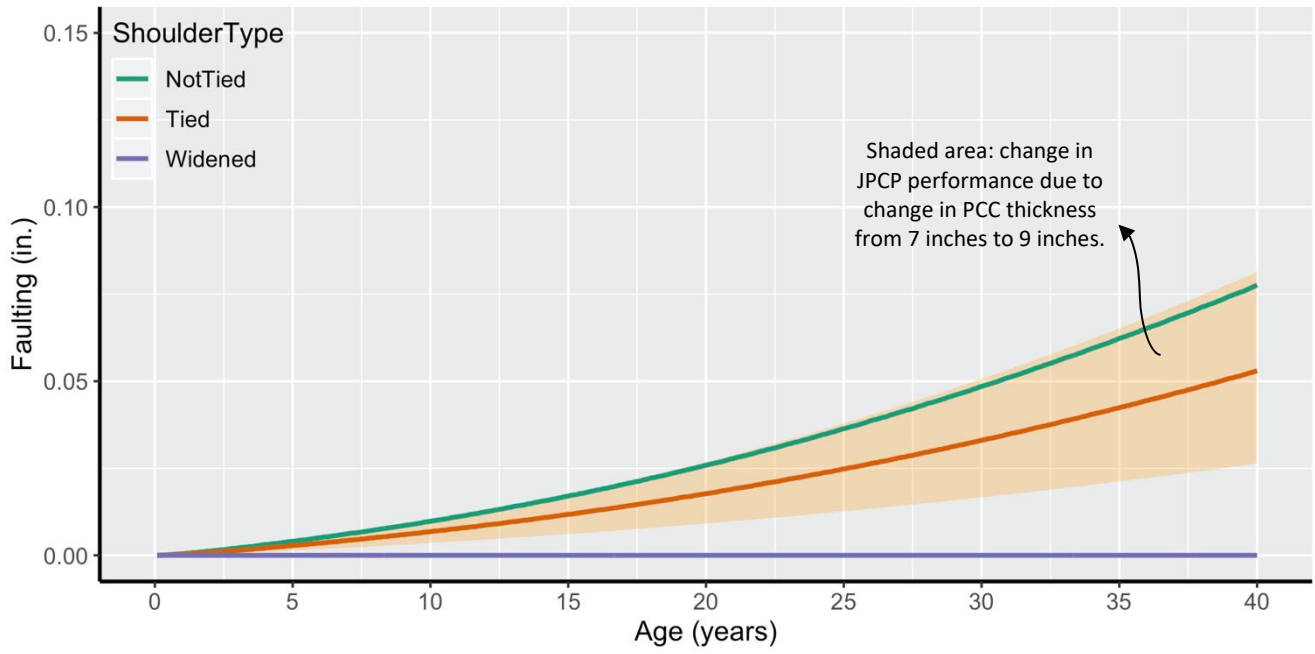


Figure 4.18: Effects of shoulder type on faulting with 50% reliability.

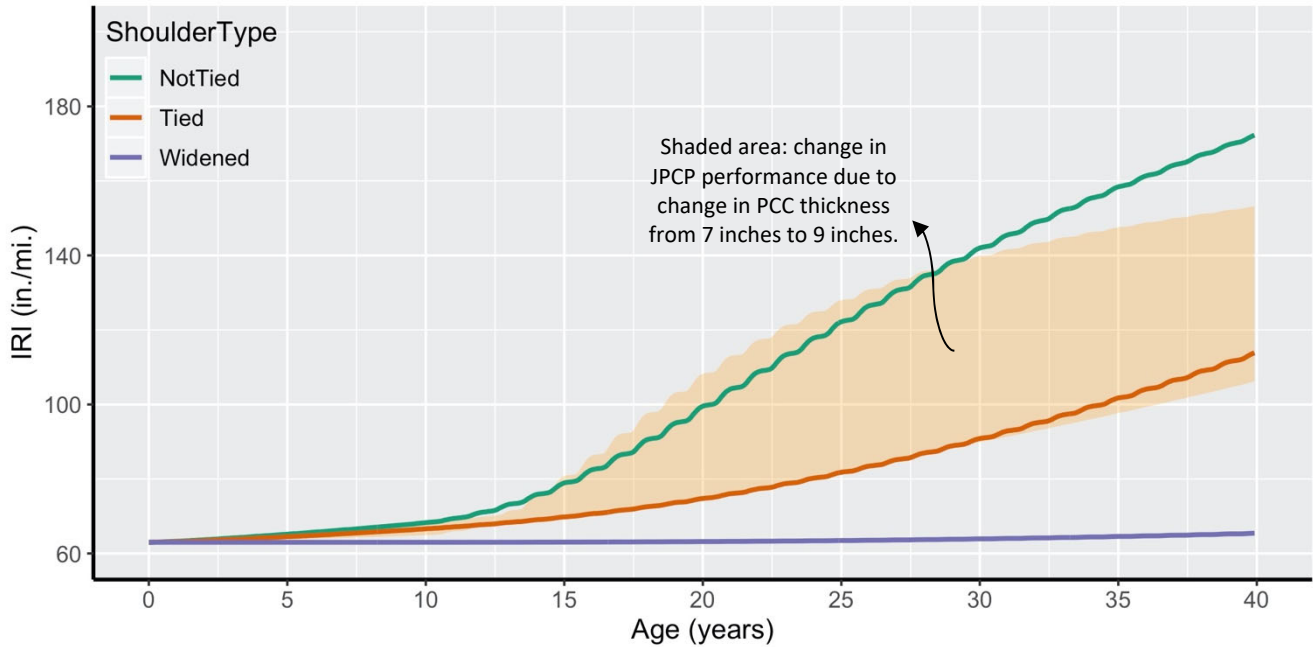


Figure 4.19: Effects of shoulder type on IRI with 50% reliability.

4.2.7 Subgrade Type

In Pavement ME, subgrade and unbound pavement layers are characterized using their resilient moduli. For rigid pavement design, the subgrade k-value needed for the structural analysis is obtained through a conversion process that transforms the actual pavement structure into an equivalent structure that consists of a PCC slab, base, and an “effective dynamic k-value” for all the layers underneath the base. The effective dynamic k-value represents the compressibility of all the layers beneath the PCC slab and base course. The effective dynamic k-value of the subgrade is calculated for each month of the year and utilized directly to compute critical stresses and deflections in the incremental damage accumulation over the design life of the pavement. Factors such as water table depth, depth to bedrock, and frost penetration depth (frozen material) can significantly affect the effective dynamic k-value.

In this study, three types of subgrade were considered: clay (A-5), gravel and sand (A-1a), and sand (A-3). Figure 4.20 shows the effects of subgrade on the transverse cracking of JPCP. It can be seen that the gravel and sand, and the sand subgrades had nearly identical performance, and the clay subgrade performed the best. However, Figure 4.21 and Figure 4.22 show that the clay subgrade had higher values for both faulting and IRI.

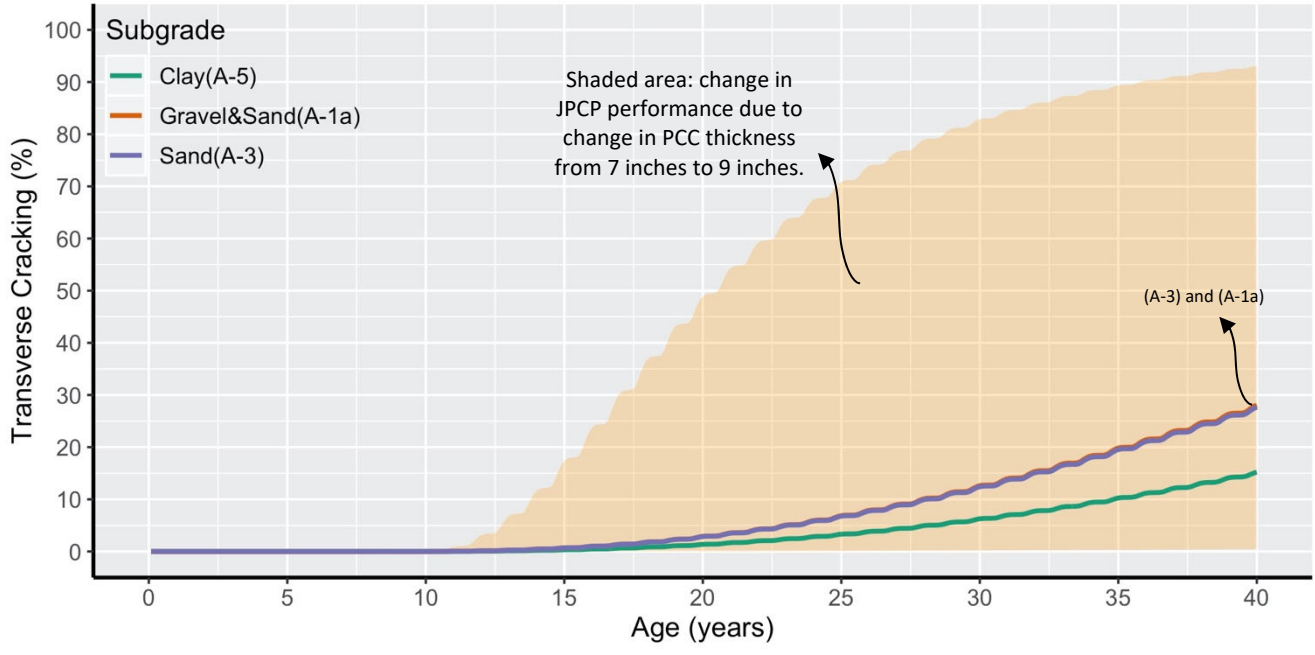


Figure 4.20: Effects of subgrade type on transverse cracking with 50% reliability.
 (Note: the figure has two lines that are nearly identical, one for A-3 and one for A-1a.)

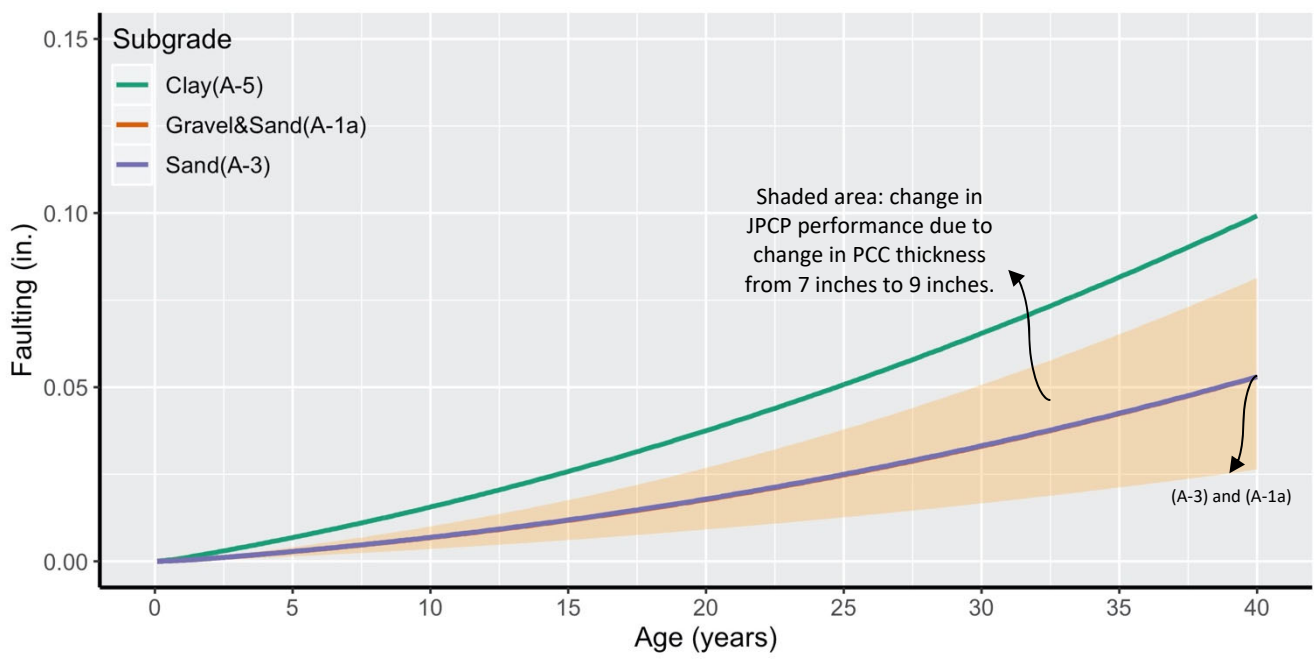


Figure 4.21: Effects of subgrade type on faulting with 50% reliability.

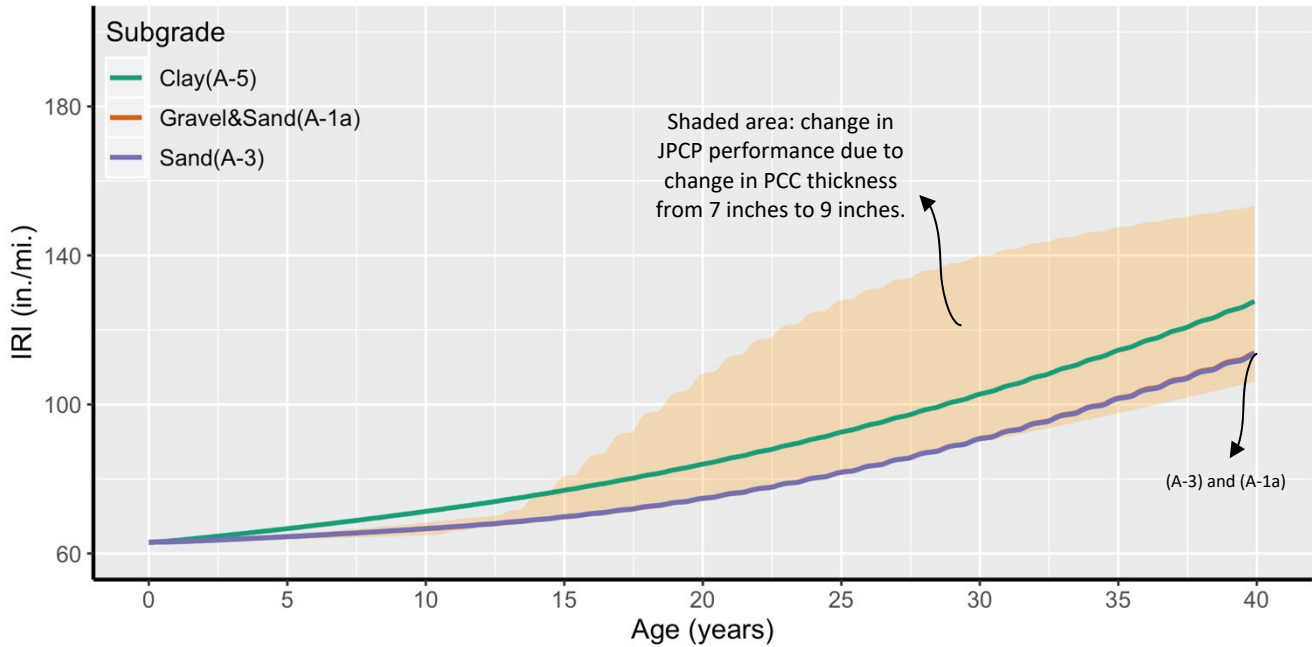


Figure 4.22: Effects of subgrade type on IRI with 50% reliability.
 (Note: the figure has two lines that are nearly identical, one for A-3 and one for A-1a.)

4.2.8 Erodibility Index

According to the Pavement ME documentation, the erosion potential of the base or subbase (the layer directly beneath the PCC layer) has a significant impact on the initiation and propagation of pavement distress. Different base types are classified based on long-term erodibility behavior as follows:

- Class 1: Extremely erosion-resistant materials
- Class 2: Very erosion-resistant materials
- Class 3: Erosion-resistant materials
- Class 4: Fairly erodible materials
- Class 5: Very erodible materials

In this study, Classes 1, 2, and 4 were considered. Class 1 is applicable to cement-treated base (CTB) and hot mix asphalt (HMA), Class 2 to CTB, and Class 4 to aggregate base (AB). Figure 4.23 shows that the erodibility index has no effect on transverse cracking performance, as expected. As was also expected, Figure 4.24 and Figure 4.25 show that the base with more erodible material will cause more faulting in JPCP and, consequently, it will result in a rougher pavement.

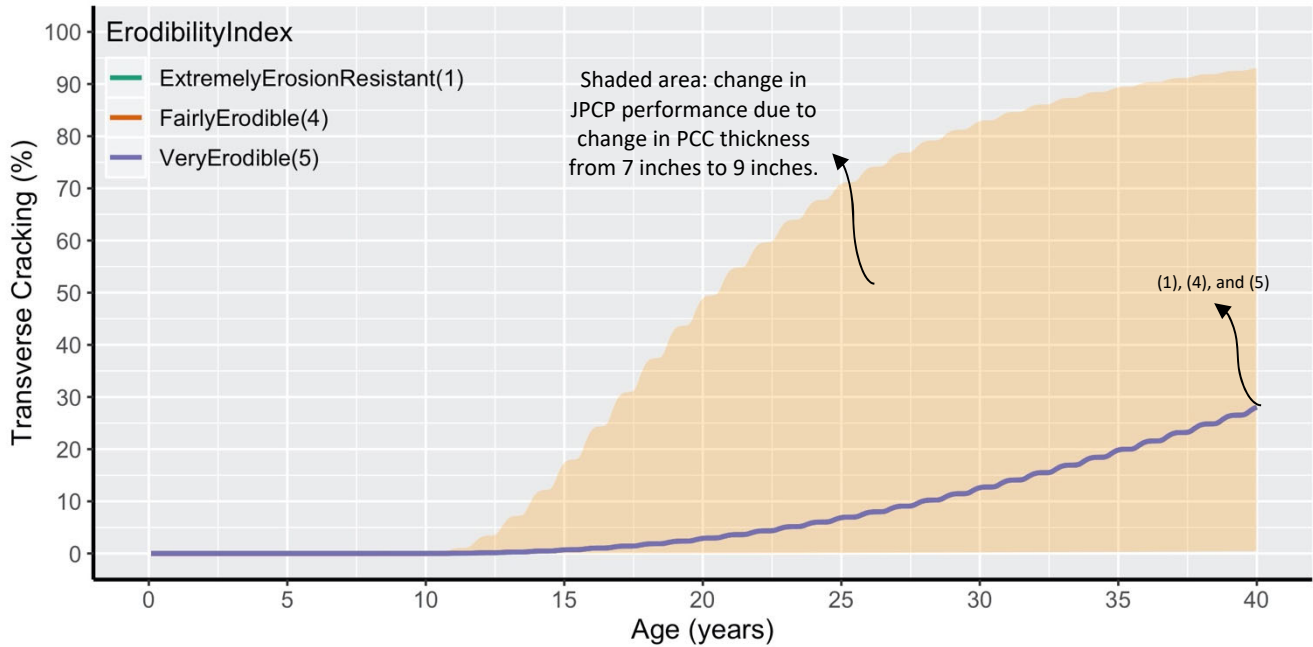


Figure 4.23: Effects of erodibility index on transverse cracking with 50% reliability.
(Note: the figure has three lines, one each for (1), (4), and (5), that are nearly identical and indistinguishable.)

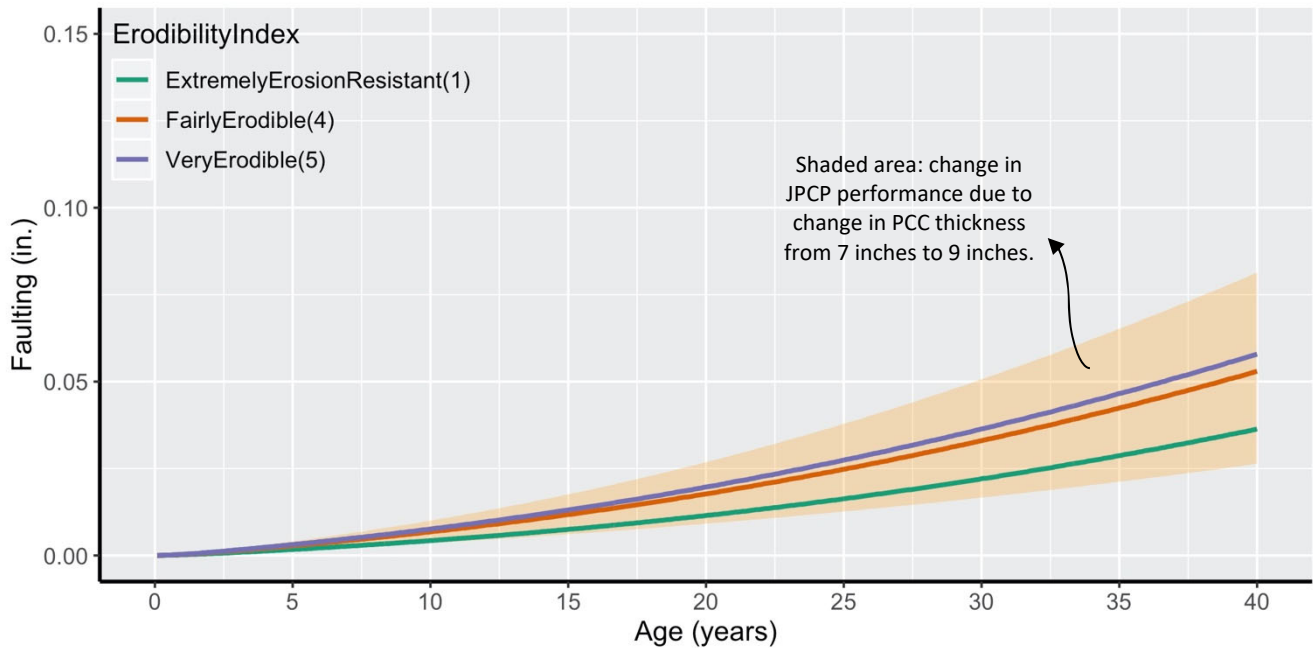


Figure 4.24: Effects of erodibility index on faulting with 50% reliability.

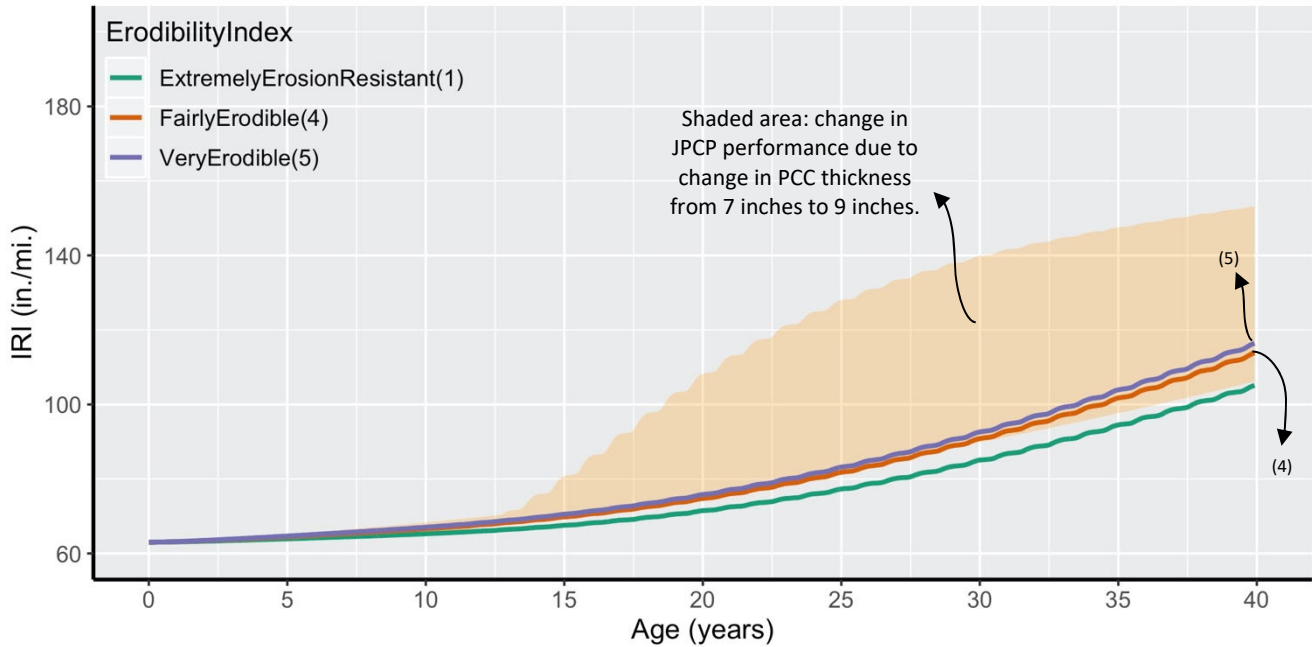


Figure 4.25: Effects of erodibility index on IRI with 50% reliability.

4.3 Pavement Material Inputs

Pavement material inputs are the variables generally unknown to a designer at the design stage and are not readily available for most of the JPCP projects constructed in California. This makes calibrating Pavement ME against the Caltrans PMS data a challenge. However, over the past few years, the UCPRC has obtained some material input data by sampling from various research projects with JPCP construction sites. Data from these projects can be used to understand the distribution of pavement material variables and their within-project and between-project variabilities to calibrate Pavement ME more efficiently. The material inputs data collected were PCC compressive strength, PCC modulus of elasticity, PCC coefficient of thermal expansion (CTE), PCC surface absorptivity, and PCC density.

Five data sources were used to set up the material input database.

- *Ground penetrating radar (GPR) data.* The objective of an earlier UCPRC GPR study was to create a lane-based pavement structure inventory database consisting of layer thickness and material types for the entire state highway network. The data collected as part of this project were used to establish fixed management sections for network-level and project-level PMS operations. As part of this project, some Blind Verification Sections (BVS) were established to provide additional quality assurance, and a large number of cores were taken that were later tested for CTE. In this current report, PCC CTE was the project-specific variable obtained from this GPR study.

- *Previous MEPDG calibration data.* These data were obtained from cores taken from different pavement sections across the California as part of an earlier UCPRC MEPDG calibration project (3).
- *Alkali-silica reaction (ASR) data.* The objective of an earlier UCPRC ASR project was to look for the presence of alkali-silica reaction in California's pavements and bridges by evaluating the core samples taken from the pavement sections across the state (7).
- *Stantec data.* These data were obtained by drilling core specimens to study the influence CTE on JPCP cracking (8).
- *Caltrans CTE database.* After the 2006 sensitivity analysis that showed a very high sensitivity of transverse cracking in the MEPDG models to CTE, Caltrans required contractors to test and report CTE for several years. This database has the CTE test results taken from the JPC pavements while under construction during that period.

Further discussion on pavement material inputs is provided in the appendix at the end of this report.

4.3.1 PCC Compressive Strength

The compressive strength of PCC materials can be used to estimate the elastic modulus, flexural strength, and indirect tensile strength if no directly measured information for these properties are available as inputs. In Pavement ME, the processed inputs for PCC strength and modulus properties are the monthly strength and modulus values for the entire design period. According to the Pavement ME documentation, an increase in PCC compressive strength, which is used to model commensurate increases in flexural strength, leads to lower fatigue damage; however, since the PCC modulus of elasticity also increases with increased compressive strength, the bending stress due to shrinkage and thermal gradients will also increase. Thus, the reduction in fatigue damage is not as dramatic as might be expected when PCC strength (flexural strength estimated from compressive strength) is increased. In addition, a higher-strength PCC obtained through increased cement content may result in greater shrinkage of the hardened mixture, although this is not modeled in Pavement ME. If this higher shrinkage occurs, it will lead to greater warping, which will increase tensile stresses at the top of the slab and, consequently, top-down cracking.

The compressive strengths were measured on cores taken at least several years and often many years after construction. The values were converted from the long-term strengths to equivalent 28-day strengths based on Pavement ME formula, which include the ACI formula that relates flexural (MR) and compressive strength, a default time evolution function for flexural strength, and a default 1.2 ratio between 20-year and 28-day flexural strength. In practice, all flexural strength values were divided by 1.2 in order to estimate the 28-day flexural strength, regardless of concrete age. For any given time, the ratio between MR and 28-day MR is a function of age; thus, applying a 1.2 factor to all projects regardless of age is a simplification. The Pavement ME default time function is logarithmic. It increases very quickly at the beginning and very slowly after a few years (as expressed in actual concrete mechanical properties). For example, for 3-year old concrete, the ratio between MR and 28-day

MR is 1.16, which is very close to 1.2. In other words, the age correction of field specimens can be simplified by applying a 1.2 factor as soon as the project is a few years old. Finally, the 28-day flexural strength values were converted back to compressive strengths using the ACI formula.

A hierarchical input level in the MEPDG input scheme allows a designer to categorize their knowledge of an input parameter into one of three levels, and in this way the catalog can determine the input values for most of the material and traffic parameters. The following defines each hierarchical input level that a designer can use:

- Input Level 1: This input parameter is measured directly; it is site- or project-specific. This level represents the greatest knowledge about the input parameter for a specific project, but the testing and data collection costs for determining this parameter's input value are the highest of the three possible levels. Level 1 should be used for pavement designs that have unusual site features, materials, or traffic conditions that are outside the inference-space used to develop the correlations and defaults included for Input Levels 2 and 3.
- Input Level 2: This input parameter is estimated from correlations or regression equations. The input value is calculated from other site-specific data or parameters that are less costly and/or easier to measure than they are for Level 1. Input Level 2 can also represent measured regional values that are not project specific.
- Input Level 3: This input parameter is based on "best-estimated" or default values. Level 3 inputs are based on global or regional default values—the median value from a group of data with similar characteristics. This input level reflects the least knowledge about the input parameter for the specific project, but it has the lowest testing and data collection costs.

Level 3 was selected for concrete strength/stiffness properties. This means that the only input is the 28-day compressive strength. Then Pavement ME uses the ACI formula to estimate 28-day flexural strength and modulus of elasticity, and a default time evolution function applicable to both flexural strength and modulus of elasticity.

In this study, three different values were considered for PCC compressive strength. These values were chosen based on the PCC compressive strength data distribution shown in the appendix.

Figure 4.26 shows the transverse cracking model's sensitivity to changes in the compressive strength of the PCC slab (and the associated changes in flexural strength and modulus of elasticity). It can be seen that increasing the slab's compressive strength from 4,730 psi to 6,730 psi (32.6 MPa to 46.4 MPa) decreased the transverse cracking from 70 percent to about 8 percent in a 40-year service life.

Figure 4.27 shows that the faulting model is less sensitive to changes in PCC strength (and the associated changes in flexural strength and modulus of elasticity) than the transverse cracking model was. Figure 4.28 shows that increasing the PCC compressive strength decreased the IRI, as less transverse cracking occurred with a stronger PCC.

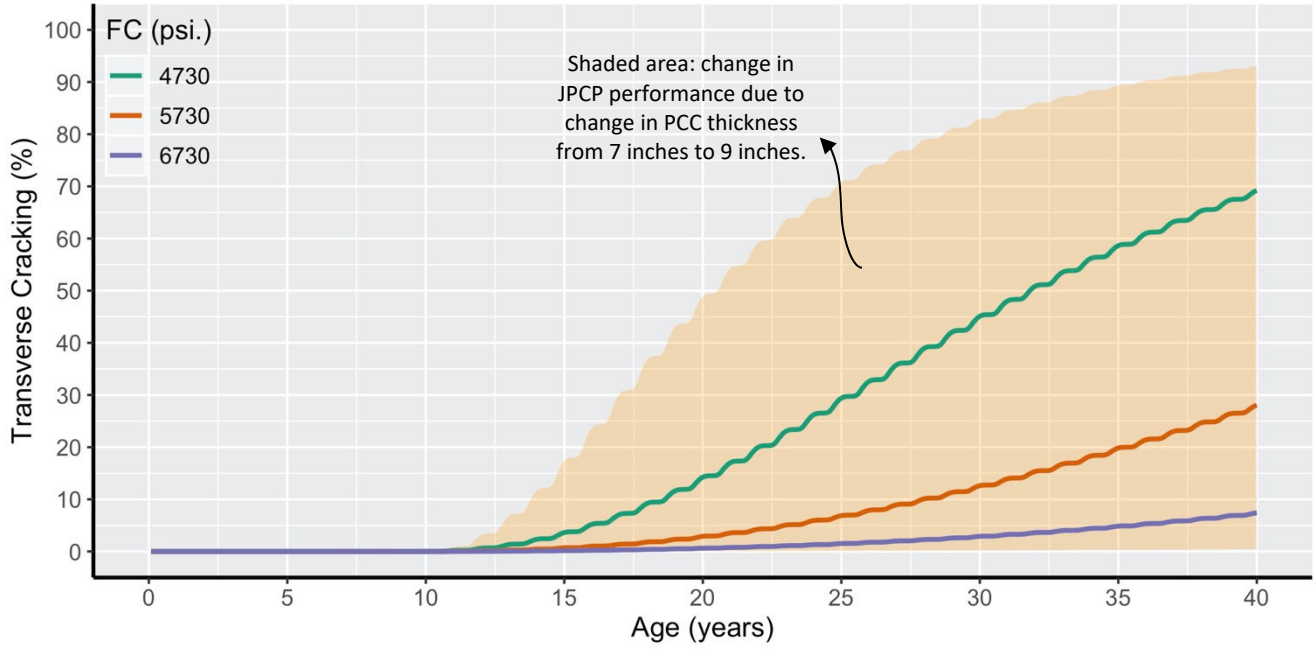


Figure 4.26: Effects of PCC compressive strength and associated assumptions regarding flexural strength and stiffness on transverse cracking with 50% reliability.

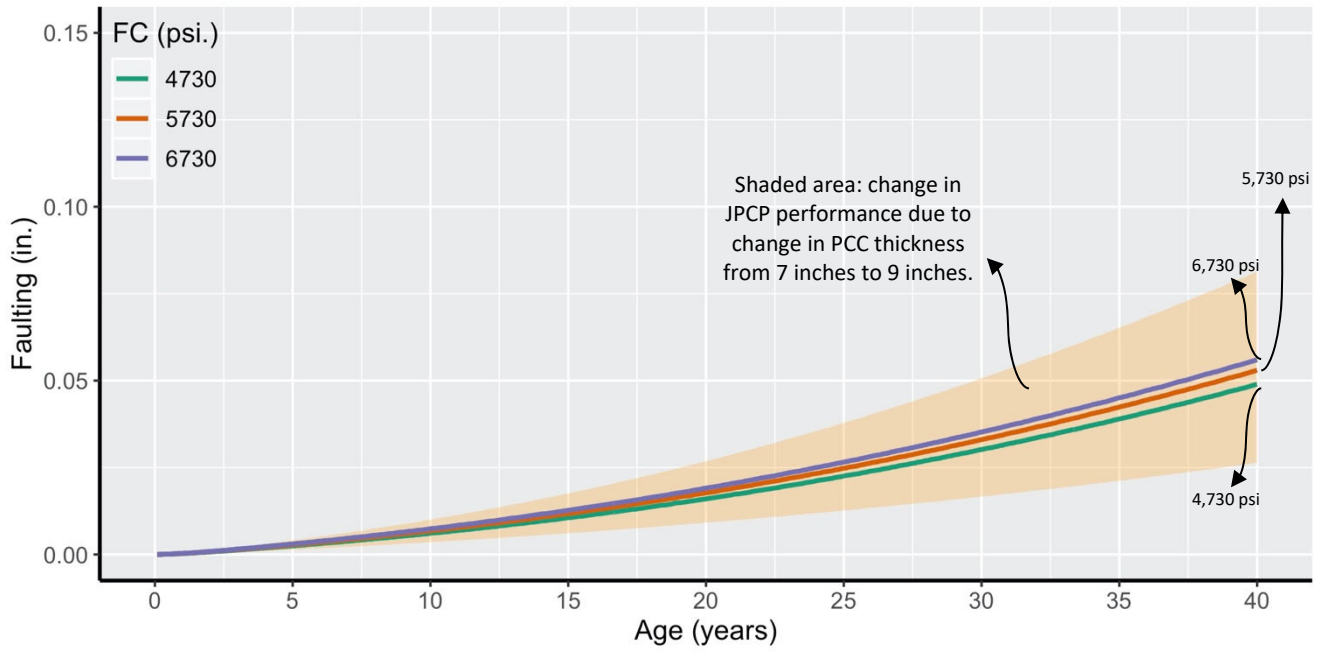


Figure 4.27: Effects of PCC compressive strength and associated assumptions regarding flexural strength and stiffness on faulting with 50% reliability.

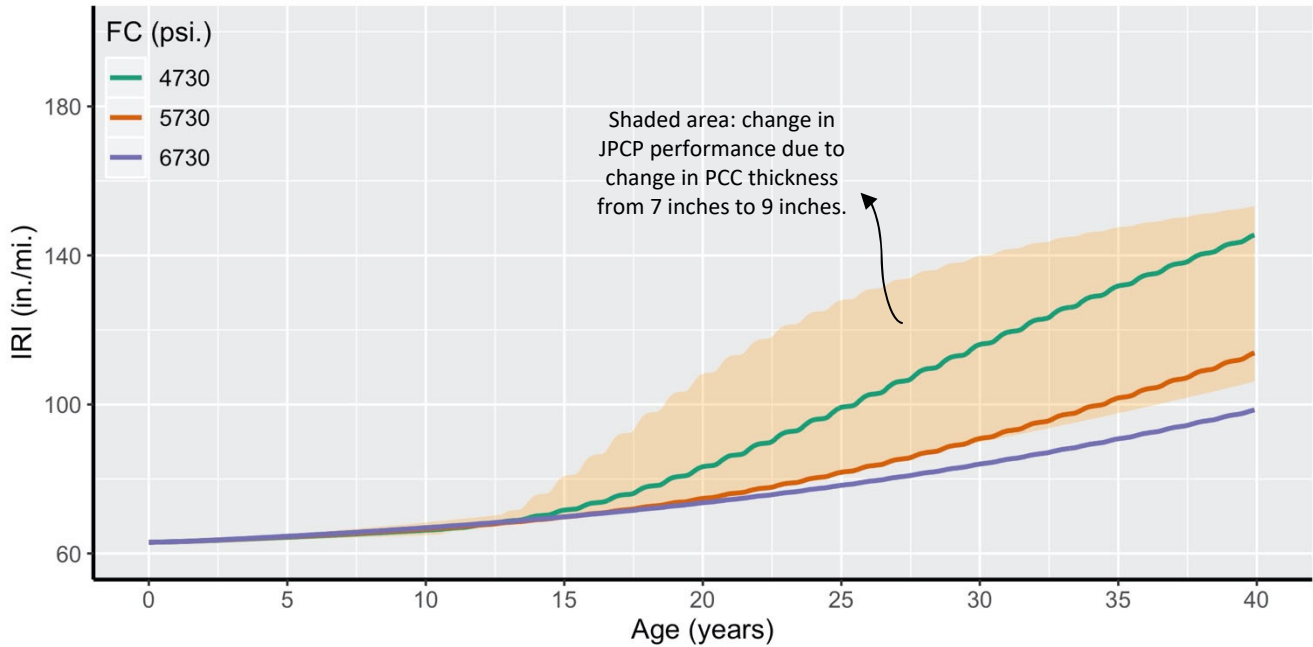


Figure 4.28: Effects of PCC compressive strength and associated assumptions regarding flexural strength, and stiffness on faulting on IRI with 50% reliability.

4.3.2 PCC Coefficient of Thermal Expansion

The coefficient of thermal expansion (CTE) is defined as the change in unit length per degree of temperature change. CTE affects both critical slab stresses and transverse joint openings. The magnitude of calculated curling stress (caused by temperature difference through the slab thickness) is very sensitive to CTE. According to the MEPDG (1), under certain exposure conditions, curling stresses can comprise 50 percent or more of the critical stress experienced by a loaded JPCP slab, which thereby affects transverse cracking significantly.

This study considered three CTE values that were chosen using the CTE data distribution shown in Figure A.17 in the appendix: $5 \text{ microstrain}/^{\circ}\text{F}^{-1}$, which is close to the median value shown in the appendix, and one standard deviation above and below. Figure 4.29 shows the significant effect CTE has on the transverse cracking performance of JPCP. Figure 4.30 and Figure 4.31 also show that increasing CTE in JPCP will cause a significant increase in both faulting and IRI because of greater curling.

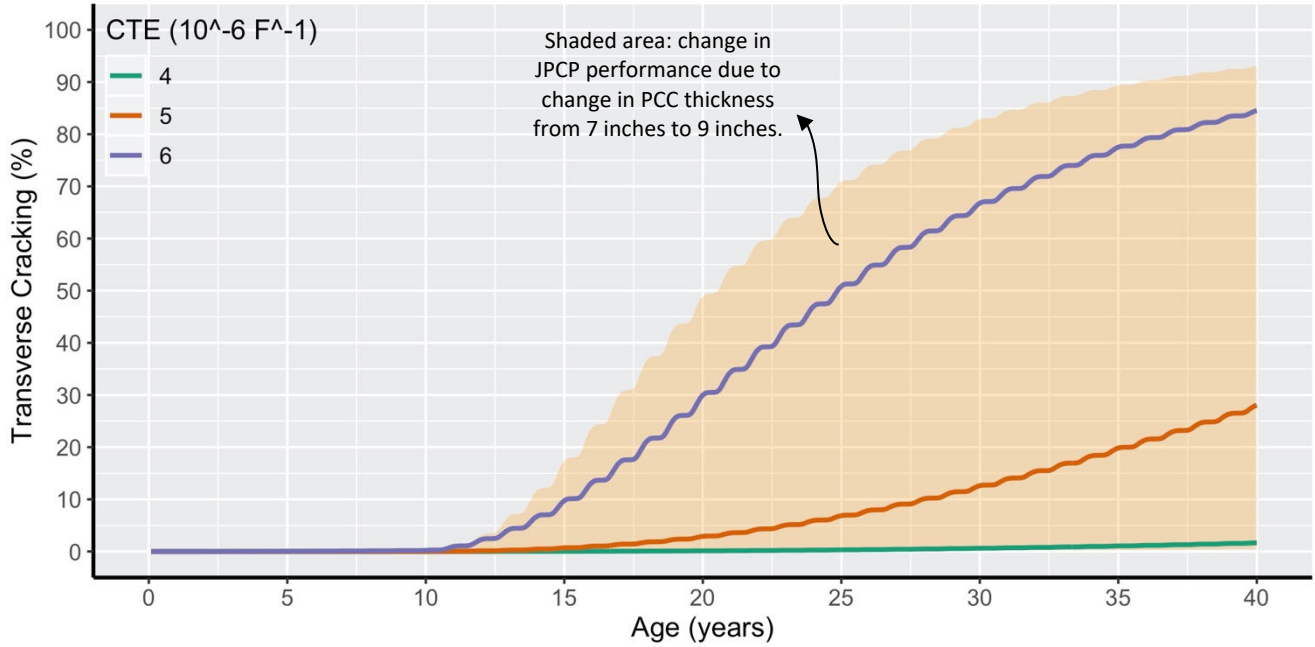


Figure 4.29: Effects of PCC CTE on transverse cracking with 50% reliability.

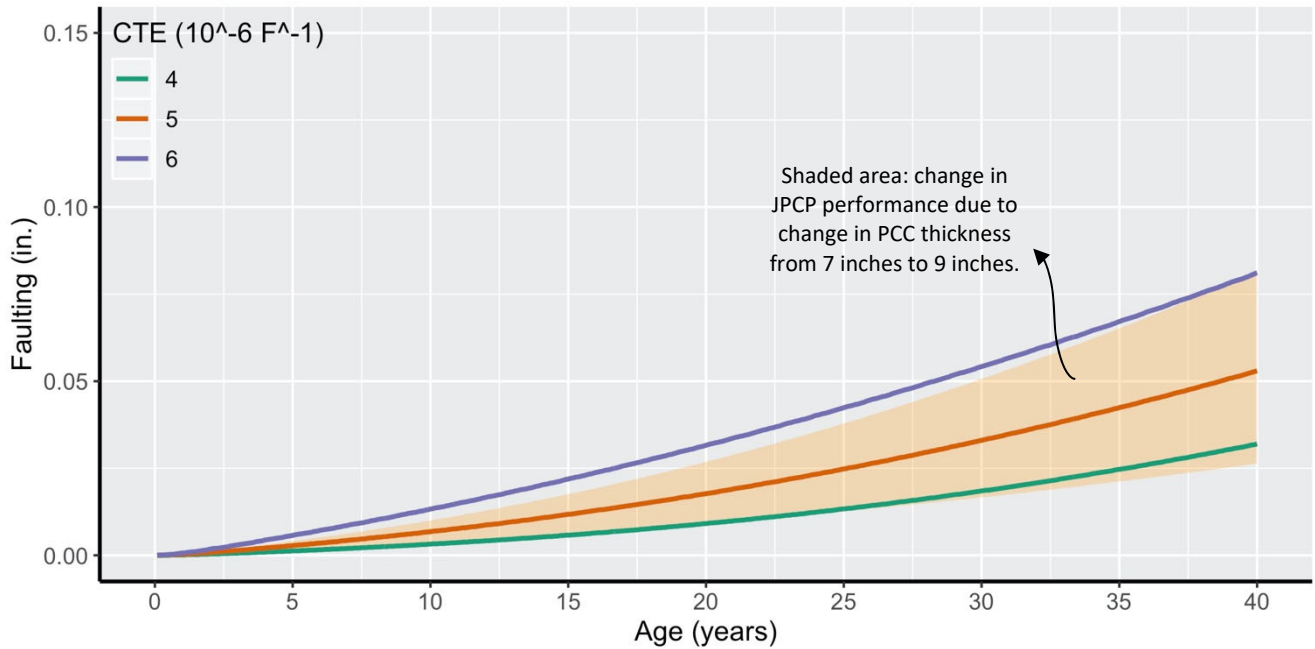


Figure 4.30: Effects of PCC CTE on faulting with 50% reliability.

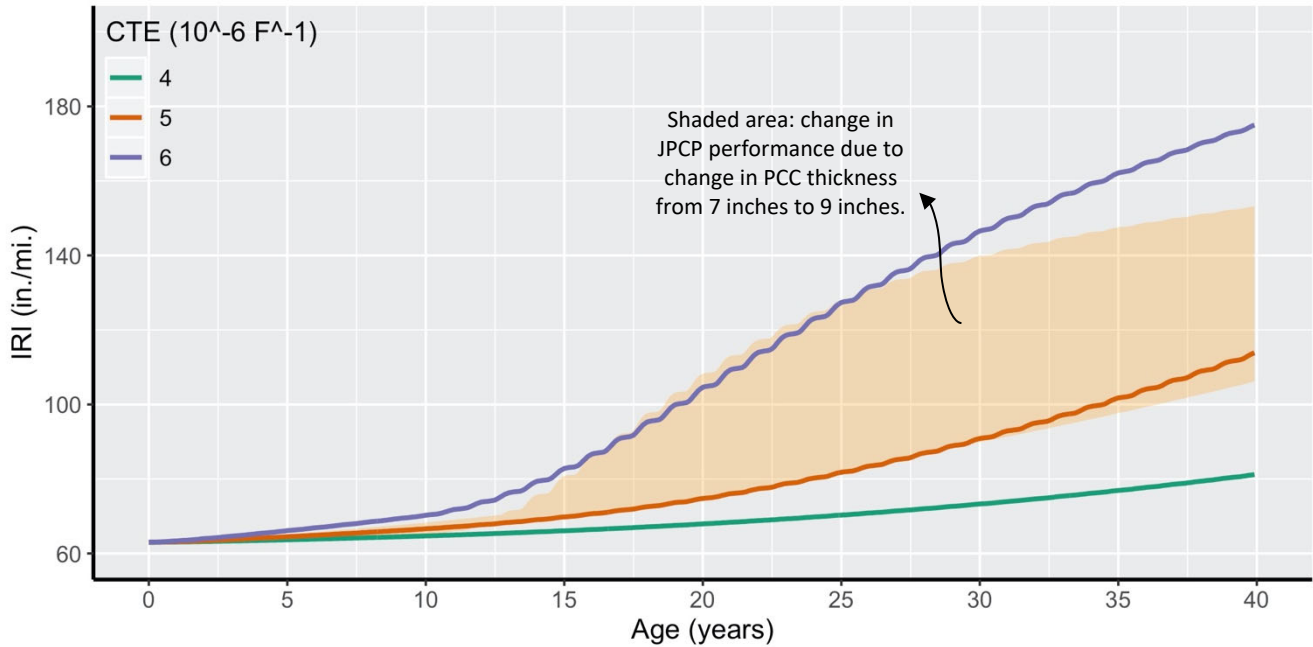


Figure 4.31: Effects of PCC CTE on IRI with 50% reliability.

4.3.3 PCC Shortwave Absorptivity

The shortwave absorptivity of a pavement surface depends on its pavement composition, color, and texture. *Shortwave absorptivity* is the ratio of the amount of solar energy absorbed by the pavement surface to the total energy the surface was exposed to, and it naturally affects the temperature regime within the pavement structure and its associated structural response. This input ranges from 0 to 1. The more reflective a surface is, the lower its shortwave absorptivity will be.

The Pavement ME software recommends a shortwave absorptivity range between 0.5 and 1.0. In this study, four values for PCC shortwave absorptivity were considered, 0.65, 0.7, 0.8, and 0.9, based on the shortwave absorptivity data distribution in Figure A.20 in the appendix and the Pavement ME-recommended range. The default value in Pavement ME is 0.85. The shortwave absorptivity data distributions provided in the appendix were obtained from just three projects, which have all been in service for many years, and were therefore expected to show high values. The average of the shortwave absorptivity data in the appendix was 0.91, and this is why the top of the shortwave absorptivity range was set to 0.9. The rest of the values were considered since the JPCP at its initial service life had lower shortwave absorptivity values. Figure 4.32 shows the effect that PCC shortwave absorptivity had on results from the transverse cracking model. It can be seen from the figure that reducing the PCC shortwave absorptivity from 0.9 to 0.65 had a large impact on transverse cracking performance, an impact

similar to the one resulting from an increase in PCC slab thickness from 7 inches to 9 inches. Figure 4.33 and Figure 4.34 show the impact of PCC shortwave absorptivity on faulting and IRI, which in both cases is significant.

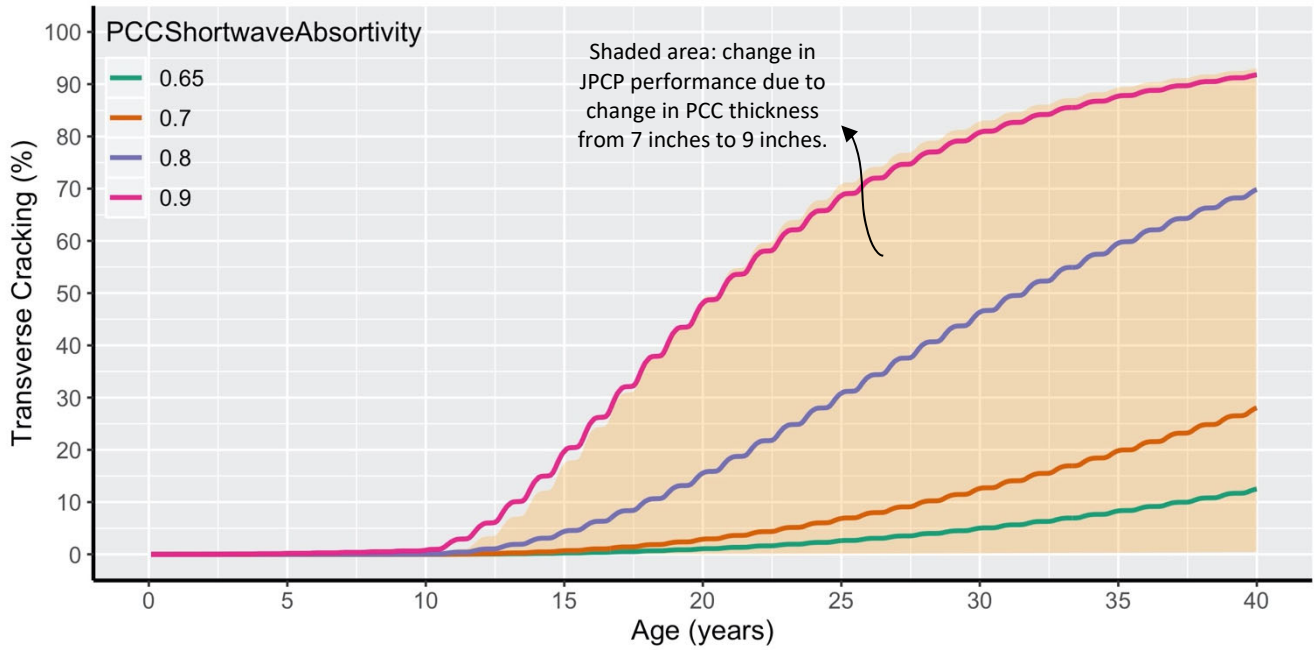


Figure 4.32: Effects of PCC shortwave absorptivity on transverse cracking with 50% reliability.

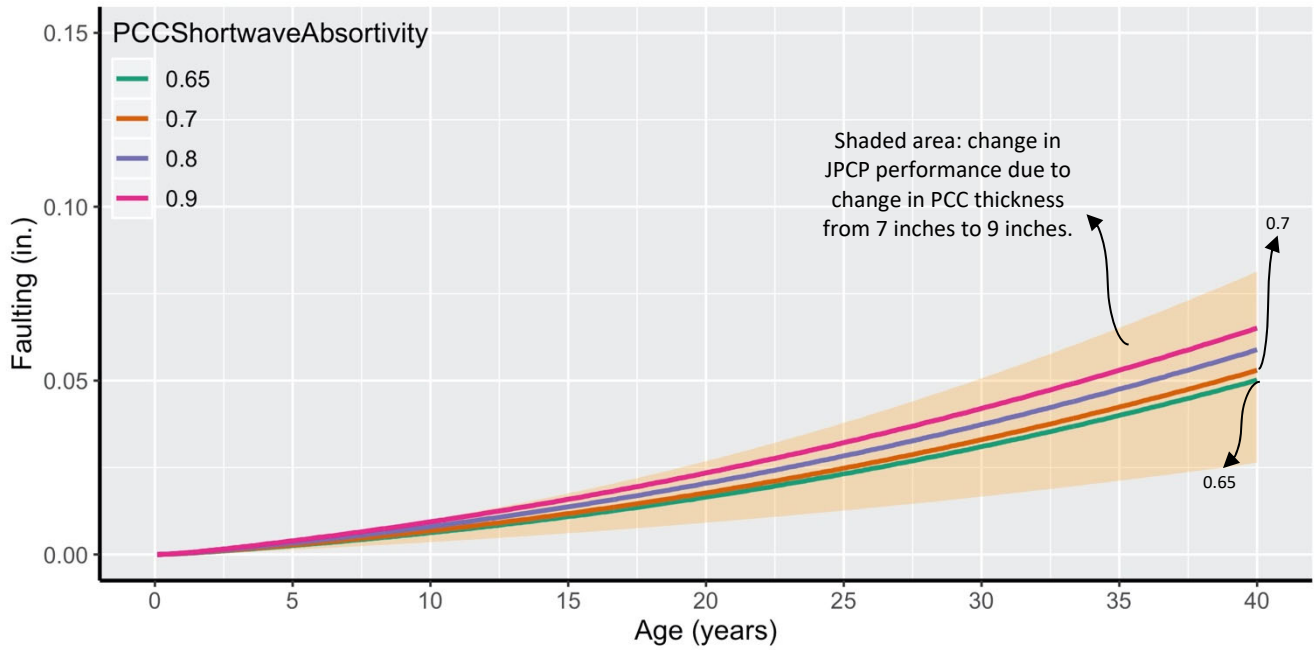


Figure 4.33: Effects of PCC shortwave absorptivity on faulting with 50% reliability.

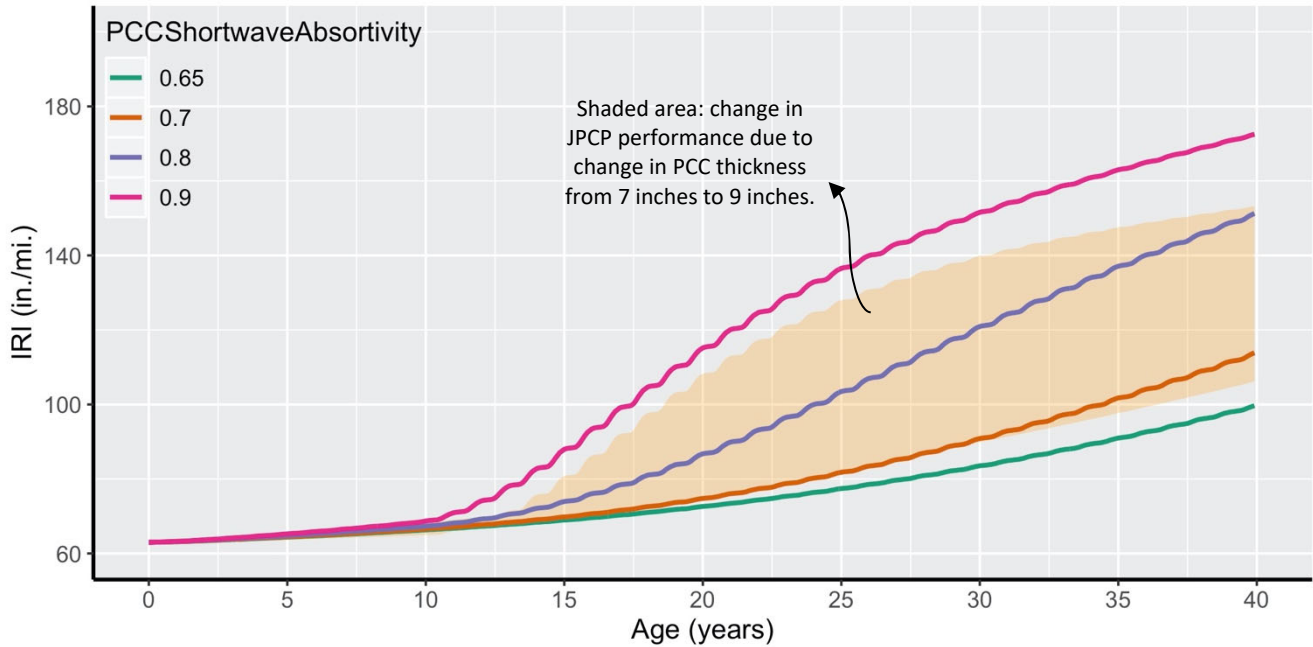


Figure 4.34: Effects of PCC shortwave absorptivity on IRI with 50% reliability.

4.3.4 PCC Heat Capacity

PCC heat capacity is the heat required to raise the temperature of a unit mass of material by a unit temperature. No PCC heat capacity data are available in the UCPRC database. The Pavement ME software recommends a heat capacity range between 0.1 and 0.28. Based on that recommendation, this study considered three values: 0.2, 0.24, and 0.28 (Pavement ME default value). It was found that values less than 0.2 did not produce a result in Pavement ME. The figures below show that this variable does not have much of an effect on the transverse cracking, faulting, and IRI models.

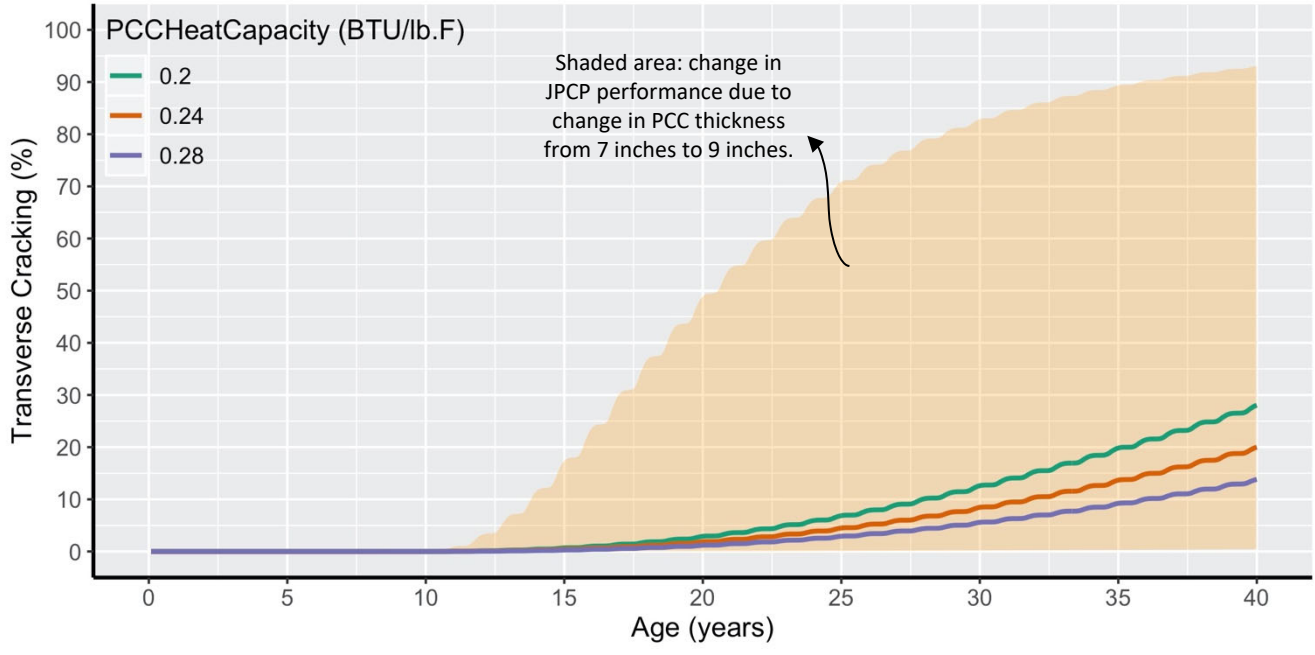


Figure 4.35: Effects of PCC heat capacity on transverse cracking with 50% reliability.

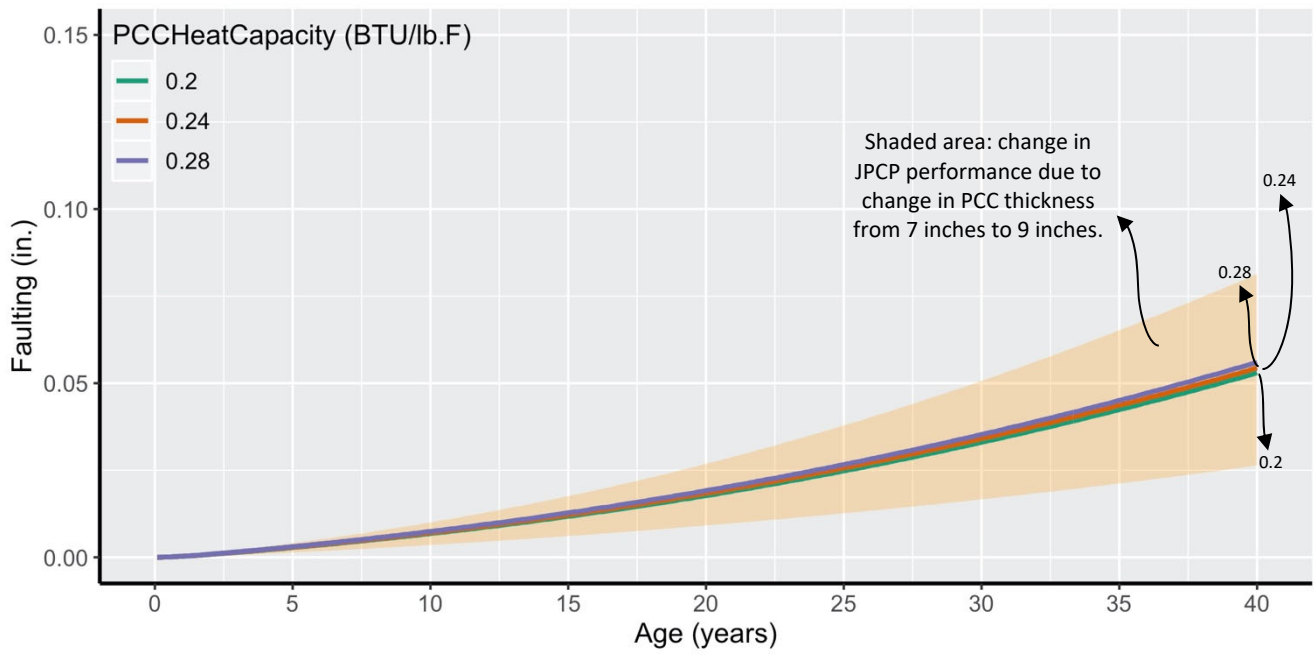


Figure 4.36: Effects of PCC heat capacity on faulting with 50% reliability.

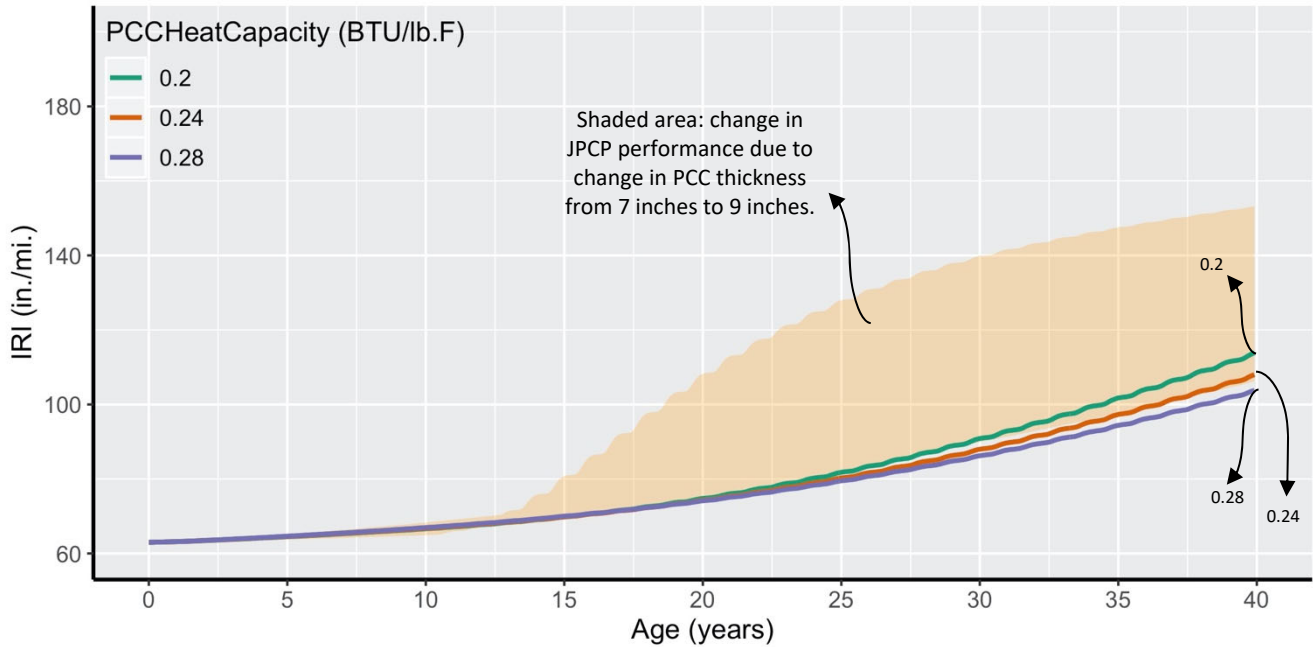


Figure 4.37: Effects of PCC heat capacity on IRI with 50% reliability.

4.3.5 PCC Thermal Conductivity

Thermal conductivity is the quantity of heat that flows normally across a surface of unit area per unit of time and per unit of temperature gradient. No PCC thermal conductivity data are available in the UCPRC database. Pavement ME recommends a range of 1.0 to 1.5 for this variable, and therefore this study considered four PCC thermal conductivity values: 1.0, 1.15, 1.25 (the Pavement ME default value), and $1.5 \frac{\text{BTU}}{\text{hr.ft.}^{\circ}\text{F}}$. Figure 4.38, Figure 4.39, and Figure 4.40 show that thermal conductivity has a significant impact on JPCP transverse cracking and smoothness performance but does not affect faulting much. However, there is not a monotonic relationship between thermal conductivity and Pavement ME predicted cracking, faulting, and IRI. This outcome was not unexpected since the implications of thermal conductivity are complex, and one should not expect a monotonic relation between this variable and Pavement ME distress outputs.

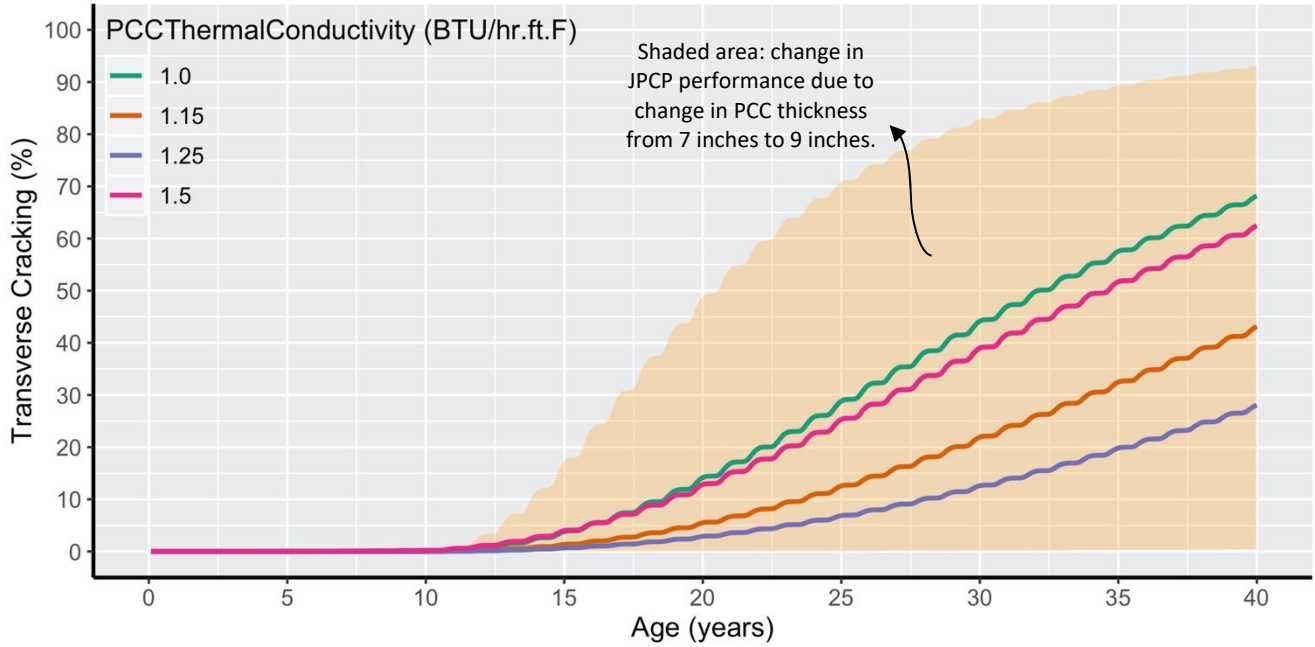


Figure 4.38: Effects of PCC thermal conductivity on transverse cracking with 50% reliability.

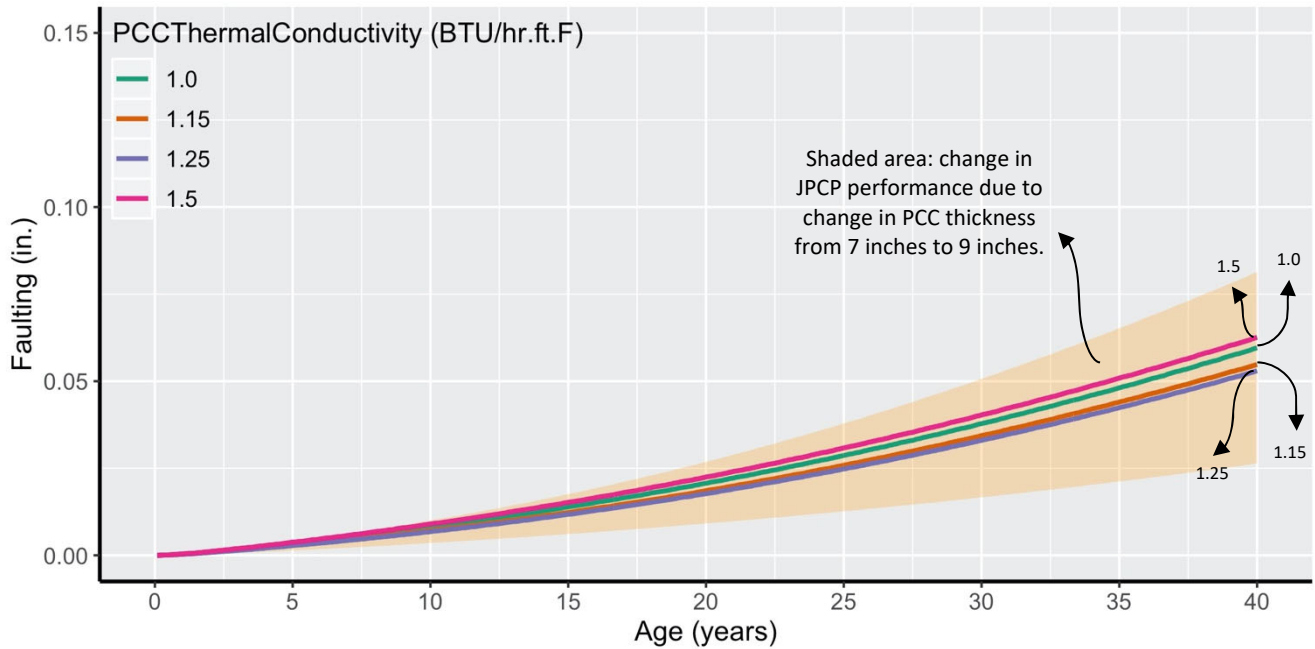


Figure 4.39: Effects of PCC thermal conductivity on faulting with 50% reliability.

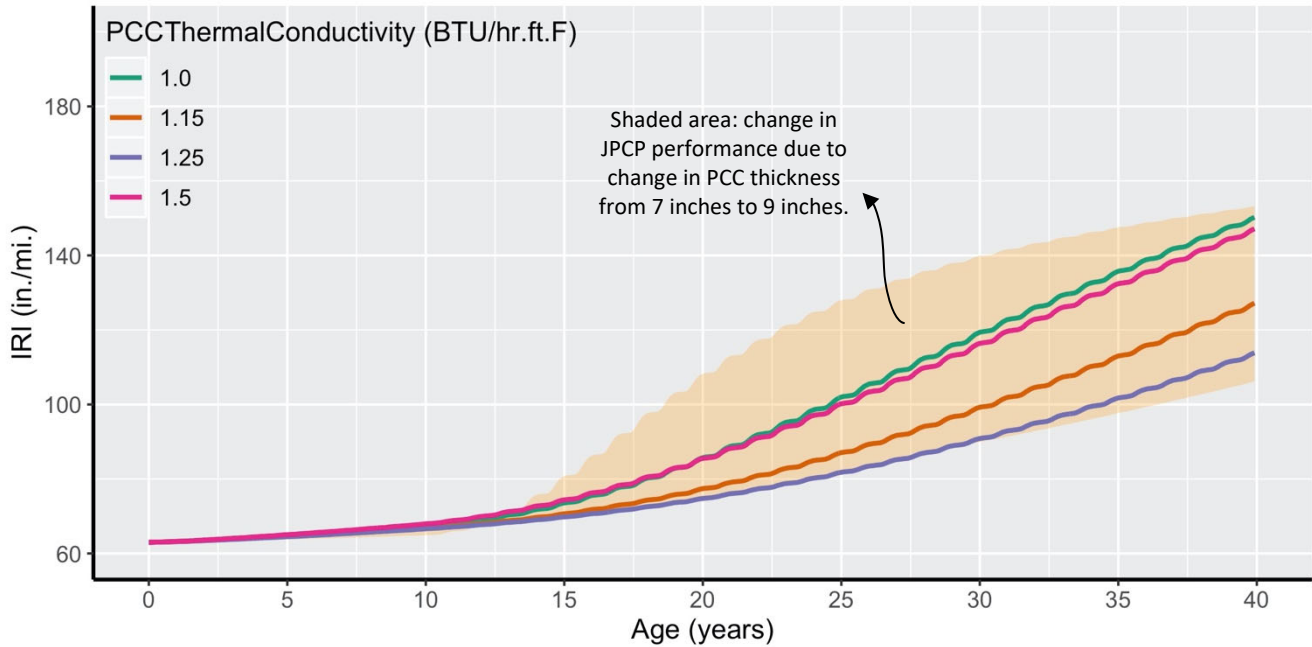


Figure 4.40: Effects of PCC thermal conductivity on IRI with 50% reliability.

4.3.6 PCC Built-In Curl-Warp Temperature

According to the Pavement ME documentation, PCC paving is often performed during the morning on hot, sunny days, in conditions that tend to expose the newly paved PCC slabs to a high positive temperature difference from intense solar radiation. Therefore, the PCC slabs are flat when they harden, but they are hardening when there is a large positive temperature gradient (the upper portion of the slab is much warmer than the bottom). This temperature gradient has been termed the *zero-stress temperature gradient*. Whenever the temperature gradient in the slabs falls below the zero-stress gradient locked into them at the time of construction, the slabs will curl upward, causing tensile stress at the top of the slab that can lead to top-down cracking of JPCP. Thus, to prevent, reduce, or eliminate the upward curling, the slabs are constructed to take advantage of several factors that act to reduce the built-in effective negative temperature gradient: the slab self-weight, dowels, and the weight of any base course bonded to the slab. These factors affect the amount of actual permanent curl, as well as the amount of creep relaxation that may take place. The Pavement ME documentation states that if PCC paving is performed later in the afternoon or at night, so that the highest temperature from the heat of hydration does not correspond with the most intense solar radiation, the temperature gradient at the time of hardening will be much lower and could potentially even be negative.

Differential shrinkage (top versus bottom of the slab) also produces permanent warping that is superimposed on the zero-stress thermal gradient and is modeled in the same way as permanent curling. The permanent components of curling and warping are, therefore, considered together. It is important to note that only a portion of permanent curl/warp actually affects pavement response, because the PCC creep and slab foundation permanent deformation that occur over time negate some of the effects of the permanent curvature present in PCC slabs.

No PCC built-in curl-warp temperature data are available in the UCPRC database. However, Pavement ME recommends a range of -30 to 0°F, so this study considered four built-in curl-warp temperature values: 0, -5, -10 (Pavement ME default value), and -15°F. Decreasing the built-in curl-warp equivalent temperature gradient (cooler-on-top), which the Pavement ME models assume comes from a combination of the drying shrinkage gradient and the thermal gradients when the concrete sets, results in larger tensile stresses at the top of the slab (which entails more top-down transverse cracking) and larger corner deflections (which entails larger differential deflection energy and, consequently, more faulting). Pavement ME cracking, faulting, and IRI predictions for the different built-in curl-warp temperatures are shown in Figure 4.41, Figure 4.42, and Figure 4.43, respectively. Figure 4.41 shows the significant impact of the built-in curl-warp temperature on JPCP transverse cracking. However, while a monotonic relationship between this variable and both top-down and bottom-up cracking is expected, the same is not true for total cracking. The reason is that total cracking is a combination of top-down and bottom-up, with the former worsening and the latter improving as the built-in curl temperature increases (in absolute value). As shown in Figure 4.41, the total cracking reaches a minimum when the built-in curl is -10°F, and it increases when this variable either decreases or increases. However, as expected, a monotonic relationship existed between the built-in curl temperature and both top-down and bottom-up cracking independently of each other, as shown in Figure 4.44. That figure shows the effects of built-in curl temperature on bottom-up, top-down, and total (bottom-up + top-down) cracks separately.

The relationship between faulting and built-in curl-warp temperature (Figure 4.42) is as expected: the larger the built-in curl-warp is the larger the deflections and the differential deflections are, and, consequently, the larger the differential deflecting energy and the subsequent faulting will be. The relationship between built-in curl-warp temperature and IRI is more complicated, as IRI is a function of both faulting—to which built-in curl-warp is monotonically related—and transverse cracking—to which built-in curl-warp is not monotonically related.

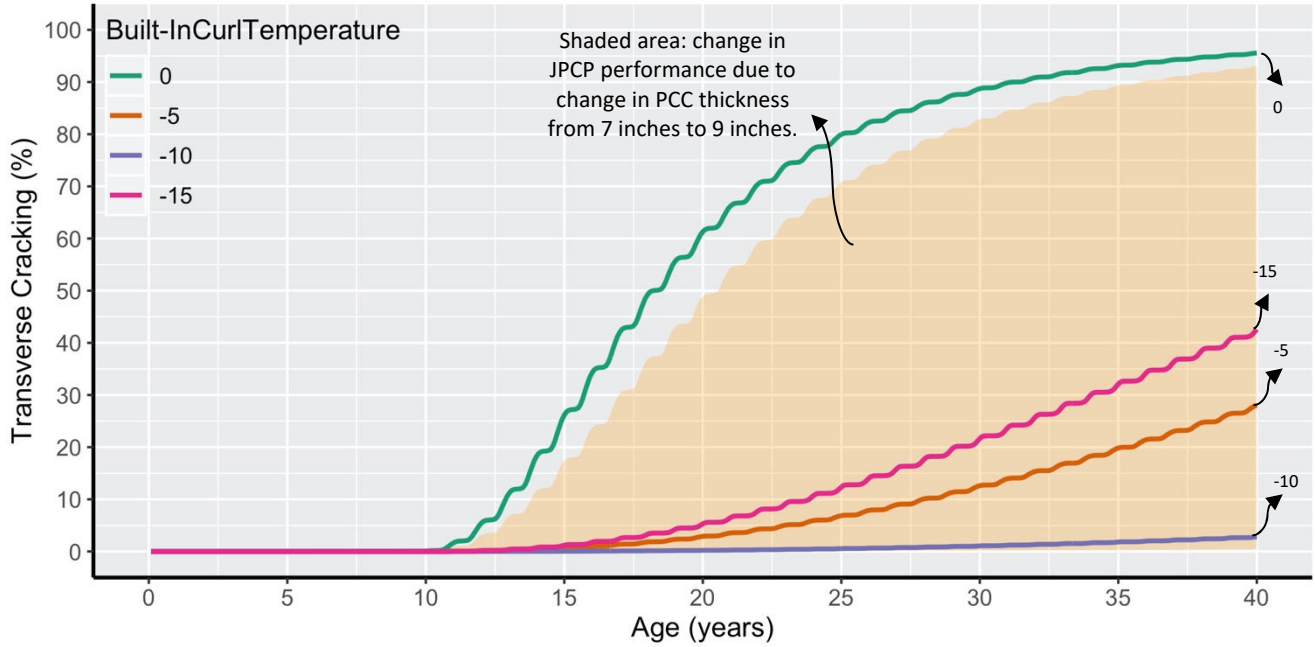


Figure 4.41: Effects of built-in curl-warp temperature on transverse cracking for 8-inch slabs with 50% reliability.

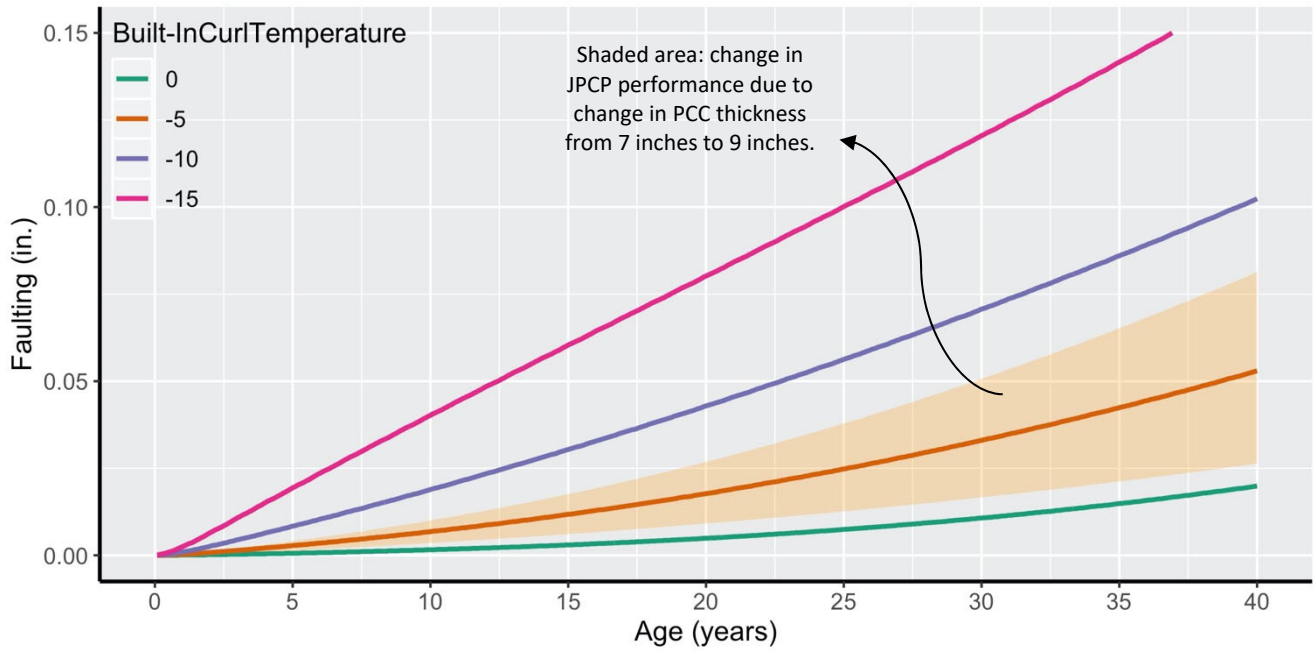


Figure 4.42: Effects of built-in curl-warp temperature on faulting with 50% reliability.

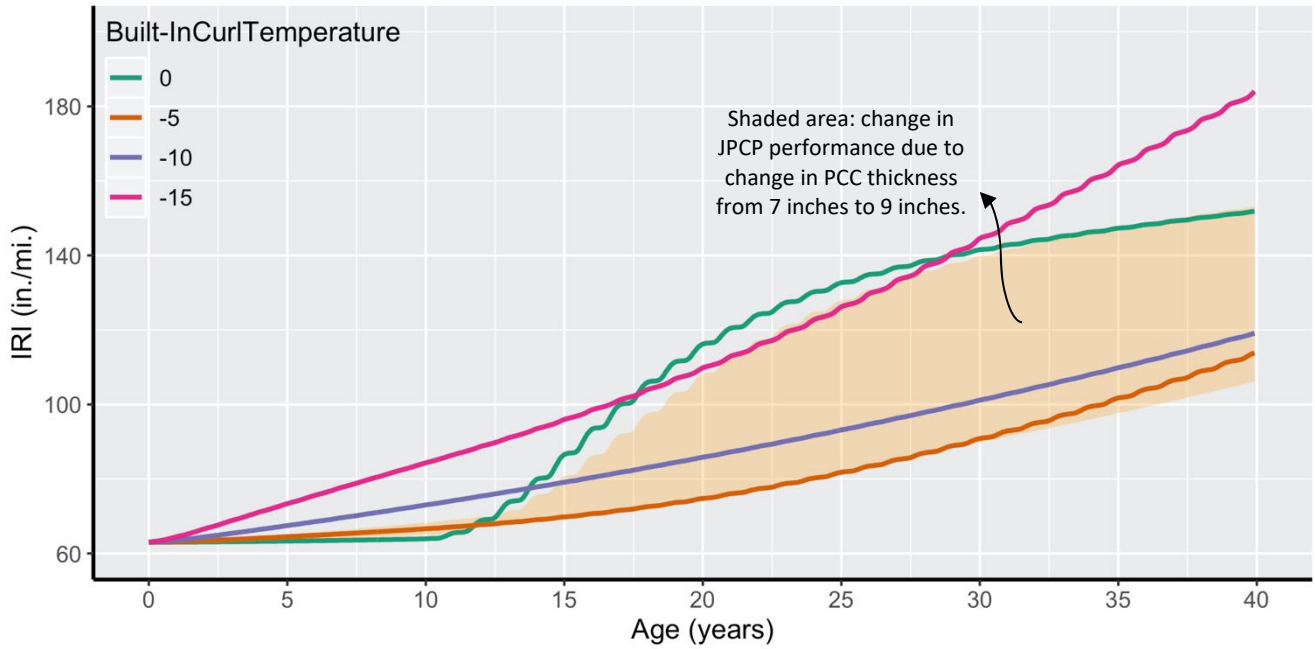


Figure 4.43: Effects of built-in curl-warp temperature on IRI with 50% reliability.

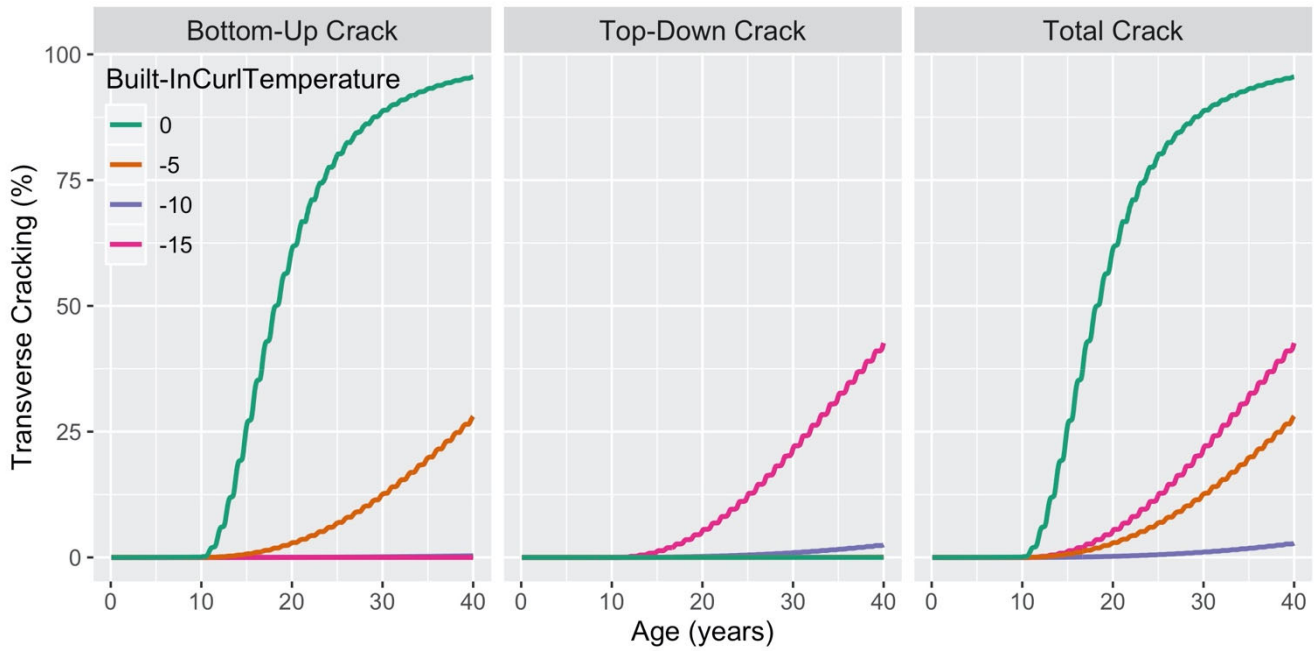


Figure 4.44: Effects of built-in curl-warp temperature on bottom-up, top-down, and total transverse cracking for 8-inch slabs with 50% reliability.

4.4 Traffic Inputs

4.4.1 Average Annual Daily Truck Traffic

Traffic data are one of the key data inputs required for the analysis and design of pavement structures. The Pavement ME software considers truck traffic loading in terms of axle load spectra and *average annual daily truck traffic* (AADTT), which is the bidirectional average annual daily truck traffic for two lanes.

This study considered five AADTT values, 7,000, 12,000, 14,000, 16,000, and 20,000; and it assumed WIM Spectra 3 (WIM 3) as the default spectrum. The AADTT values are bidirectional with two lanes in each direction. These values were picked based on the AADTT distribution shown in Chapter 2. These heavy truck traffic values were chosen to be high to evaluate the sensitivity to traffic. The directional and truck lane distribution factors were assumed to be 50 and 95 percent, respectively. Five WIM spectra characterize the truck loads for the different highways in the Caltrans road network. Each WIM spectra (1 through 5) includes a particular distribution of truck classes and axle load distributions for each truck class and axle type. The use of WIM spectra constitutes Level 2 traffic inputs in Pavement ME. The WIM spectra are described in the appendix. Using the Caltrans method of calculating *equivalent single axle loads* (ESALs), the truck traffic levels included in this sensitivity analysis along with the WIM 3 assumption translate to 40-year ESALs of x, y, z, k, and j respectively, which represent Caltrans Traffic Index values of 15, 16, 16, 16.5, and 17 when rounded to the nearest 0.5. It must be made clear that ESALs are not used in Pavement ME. Instead, an axle load spectra must be used with truck classification count data.

Figure 4.45, Figure 4.46, and Figure 4.47 show that as AADTT increased, transverse cracking, faulting, and IRI increased, as expected. This sensitivity is such that doubling truck traffic from 7,000 to 14,000 trucks per day resulted in approximately the same increase in transverse cracking that resulted from reducing the slab thickness from 9 inches to 8 inches when the AADTT is 14,000.

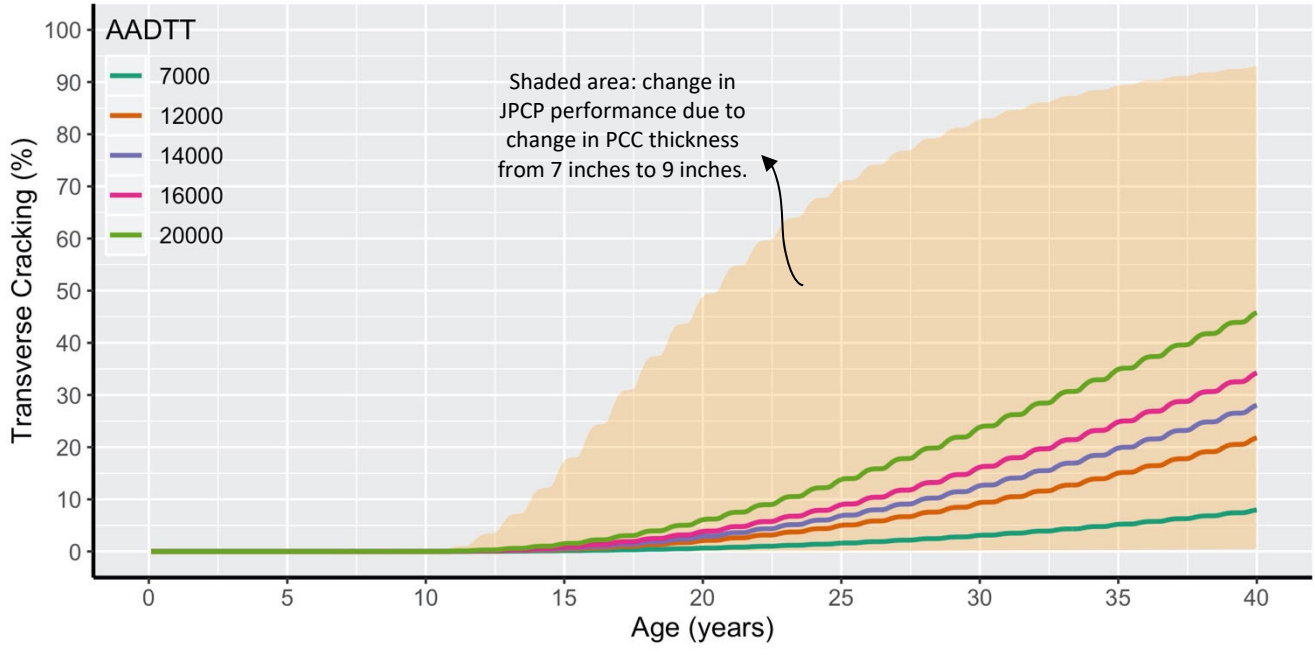


Figure 4.45: Effects of AADTT on transverse cracking with 50% reliability.

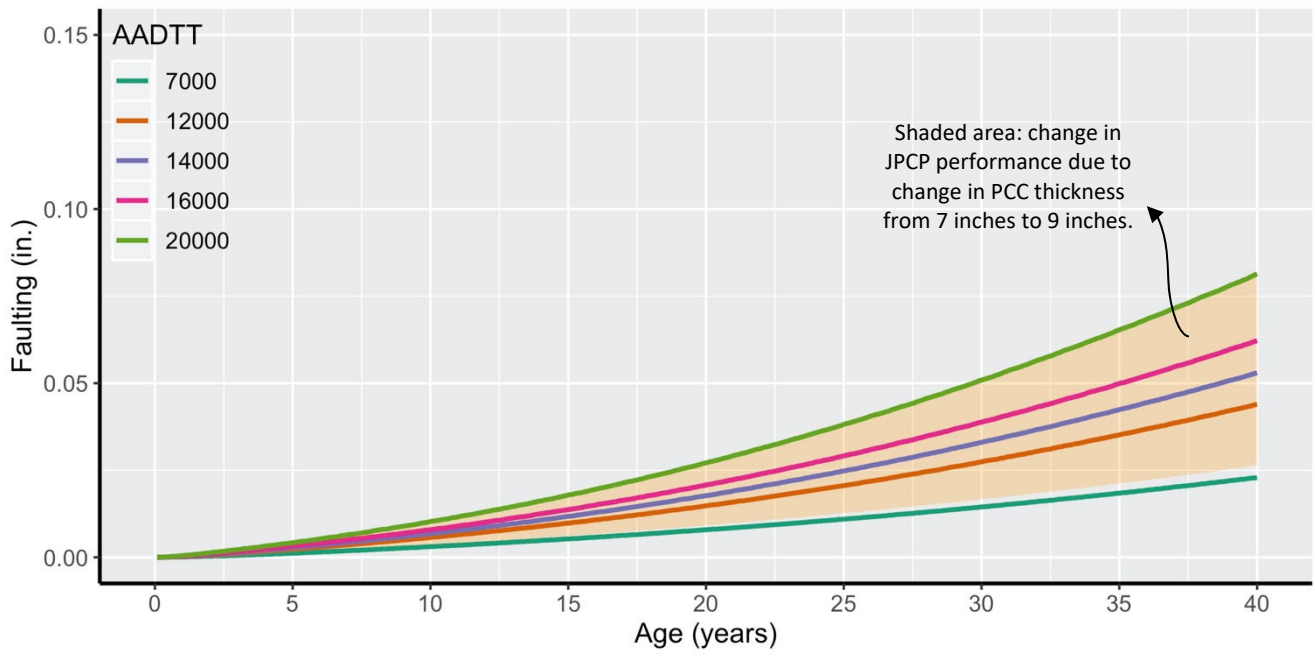


Figure 4.46: Effects of AADTT on faulting with 50% reliability.

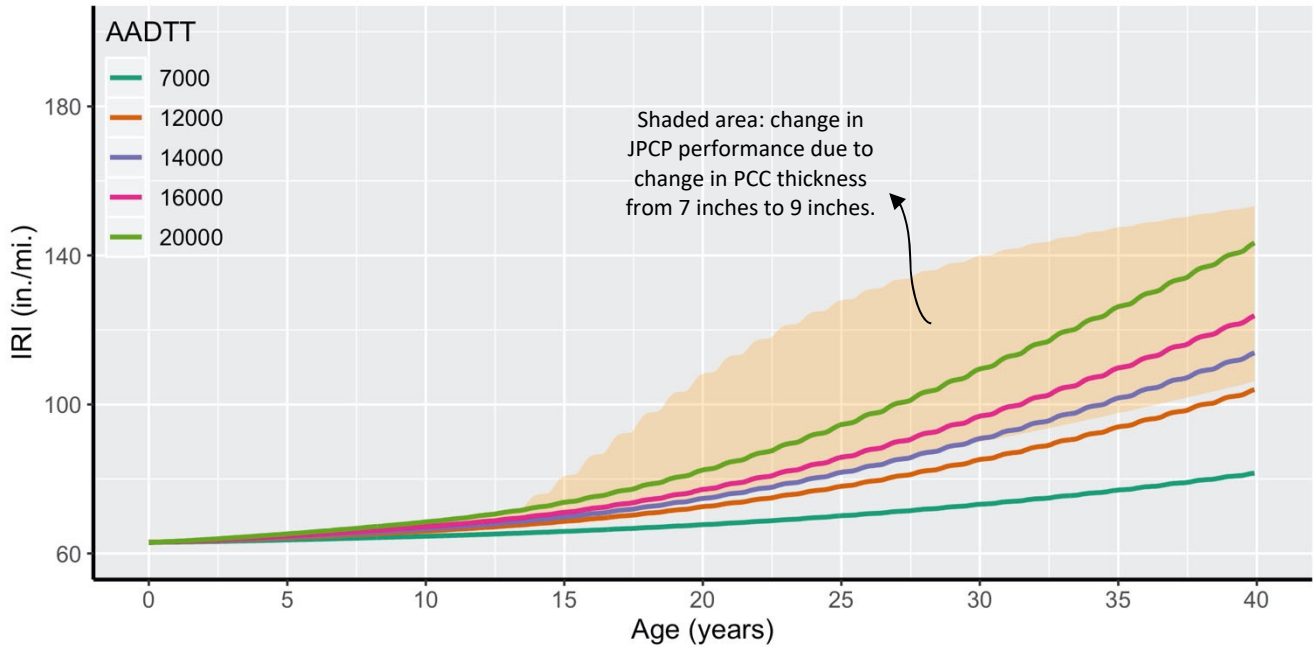


Figure 4.47: Effects of AADTT on IRI with 50% reliability.

4.4.2 Weigh-in-Motion (WIM) Spectra

Weigh-in-motion data are a tabulation of the vehicle type and the number, spacing, and weight of axles for each vehicle weighed over a period of time. WIM data are used to determine the normalized axle load distributions or spectrum for each axle type within each truck class. In other words, the load spectrum for an axle type is the percentage of loads in each load category for a given number of axles of that type. There are five WIM groups in California, three of which are considered in this study: Spectra 1, Spectra 3, and Spectra 5 (9). In general, axles get heavier as the WIM spectra changes from Spectra 1 to Spectra 5 (called “spectra” here because there is a spectrum for each axle type in each set) and therefore, more distress is expected under higher-numbered WIM groups.

Figure 4.48, Figure 4.49, and Figure 4.50 show the effect of WIM spectra on Pavement ME–predicted transverse cracking, faulting, and IRI, respectively. It was expected that an overall heavier WIM spectra, represented by a higher WIM spectra number, would result in larger predicted distresses. However, the Pavement ME–predicted cracking, faulting, and IRI were not particularly sensitive to the WIM spectra. This is because the different WIM spectra differ from one another in the middle and low load ranges, as shown in Figure 4.51; however, these load levels produce very little damage to the JPCP. On the contrary, the three WIM spectra are very similar to one another for equivalent single axle loads above 18 kips, which produce most JPCP damage, and that explains why the three result in similar cracking, faulting, and IRI. For similar reasons, one should not necessarily expect Pavement ME–predicted distresses to increase systematically as WIM spectra increases.

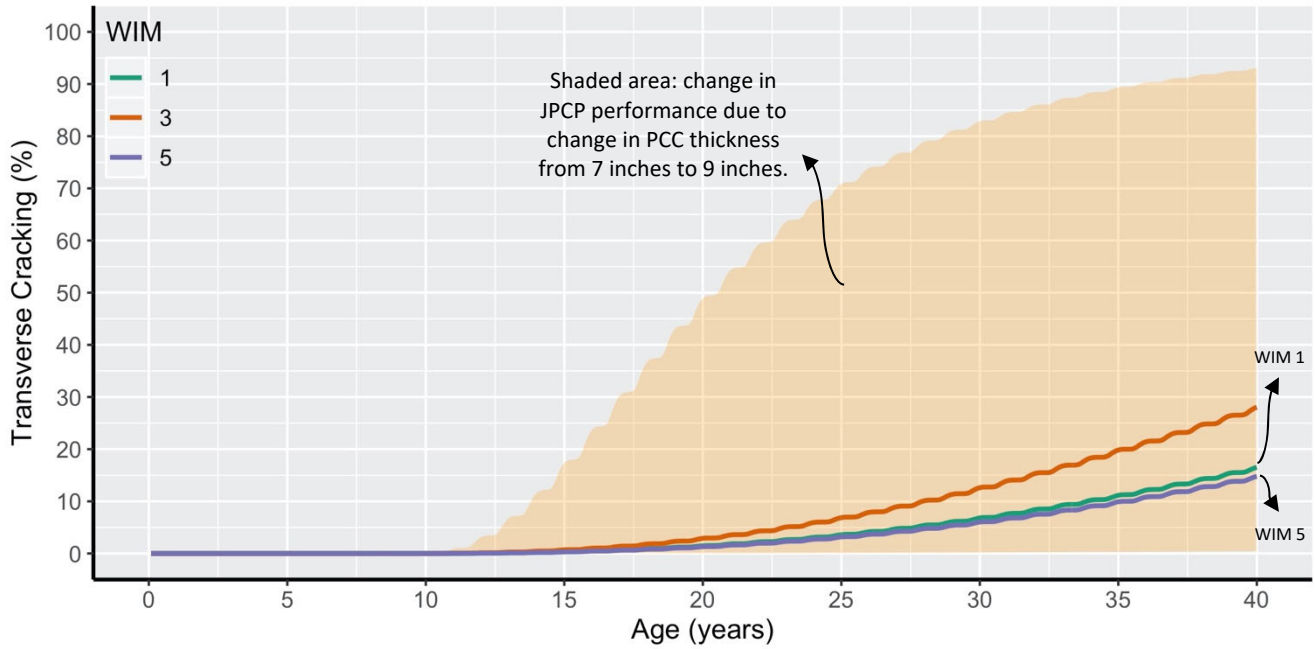


Figure 4.48: Effects of WIM spectra on transverse cracking with 50% reliability.

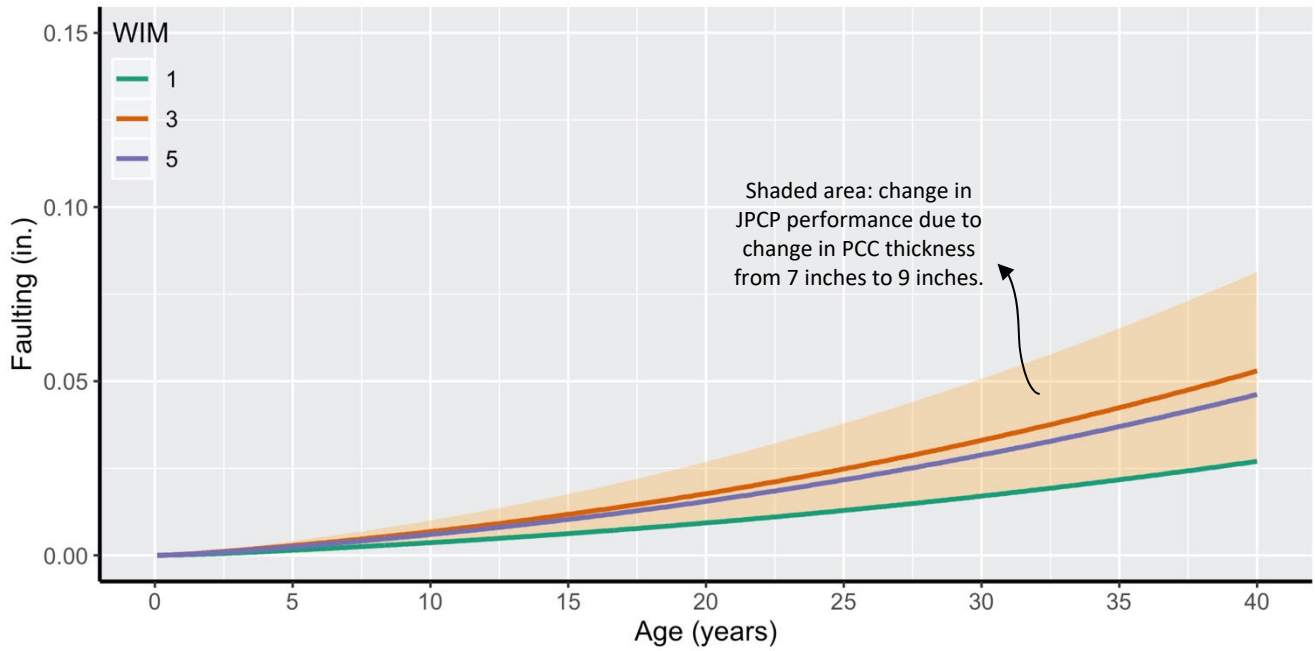


Figure 4.49: Effects of WIM spectra on faulting with 50% reliability.

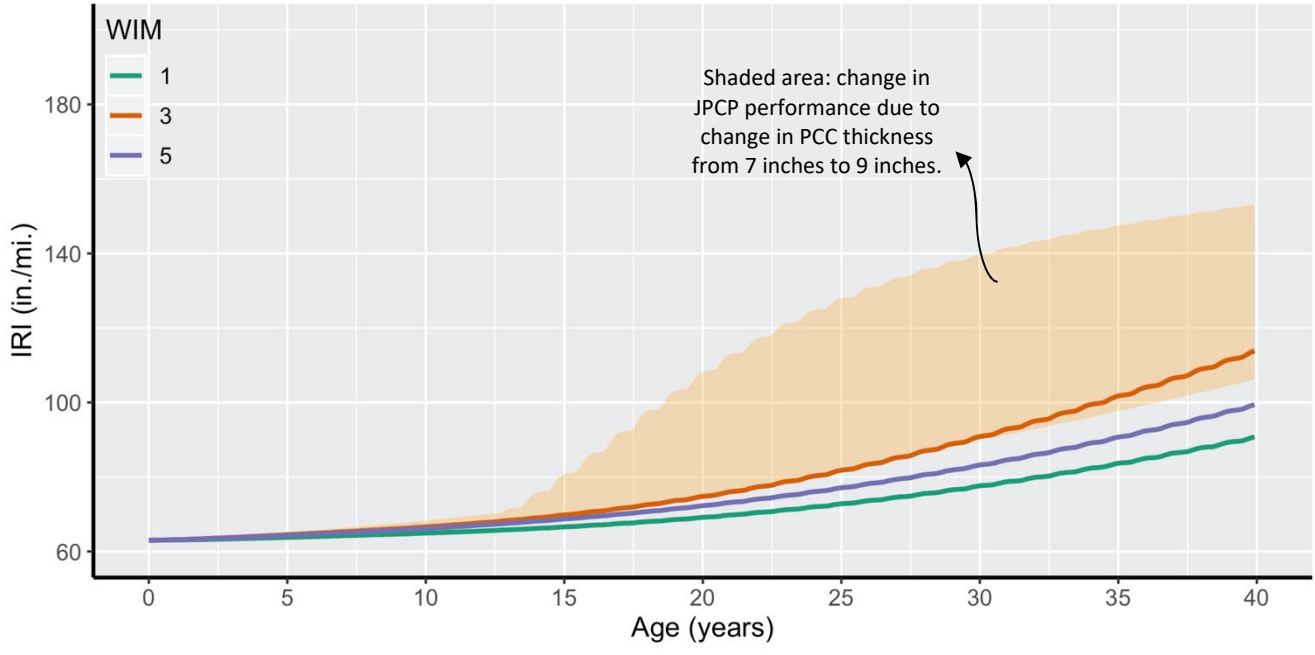


Figure 4.50: Effects of WIM spectra on IRI with 50% reliability.

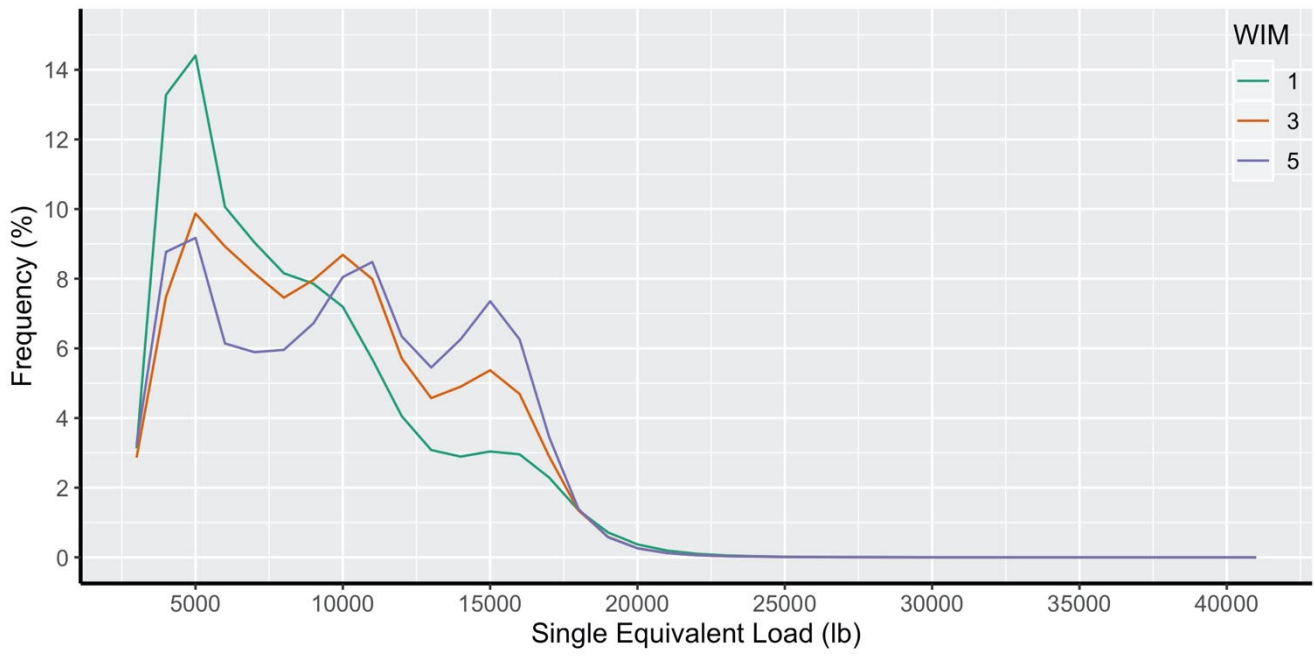


Figure 4.51: Equivalent single axle loads associated to WIM spectra.

(Note: the single equivalent load is the result of splitting tandem axles in two and tridem axles in three [e.g., one tandem becomes two singles with half the load each]. The use of single equivalent axes is a simplified way to determine the similarity between different WIM spectra. It does not impact the actual spectra being used in Pavement ME.)

4.5 Climate

According to the MEPDG, environmental conditions have a significant effect on the performance of rigid pavements. The interaction of climatic factors with pavement materials and loading is complex. Factors such as precipitation, temperature, freeze-thaw cycles, and depth to water table affect pavement and subgrade temperature and moisture content, which, in turn, directly affect the pavement layers' load-carrying capacity and ultimately pavement performance.

This study considered California's nine climate regions. The weather stations used to represent each climate region are shown in Table 4.2.

Table 4.2: Climate Regions and Corresponding Weather Stations

Climate Region	Representative Weather Station in Pavement ME	Weather Station Identification Number
Central Coast	San Francisco	23234
Desert	Riverside	03171
High Desert	Reno	23185a
High Mountain	Emigrant Pass	23225c
Inland Valley	Sacramento	23232
Low Mountain	Santa Rosa	23213
North Coast	Arcata/Eureka	24283
South Coast	Los Angeles	23174
South Mountain	Palm Springs	3104d

Figure 4.52, Figure 4.53, and Figure 4.54 show that all the distress models are significantly affected by climate region. The transverse cracking results are somewhat unexpected with respect to the South Coast region, which might be considered a relatively benign climate region based on the observed performance data, but which had the third-most cracking of all the regions, and the harsher High Desert region, which showed the least amount of cracking.

However, appearances can be deceptive. In a study conducted as part of the earlier Pavement ME calibration, temperature gradients were calculated using (a) the stand-alone version of the *Enhanced Integrated Climate Model* (EICM) coded into Pavement ME and 30 years of climate data (10) and (b) six of the current nine climate regions that Caltrans designs for; the High Mountain, South Mountain and Low Mountain regions were not included in the calculations at first but were added later. Further, the North Coast region was not included in this sensitivity analysis because there are few concrete pavements there.

In Figures 25 and 26 in Reference (10), the ranking in terms of distributions of positive temperature gradients that would contribute to bottom-up transverse cracking showed that the South Coast, Inland Valley, and Desert regions had similar high positive gradients, while the High Desert and Central Coast regions had similar low positive gradients. The ranking in terms of distributions of negative temperature gradients that would contribute to top-down transverse cracking were the High Desert, Desert, and Inland Valley regions with similar high negative gradients, while the Central Coast and South Coast regions had similar low negative gradients. Based on the temperature gradients from the previous study, the region with both low positive and negative gradients is the Central Coast, and it had the second lowest amount of cracking of the regions common to both studies, as shown in Figure 4.52. The regions with the highest positive temperature gradients common to both studies were the Desert, South Coast, and Inland Valley, which are the three regions with the most cracking, as shown in Figure 4.52. The anomaly in the results is the High Desert, which has the least cracking, but which also has high negative gradients. A comparison of cracking trends for the different climate regions in the PMS data will help identify whether the Pavement ME results match field performance with respect to ranking of cracking for the different climate regions.

The results for faulting are more consistent with the expectation that climate regions with greater negative temperature gradients will have more faulting.

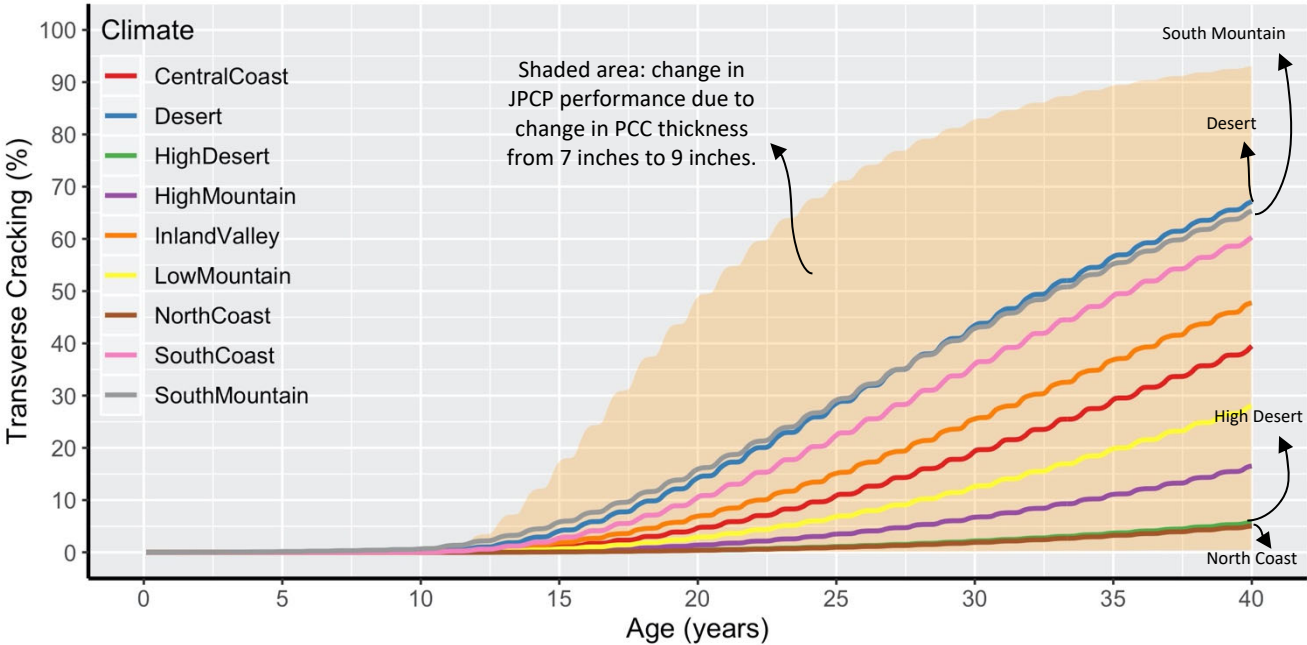


Figure 4.52: Effects of climate on transverse cracking with 50% reliability.

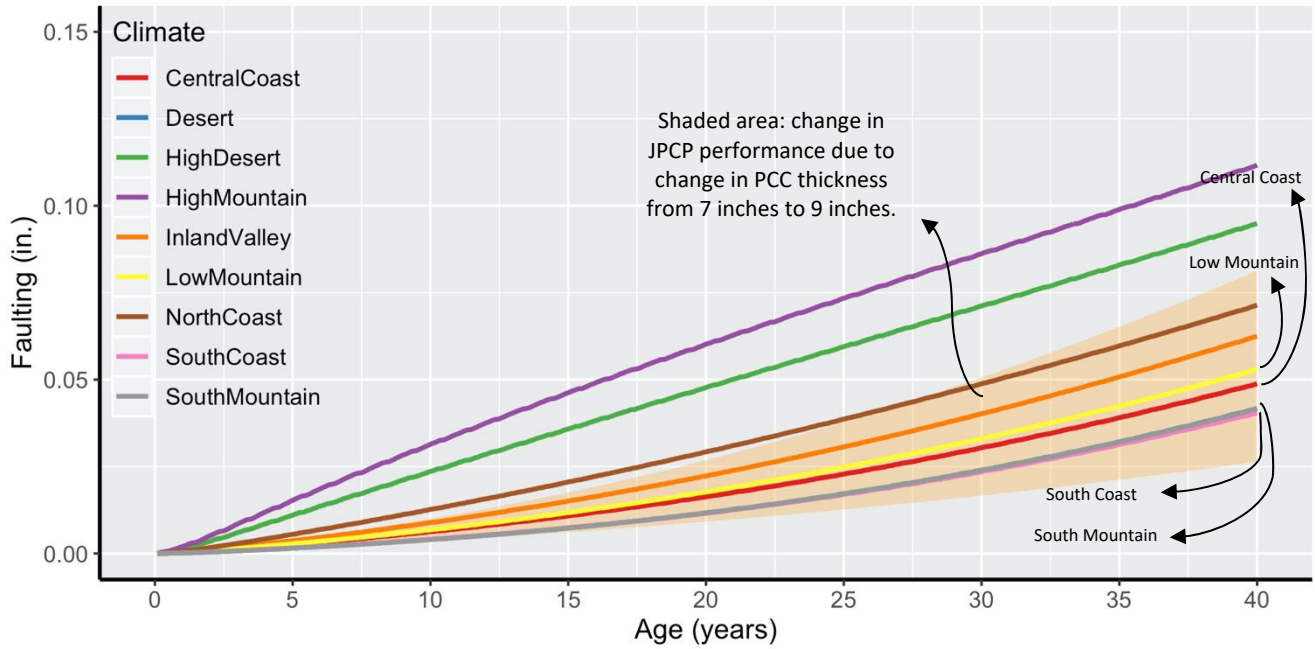


Figure 4.53: Effects of climate on faulting with 50% reliability.

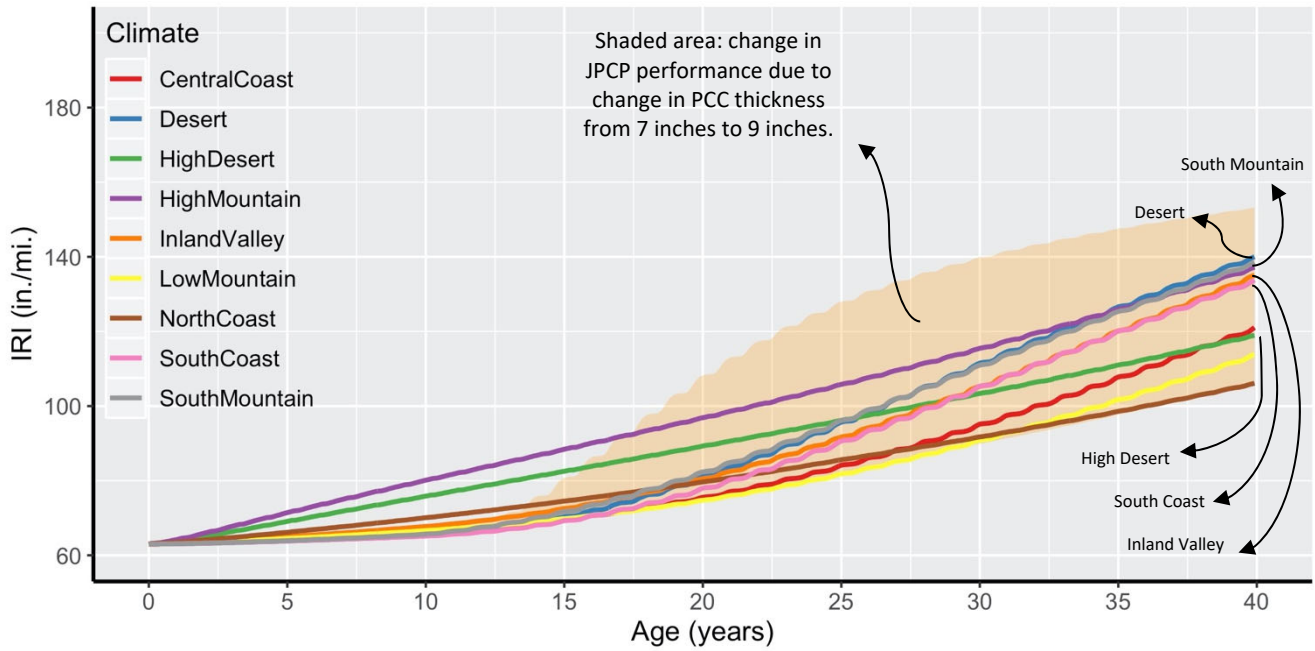


Figure 4.54: Effects of climate on IRI with 50% reliability.

5 SUMMARY AND CONCLUSIONS

In this study, a sensitivity analysis study was performed as a first step in the calibration of Pavement ME. This is part of a project undertaken to provide Caltrans with updated tools for the design and analysis of jointed plain concrete pavements (JPCPs) in California. The sensitivity analysis identified the importance of different input variables and their effects on the outputs generated by Pavement ME's performance models for transverse cracking, faulting, and IRI. These results were also used to check the reasonableness of the model predictions, to identify problems in the software, and to understand the level of difficulty involved in obtaining the inputs.

The study considered different inputs grouped as pavement structural design variables, pavement materials variables, traffic variables, and climate variables. With some exceptions, the range chosen for each of the variables generally corresponded to one of two categories. The first was the typical range of variation of the corresponding variable in the historical Caltrans road network for the time period of the projects to be used for calibration. The second category included some cases, such as AADTT, that represented values more extreme than those found in the historical database; this approach was taken to identifying sensitivity where it would not otherwise have been observable. As stated earlier, it is important to note that the historical ranges and the more extreme values chosen for each of the variables in this study are not the ranges that will be used for developing the design catalog. Figure 5.1 through Figure 5.3 summarize the sensitivity analysis for the Pavement ME transverse cracking, mean transverse joint faulting, and smoothness index (IRI) models, respectively. The red line in the figures represents the model results for the base case inputs, and each boxplot shows the effect of varying the specific variables on the distress. Therefore, boxplots with greater height identify a variable with a greater effect on the distress for the range of inputs considered. Based on these figures, the following variables were found to be the ones with the greatest influence on JPCP design. They are ranked from most to least influential:

- Transverse cracking
 - PCC slab thickness
 - Built-in curl-warp temperature
 - PCC coefficient of thermal expansion (CTE)
 - PCC shortwave absorptivity
 - PCC compressive strength, which was used with American Concrete Institute (ACI) equations implemented in Pavement ME to predict PCC flexural strength and modulus of elasticity
 - Shoulder type

- Mean transverse joint faulting
 - Load transfer* (use of dowels)
 - Built-in curl-warp temperature
 - Shoulder type
 - Climate
 - AADTT
 - PCC coefficient of thermal expansion
 - PCC thickness
 - Subgrade type
- Smoothness index
 - Load transfer* (use of dowels)
 - Shoulder type
 - Coefficient of thermal expansion
 - PCC shortwave absorptivity
 - Built-in curl-warp temperature
 - AADTT
 - PCC thermal conductivity
 - PCC thickness

*Load transfer (use of dowels) is not shown in Figure 5.2 and Figure 5.3 as its high values for the undoweled case do not allow for an effective comparison of results.

The sensitivity analysis shows that the overall JPCP performance predictions by Pavement ME are reasonable. Pavement ME–predicted distresses did not show any important unexpected trends versus any of the variables considered in this sensitivity analysis. Further, over the course of the study, no major issues were found in the running of the Pavement ME software.

Calibration of Pavement ME, the next step in this project, will proceed as planned because, except for the material inputs, the Caltrans PMS database currently includes all the other required design inputs. To help a designer overcome the lack of material inputs at the time of design, the calibration will include median values for these based on historical Caltrans projects; these should provide reasonable results and a representative “best estimate” calibration. Even so, designers will still need to keep in mind that the calibration will still include some variability due to differences in the materials supplied by different contractors on different projects (i.e., the between-project variability). This sensitivity analysis study also identified the within-project variability of construction-related variables such PCC compressive strength, PCC modulus of elasticity, and PCC CTE. The appendix at the end of this report shows the data used for the analysis.

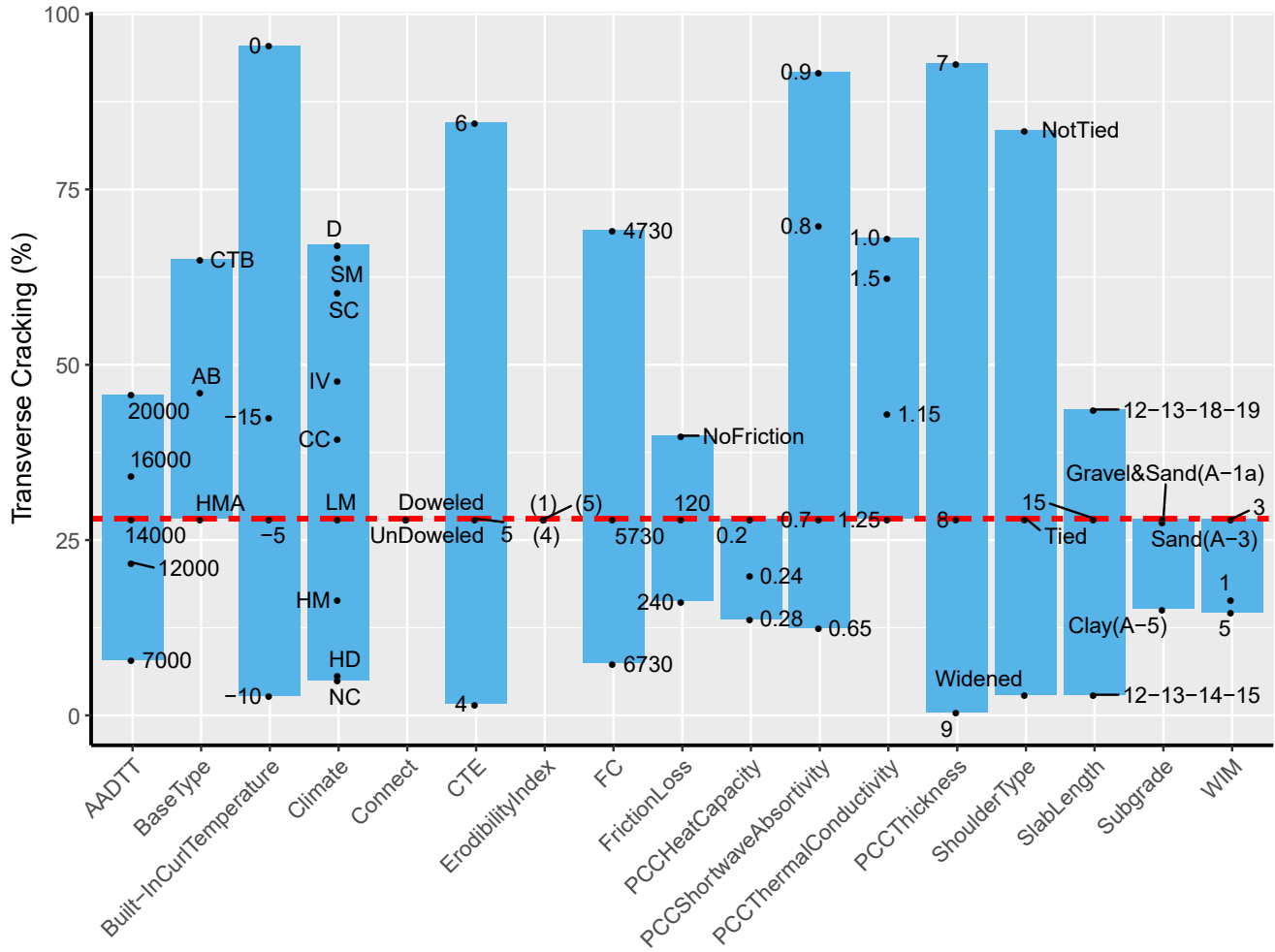


Figure 5.1: Overall sensitivity analysis of the transverse cracking model in Pavement ME.

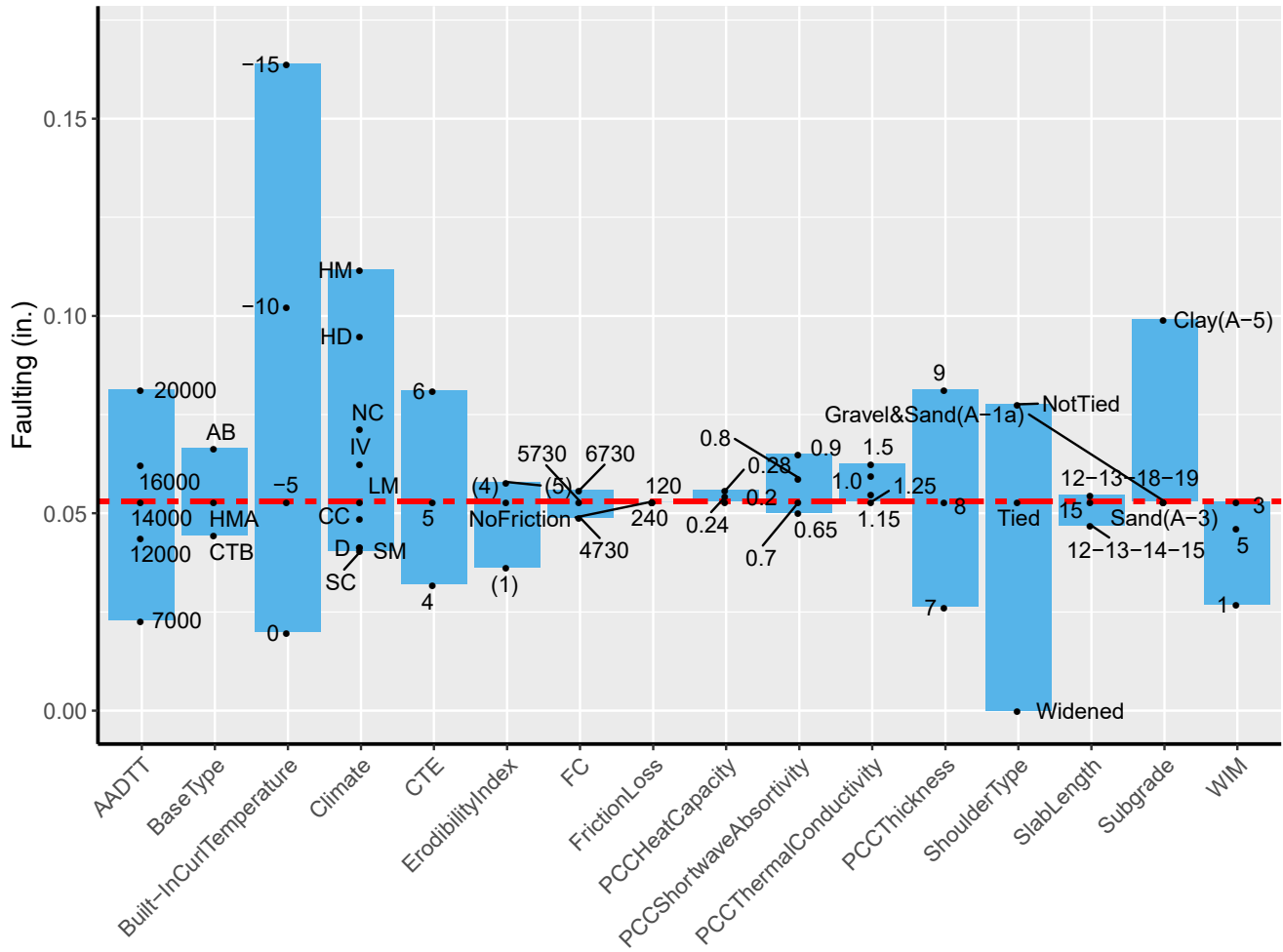


Figure 5.2: Overall sensitivity analysis of the faulting model in Pavement ME.

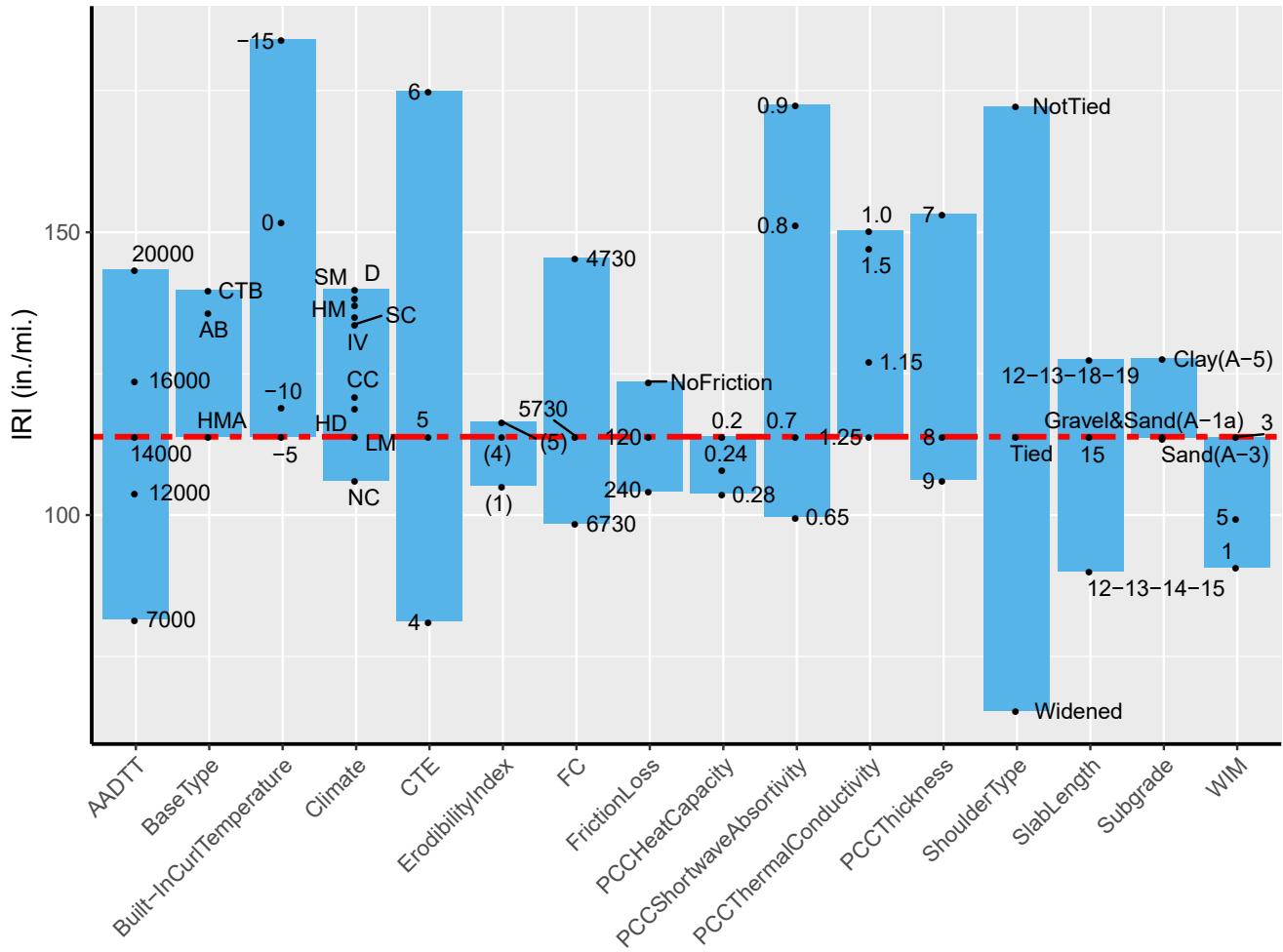


Figure 5.3: Overall sensitivity analysis of the IRI model in Pavement ME.

REFERENCES

1. National Cooperative Highway Research Program (NCHRP). 2003. Mechanistic-Empirical Pavement Design Guide of New and Rehabilitated Pavement Structures.
2. Kannekanti, V. and J. T. Harvey. 2006. Sensitivity Analysis of 2002 Design Guide Rigid Pavement Distress Prediction Models. University of California, Davis. Report No. UCD-DG-2006-01. www.ucprc.ucdavis.edu/PDF/UCPRC-DG-2006-01.pdf. (Accessed March 1, 2019)
3. Kannekanti, V. and J. T. Harvey. 2007. Field Calibration of MEPDG JPCP Distress Prediction Models. University of California, Davis. Report No. UCPRC-RR-2007-02. (Accessed March 1, 2019)
4. Kannekanti, V. and J. T. Harvey. 2006. Sample Rigid Pavement Design Tables Based on Version 0.8 of the Mechanistic Empirical Pavement Design Guide. University of California, Davis. Report No. UCPRC-TM-2006-04. www.ucprc.ucdavis.edu/PDF/MPEDG%20Stg%205%20Final%20UCPRC-TM-2006-04%20with%20FHWA.pdf. (Accessed March 1, 2019)
5. Harvey, J. T., J. Roesler, J. Farver, and L. Liang. 2000. Preliminary Evaluation of Proposed LLPRS Rigid Pavement Structures and Design Inputs. University of California, Davis. Report No. FHWA/CA/OR-2000/02. www.ucprc.ucdavis.edu/PDF/Prelim%20Eval%20of%20Prop%20LLPRS.pdf. (Accessed March 1, 2019)
6. Heath, A., J. Roesler, and J. Harvey. 2003. Modeling Longitudinal, Corner and Transverse Cracking in Jointed Concrete Pavements. *International Journal of Pavement Engineering*, Vol. 4 (1): 51–58.
7. Li, H., J. Harvey, J. Asselanis, J. Zhou, I. Guada, V. Kannekanti, and R. Wu. 2016. Preliminary Results from Visual Inspection and Laboratory Testing for ASR in Existing Concrete Cores from Bridge and Pavement in California. University of California, Davis. Report No. UCPRC-RR-2015-07. www.ucprc.ucdavis.edu/PDF/UCPRC-RR-2015-07.pdf. (Accessed March 1, 2019)
8. Kohler, E., and V. Kannekanti. 2008. Influence of Coefficient of Thermal Expansion on the Cracking of Jointed Concrete Pavements. 6th RILEM International Conference on Cracking in Pavements. Chicago.
9. Kim, C., J. D. Lea, V. Kannekanti, and J. T. Harvey. 2019. Updating Weigh-in-Motion (WIM) Spectra in Pavem. University of California, Davis. Report No. UCPRC-TM-2018-01 (draft under review).
10. Ongel, A., and J. Harvey. 2004. Analysis of 30 Years of Pavement Temperatures Using the Enhanced Integrated Climate Model (EICM). University of California, Davis. www.ucprc.ucdavis.edu/PDF/Climate%2030%20Years.pdf. (Accessed March 1, 2019)

APPENDIX: PROJECT-SPECIFIC DETAILED MATERIALS DATA

Project-specific data are variables specific to a pavement project that may vary due to different design criteria, environmental and traffic loading conditions, and/or the inherent randomness involved in pavement construction projects. These project-specific data are unavailable in the Caltrans PMS database and, therefore, they are missing for almost all JPCP projects undertaken in California. However, over the past few years the University of California Pavement Research Center (UCPRC) has obtained essential project-specific data from parts of different research projects. These data include PCC compressive strength, PCC modulus of elasticity, PCC CTE, PCC shortwave absorptivity, and PCC density. These data were obtained by sampling from the various projects. Five data sources were used to set up this material input database.

- *Ground penetrating radar (GPR) data.* The objective of an earlier UCPRC GPR study was to create a lane-based pavement structure inventory database consisting of layer thickness and material types for the entire state highway network. The data collected as part of this project were used to establish fixed management sections for network-level and project-level PMS operations. As part of this project, some stateside Blind Verification Sections (BVS) were established to provide additional quality assurance. In this current report, the PCC CTE was the project-specific variable obtained from this GPR study.
- *Caltrans CTE database (CaltransDB).* After the 2006 sensitivity analysis that showed a very high sensitivity of transverse cracking in the MEPDG models to coefficient of thermal expansion (CTE), Caltrans required contractors to test and report CTE for several years. The Caltrans CTE database has the CTE test results taken from the JPC pavements while under construction during that period. The map in Figure A.1 shows the distribution of specimens from the GPR study and the Caltrans CTE database. Many specimens in the Caltrans database had no latitude or longitude information, and therefore, there are a few data points from the Caltrans CTE database shown in the map below.

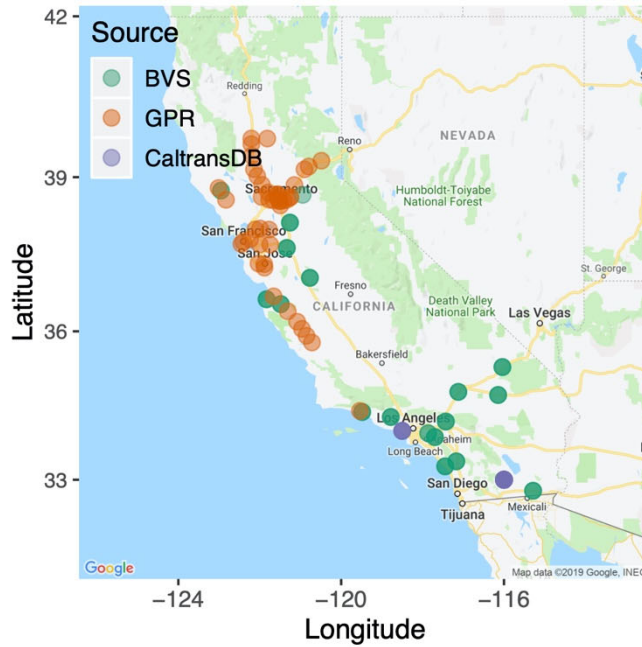


Figure A.1: Distribution map of cores taken across the state (GPR and CaltransDB).

- Previous MEPDG calibration data.* These are data obtained from cores taken from different pavement sections across California as part of a 2007 MEPDG calibration project conducted by the UCPRC (3). These pavement sections include 52 concrete sections and 43 Crack, Seat, and Overlay (CSOL) sections. Figure A.2 shows the distribution of the pavement sections across the different climate regions and Caltrans districts in California. The project-specific data obtained as part of this study were PCC compressive strength, PCC modulus of elasticity, PCC CTE, PCC density, and PCC shortwave absorptivity (3).

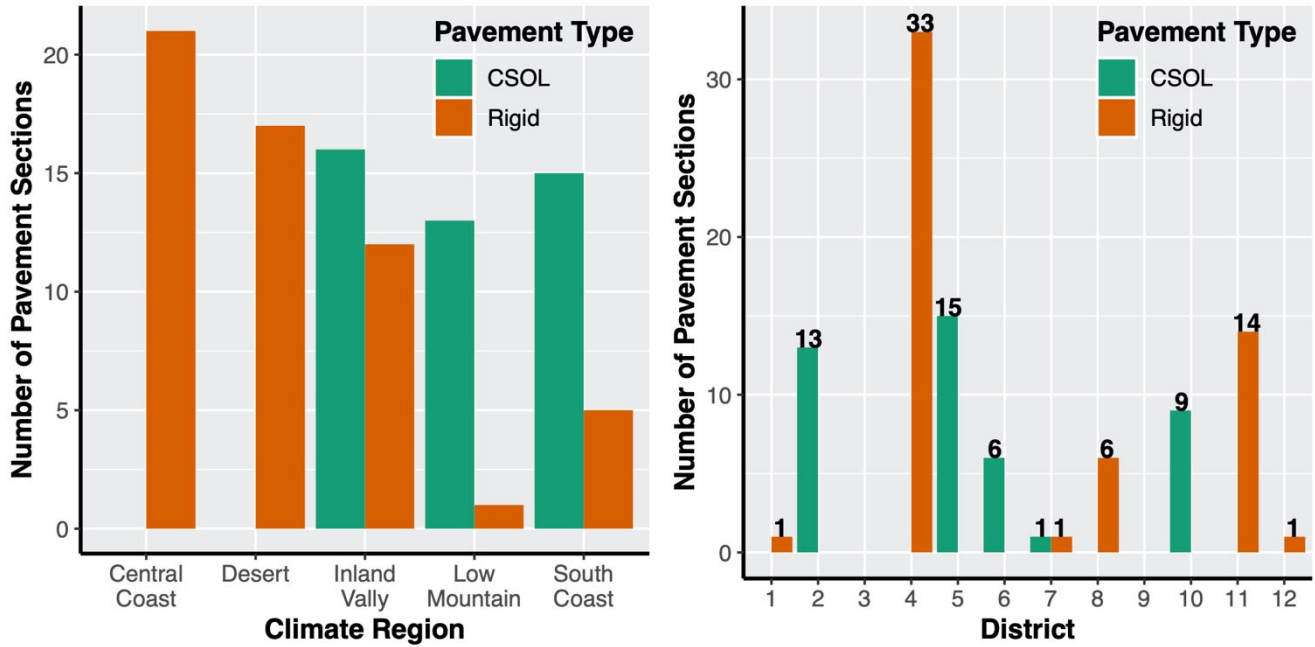


Figure A.2: Previous MEPDG calibration pavement sections distribution.

- *Alkali-silica reaction (ASR) data.* The objective of the 2016 UCPRC ASR project (7) was to look for the presence of alkali-silica reaction in California’s pavements and bridges by evaluating core samples taken from pavement sections across the state. A total of 265 specimen cores were taken as part of this study, and PCC compressive strength and PCC density were measured for the samples.

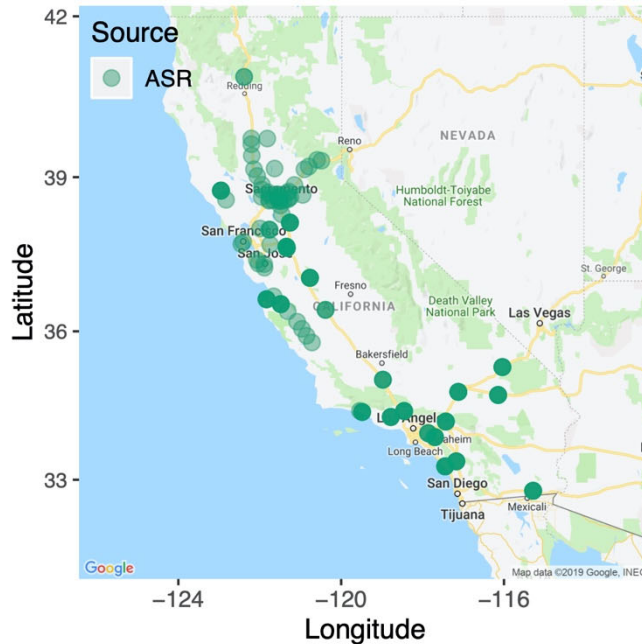


Figure A.3: Distribution map of cores taken across the state (ASR).

- *Stantec data.* These data were obtained by drilling core specimens to study the influence CTE on cracking of JPCP (8).

The following sections will show the distribution of each variable with their median and standard deviation. This information will be used in calibration of Pavement ME for pavement sections where project-specific inputs are unavailable. A more detailed discussion on this will be provided in the Pavement ME calibration report.

PCC Compressive Strength

Figure A.4 shows the distribution of the average within-project PCC compressive strength among samples taken from each project in the GPR and earlier MEPDG calibration studies. The compressive strengths were measured on cores taken at least several years and often many years after construction. The values shown have been converted from the long-term strengths to equivalent 28-day strengths using the MEPDG procedure to divide the long-term strength by a factor of 1.44. Equivalent 28-day values were used in Pavement ME. The compressive strengths adjusted to 28-day equivalents were also used for estimation of modulus of rupture and modulus of elasticity.

Compressive strength has an average of 4,539 psi with a standard deviation of 890 psi. Figure A.5 shows that the cumulative distribution of compressive strength has a 50th percentile (median) of 4,458 psi. The values shown are long-term strengths taken from cores from all the structures, in most cases many years after construction.

Figure A.6 shows the variability in compressive strength within and between the projects. The line at the mid-height of each box indicates the average value of the compressive strength, and the box's two ends indicate one standard deviation above and below the mean for each specific project. The projects with only one core sample are shown as a single line in the figure. The numbers on top of the plot indicate the number of samples taken from each project.

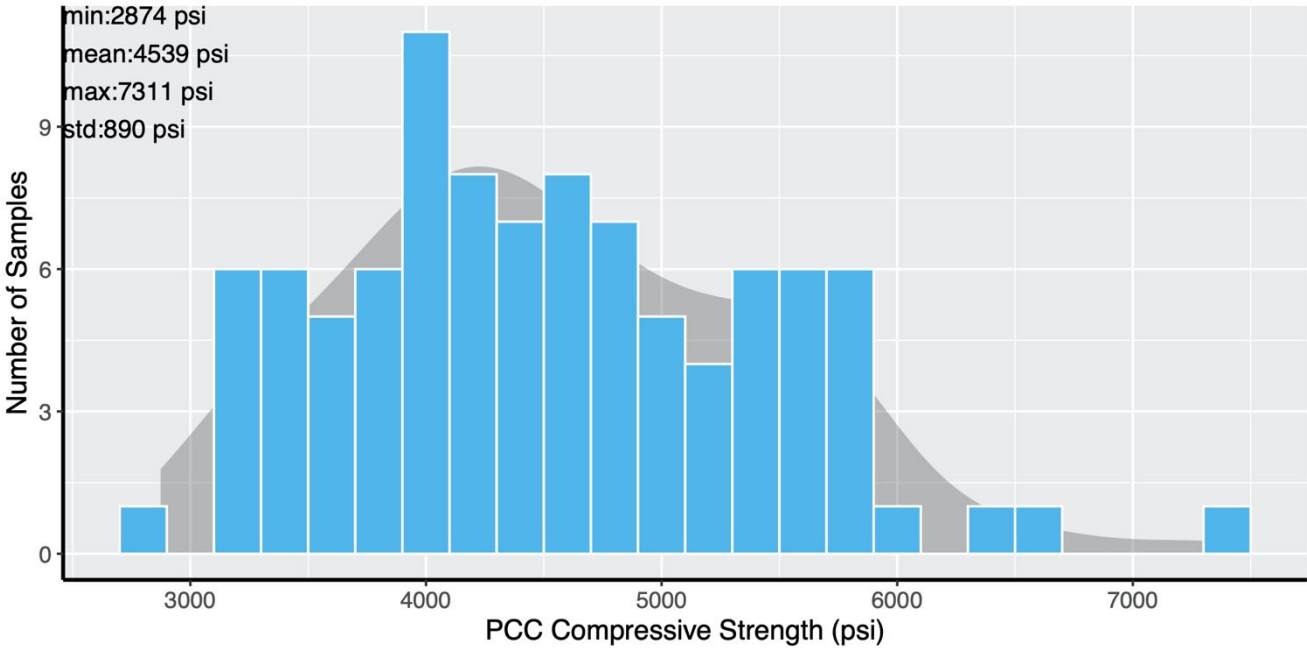


Figure A.4: PCC compressive strength distribution across all projects.

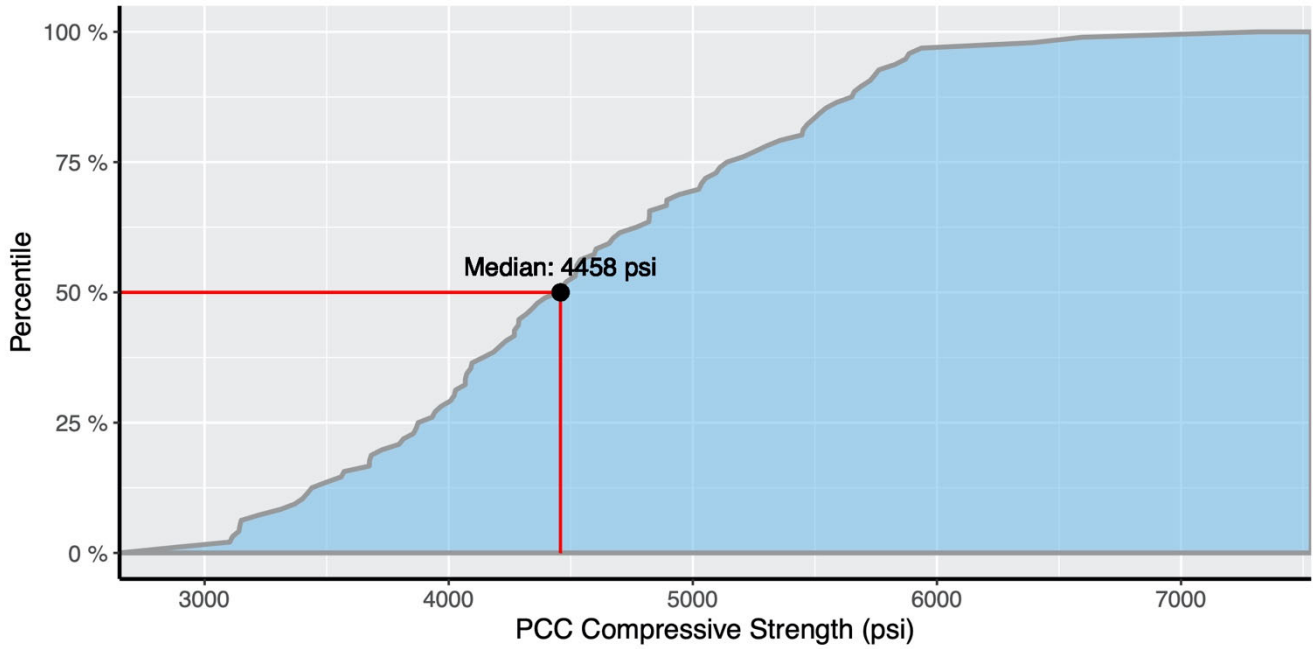


Figure A.5: PCC compressive strength cumulative distribution.

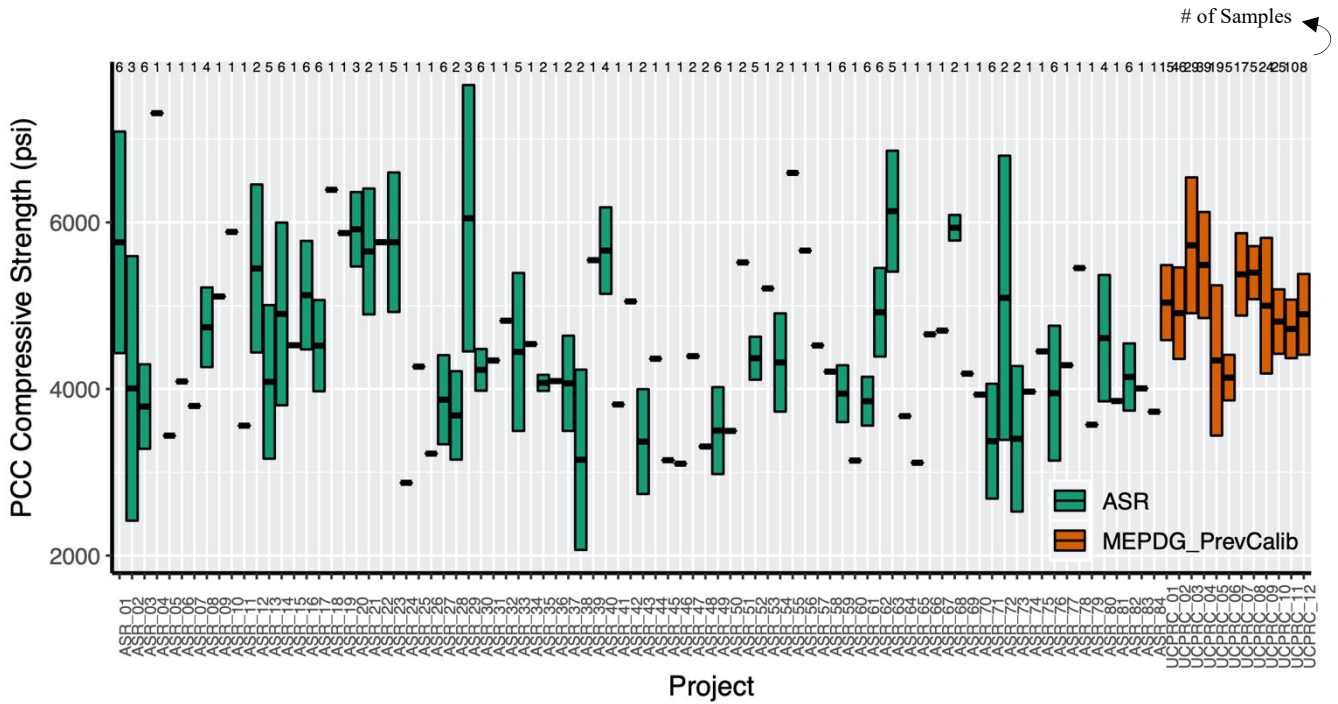


Figure A.6: PCC compressive strength variability within projects.

Coefficients of variation of measured within-project compressive strengths were:

- Average: 13.79 percent
- Median: 12.63 percent
- Standard deviation: 8.56 percent
- Maximum: 39.48 percent
- Minimum: 0.026 percent

PCC Estimated Modulus of Elasticity (28-day stiffness)

Modulus of elasticity was estimated from the PCC density and equivalent 28-day PCC compressive strengths by using the equation in the MEPDG $E_e = 33\rho^{1.5}f'_c{}^{0.5}$, where E_e is the estimated modulus of elasticity, ρ is the density, and f'_c is the compressive strength. This equation is used in Pavement ME to calculate the modulus of elasticity based on the compressive strength and density input given by the user. Based on Figure A.7 and Figure A.8, the estimated modulus of elasticity has an average of 3,947 ksi with a standard deviation of 427 ksi. The 50th percentile (median) of the estimated modulus of elasticity is 3,934 ksi. Figure A.9 shows the variability in estimated PCC modulus of elasticity within and between the projects.

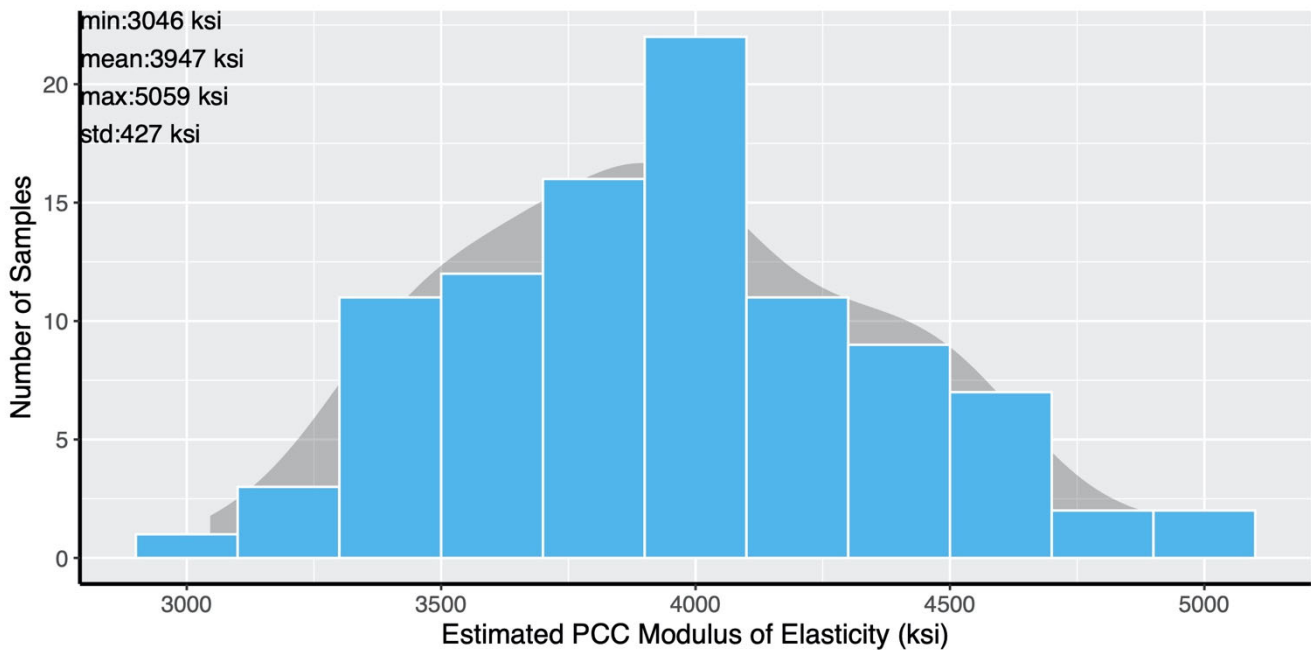


Figure A.7: PCC estimated 28-day modulus of elasticity distribution across all projects.

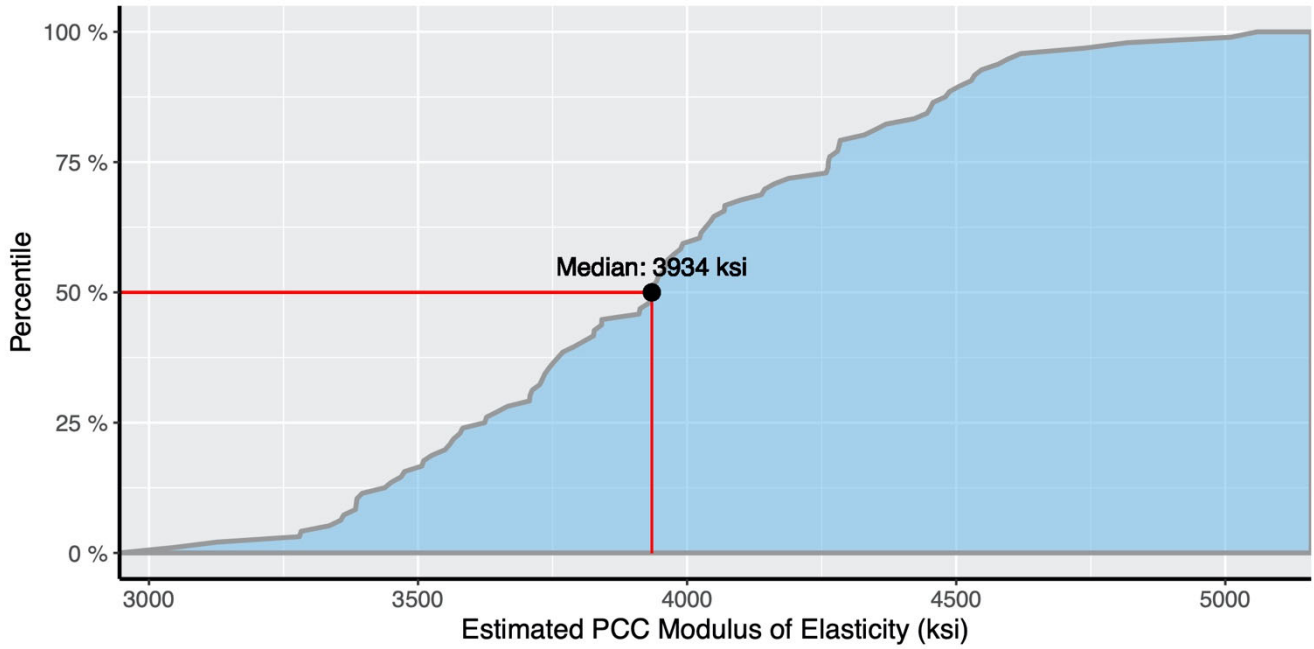


Figure A.8: PCC estimated modulus of elasticity cumulative distribution.

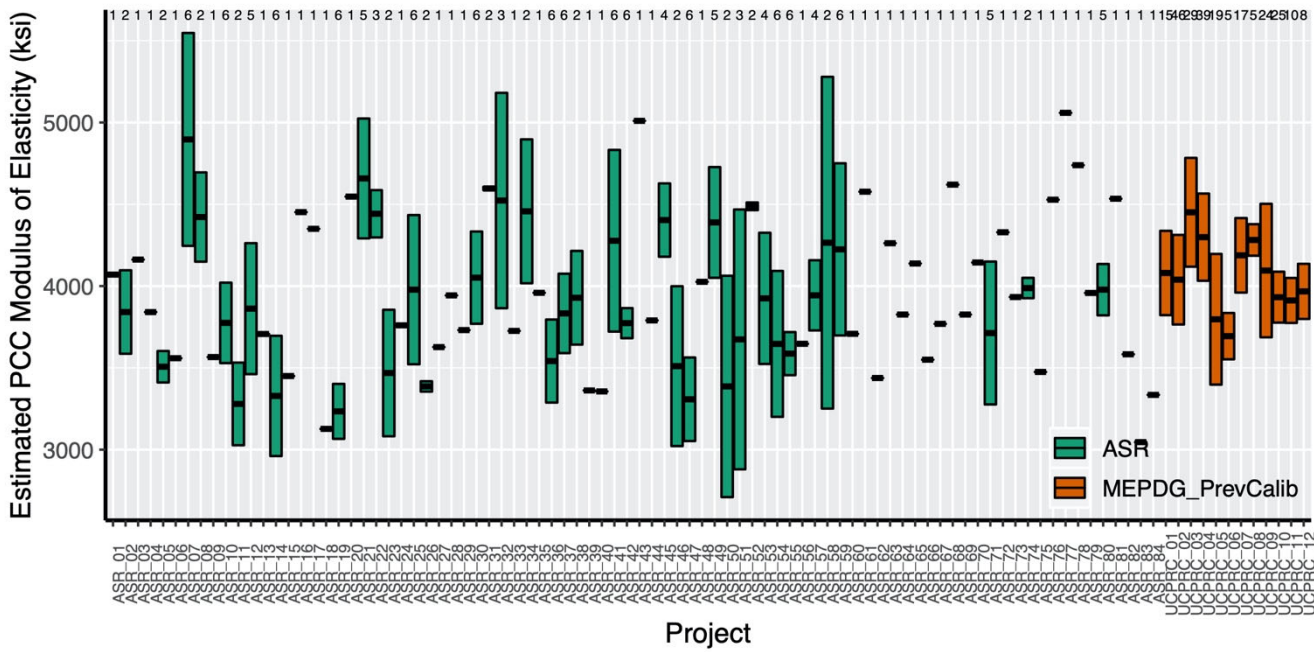


Figure A.9: PCC estimated modulus of elasticity project-level variability.

Coefficients of variation of estimated within-project modulus of elasticity values were:

- Average: 7.95 percent
- Median: 6.99 percent
- Standard deviation: 5.13 percent
- Maximum: 23.72 percent
- Minimum: 0.23 percent

Modulus of elasticity data were directly measured on cores on some sections as part of an earlier 2007 MEPDG calibration 3). Data were obtained from 224 samples across all projects. Since most of the projects had been in service for some decades at the time of the study, a factor of 1.2 was used to reduce the measurements to the 28-day stiffness. The measured modulus of elasticity from those sections had an average of 3,776 psi with a standard deviation of 347 psi. The 50th percentile (median) of the measured modulus of elasticity was estimated to be 3,786 psi. These measured values are reasonably close to those estimated from compressive strengths. The estimated values were used for the previous calibration of Pavement ME and will be used for the upcoming calibration because the MEPDG models were calibrated using estimated values, and because the methodology for measuring the modulus of elasticity was performed using a non-standard research method.

PCC Estimated Modulus of Rupture

Modulus of rupture (MR) was not measured in either the previous MEPDG calibration or ASR studies, and was estimated using the 28-day compressive strengths using the equation $MR = 9.5 f_c^{0.5}$. The estimated MR has an average of 636 psi and a standard deviation of 62 psi with a median of 633 psi. Figure A.10 shows the distribution of the average within-project estimated PCC modulus of rupture. Figure A.11 shows that the cumulative distribution of estimated PCC modulus of rupture has a 50th percentile (median) of 633 psi. Figure A.12 shows the variability in estimated PCC modulus of rupture within and between the projects.

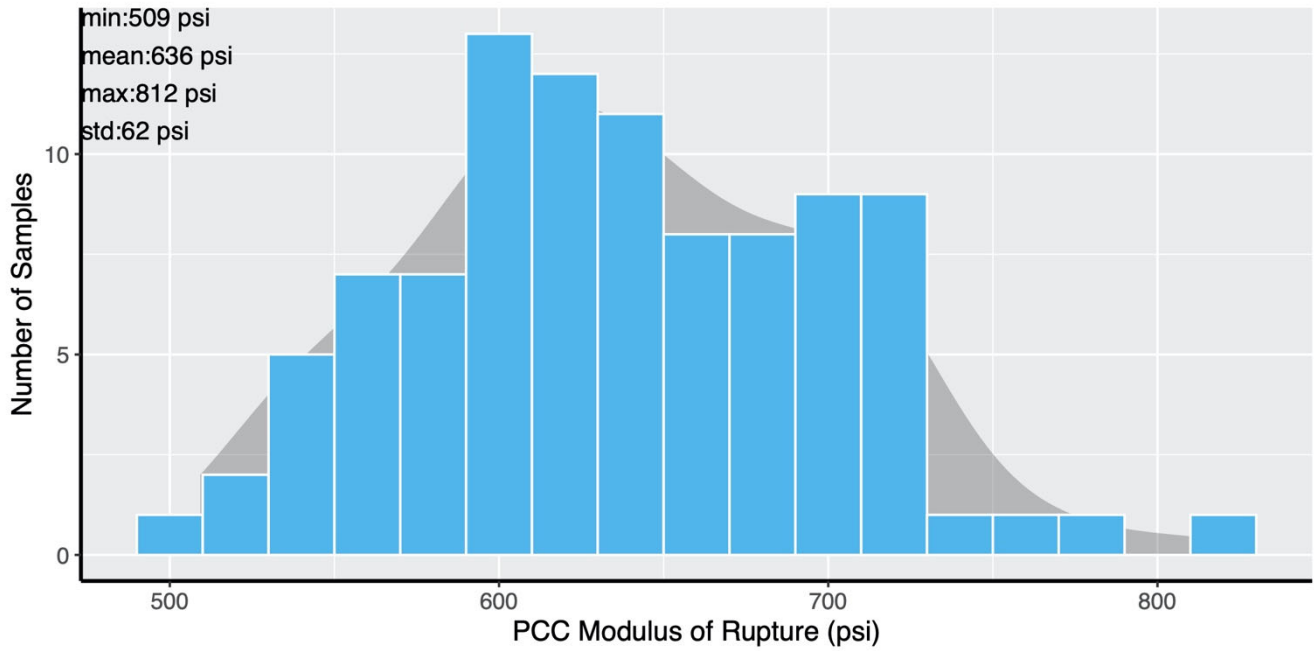


Figure A.10: PCC estimated modulus of rupture distribution across all projects.

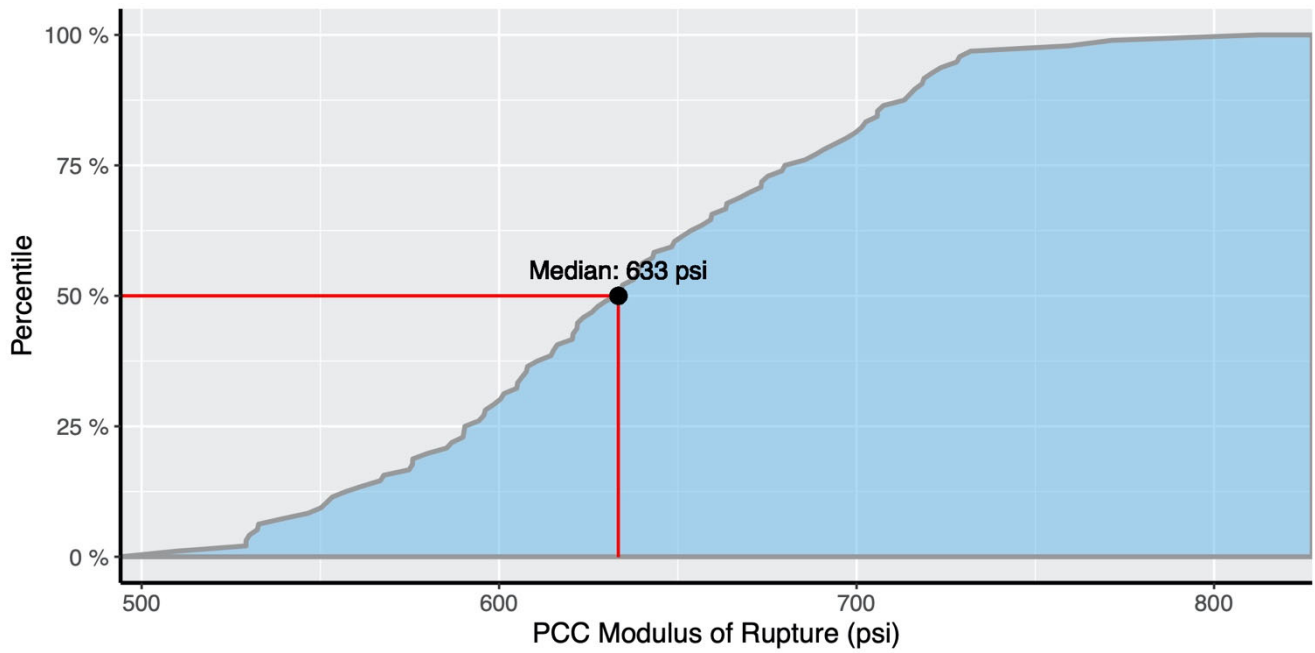


Figure A.11: PCC estimated modulus of rupture cumulative distribution.

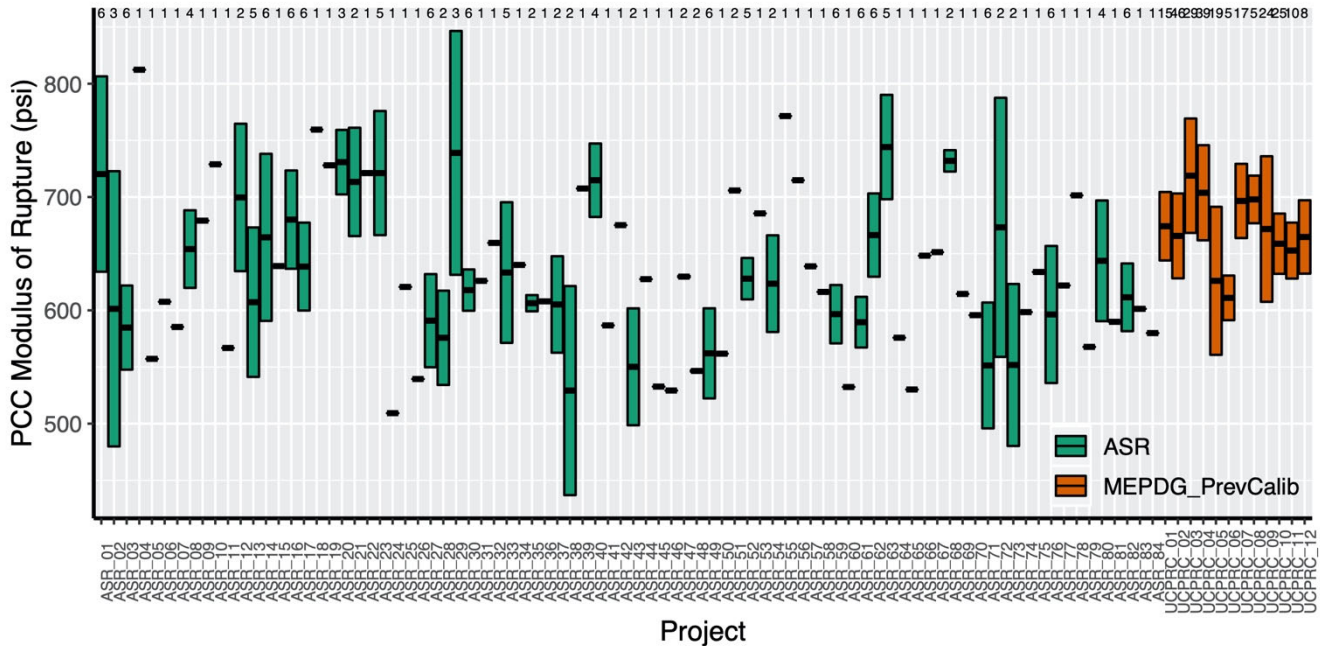


Figure A.12: PCC Estimated modulus of rupture project-level variability.

Coefficients of variation of estimated within-project modulus of rupture values were:

- Average: 6.99 percent
- Median: 6.38 percent
- Standard deviation: 4.39 percent
- Maximum: 20.43 percent
- Minimum: 0.13 percent

PCC Density

PCC density was measured as part of the ASR (7) and earlier MEPDG calibration studies (3). Density has an average of 147 pcf and a standard deviation of 3 pcf with a median of 147 pcf. Figure A.13 shows the distribution of the average within-project PCC density. Figure A.14 shows that the cumulative distribution of PCC density has a 50th percentile (median) of 147 pcf. Figure A.15 shows the variability in PCC density within and between the projects.

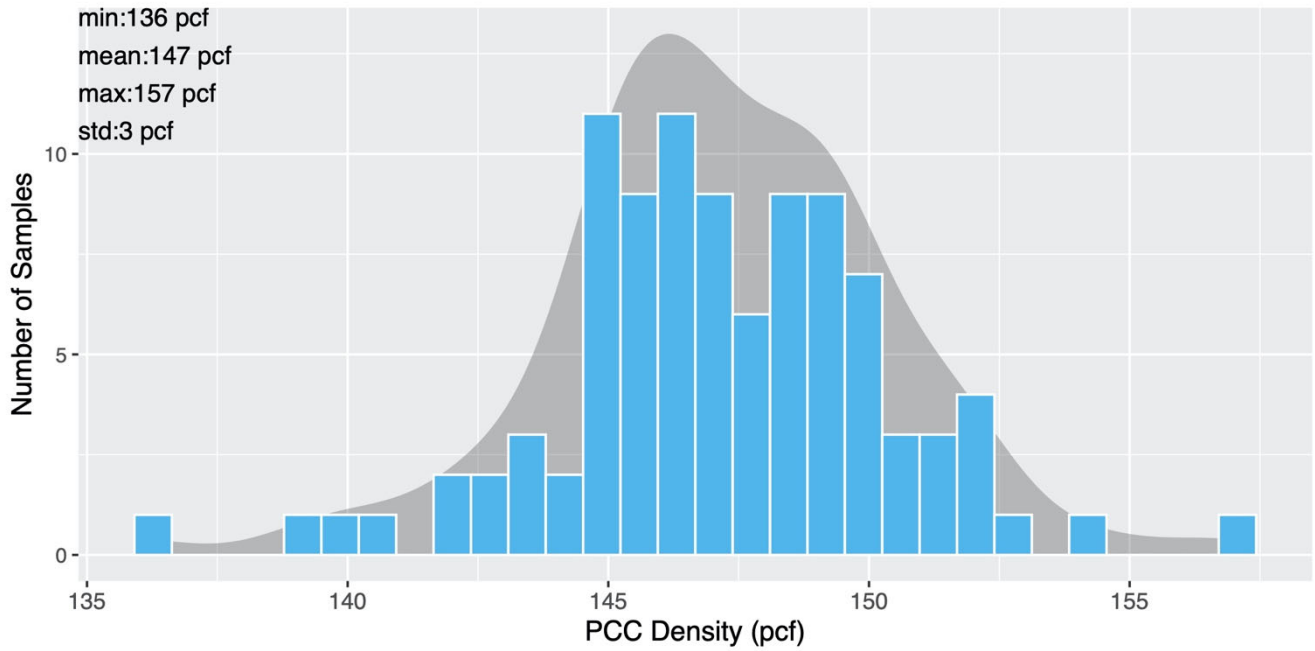


Figure A.13: PCC density distribution across all projects.

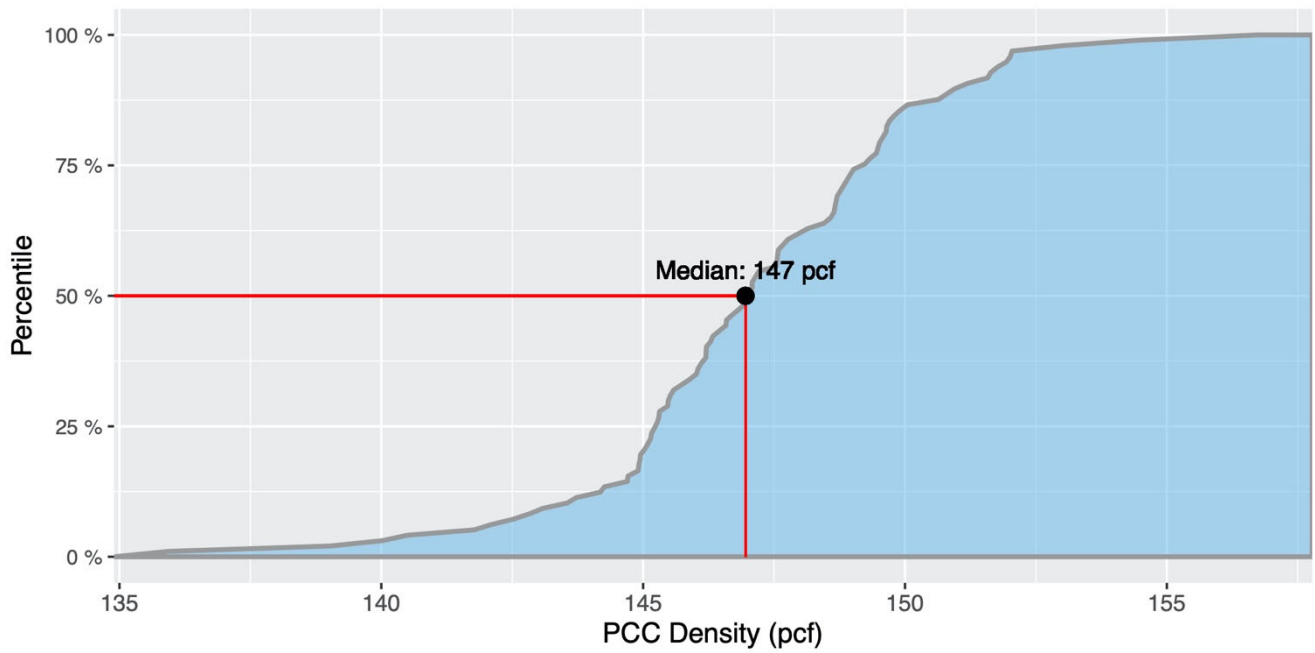


Figure A.14: PCC density cumulative distribution.

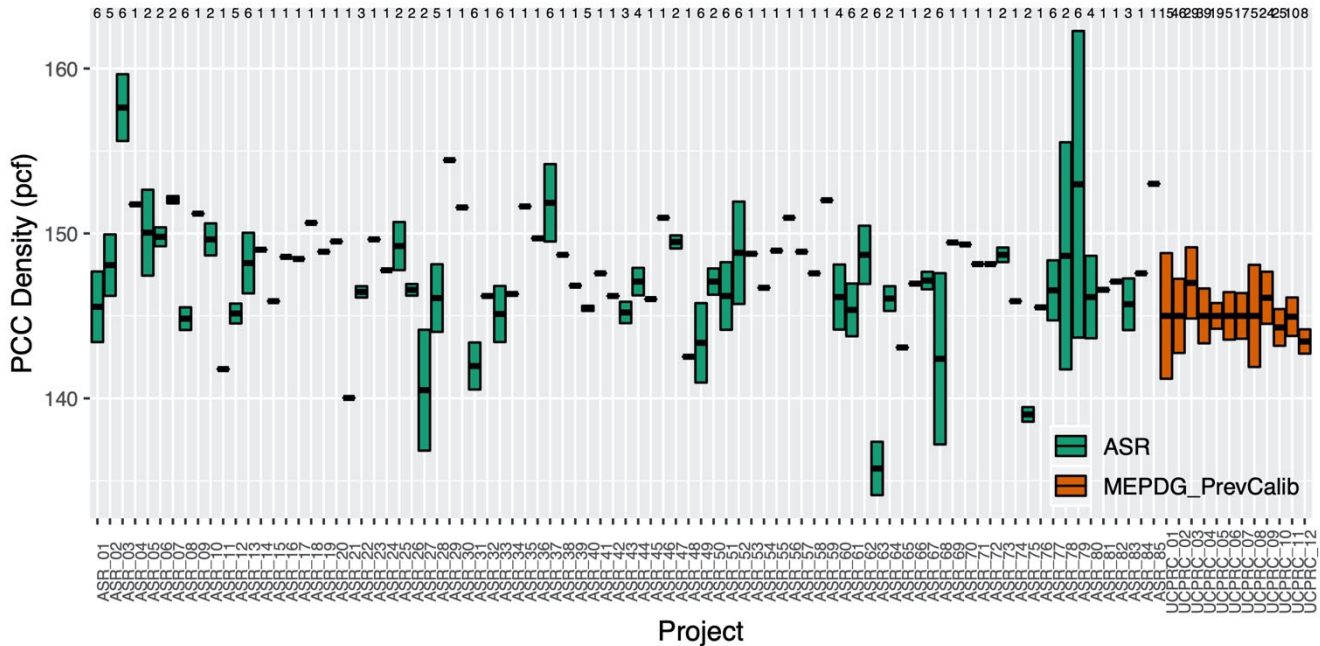


Figure A.15: PCC density project-level variability.

PCC Coefficient of Thermal Expansion

PCC CTE data were obtained from 2007 MEPDG calibration study (3), the GPR study, the Stantec project, and the Caltrans CTE database. The measured CTE values have an average of 4.91 microstrain/°F⁻¹ with a standard deviation of 0.8 microstrain/°F⁻¹ and a median of 4.8 microstrain/°F⁻¹. The measurements done by the UCPRC were not subject to the error in the reference metal identified by the Federal Highway Administration (FHWA) after the measurements were made because it was verified that the metal with the erroneous reference value was not used in the UCPRC equipment. Figure A.16 shows the distribution of the average within-project PCC CTE. Figure A.17 shows that the cumulative distribution of PCC CTE has a 50th percentile (median) of 4.8 microstrain/°F⁻¹. Figure A.18 shows the variability in PCC CTE within and between the projects.

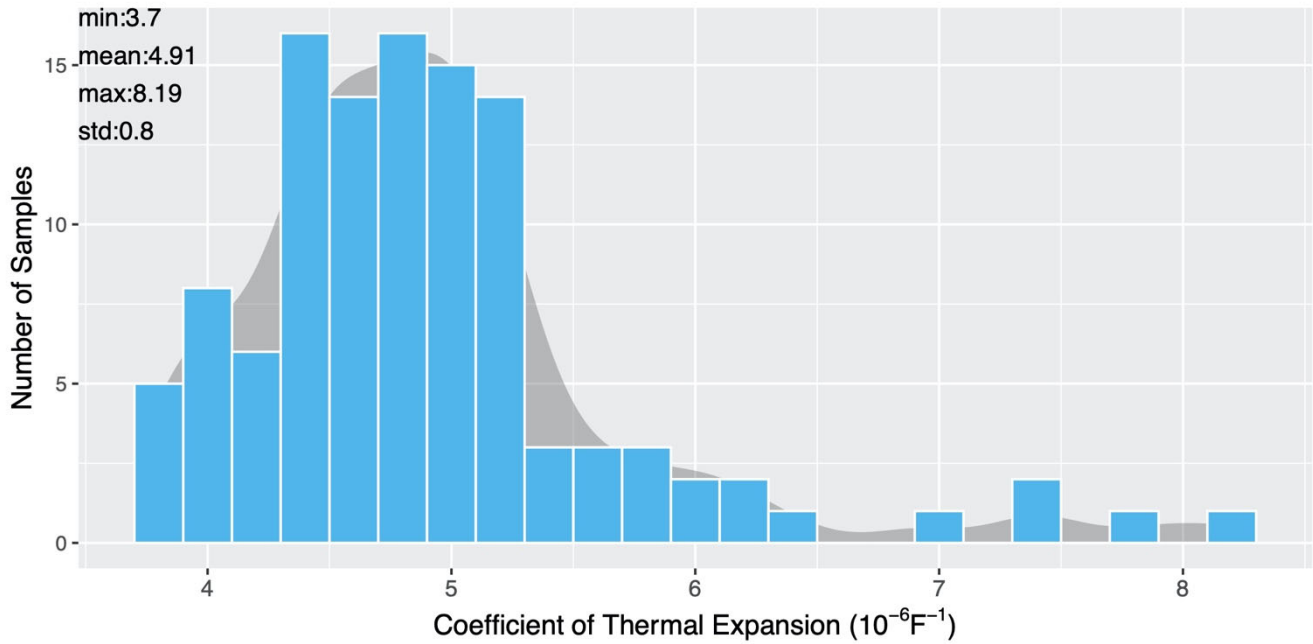


Figure A.16: PCC coefficient of thermal expansion distribution across all projects.

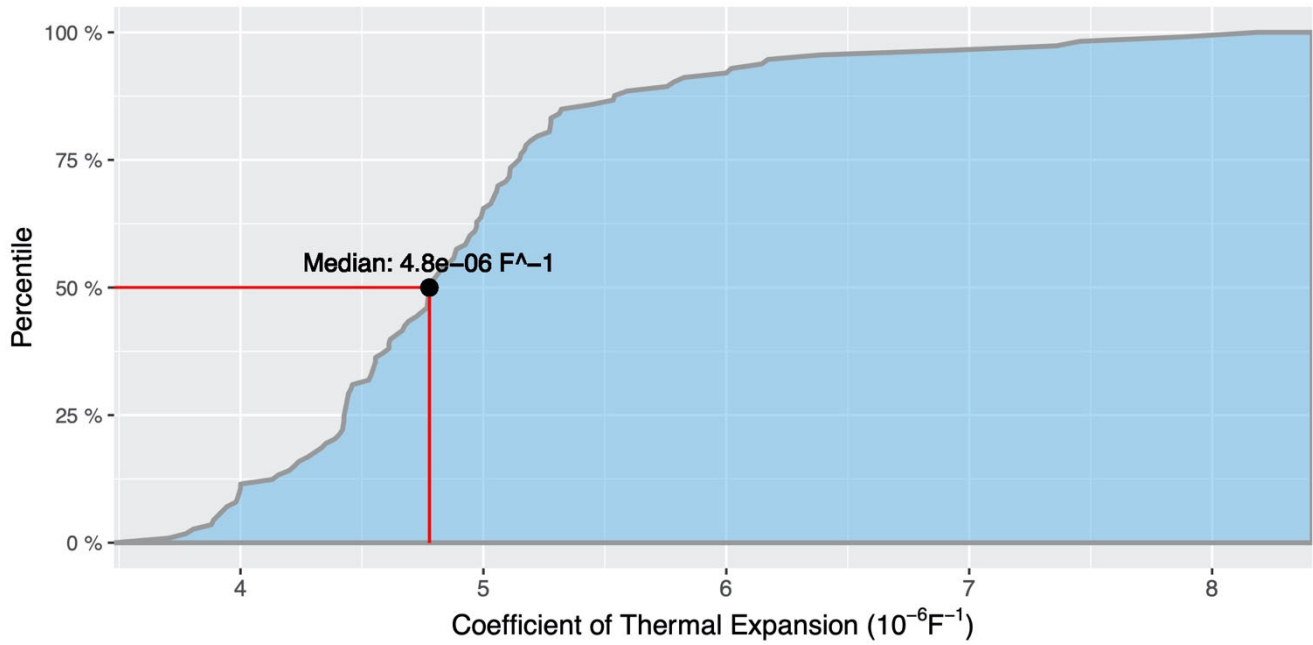


Figure A.17: PCC coefficient of thermal expansion cumulative distribution.

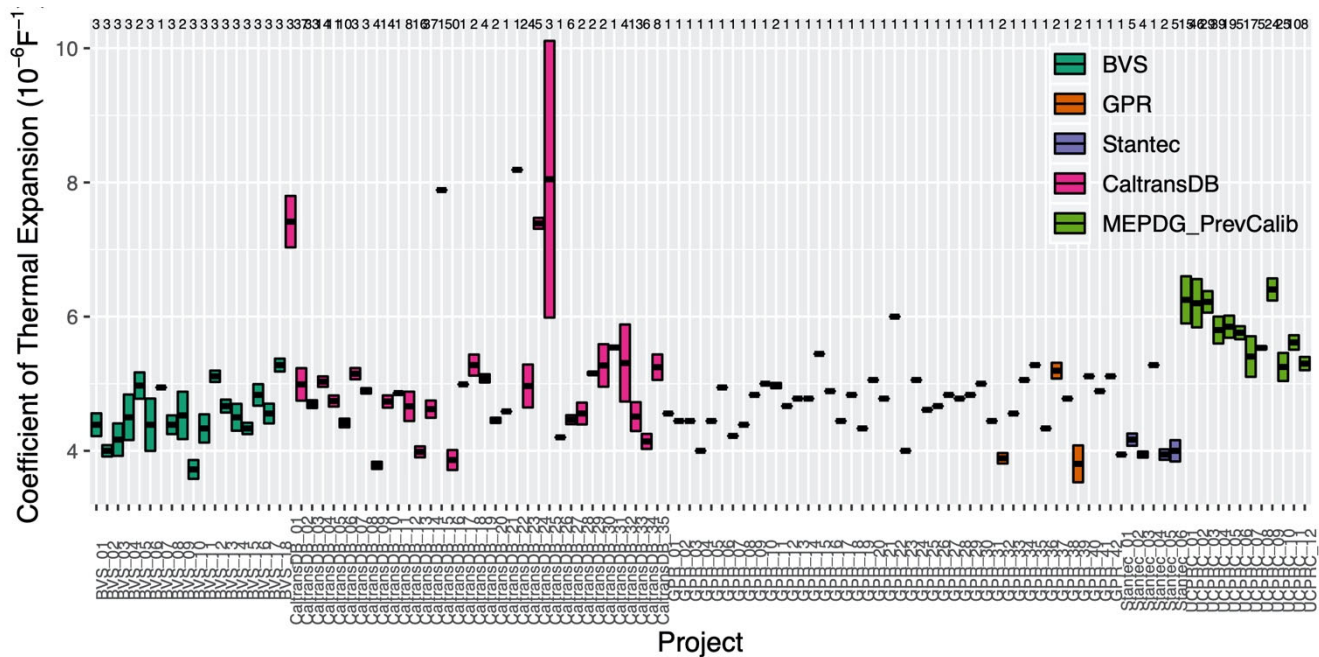


Figure A.18: PCC coefficient of thermal expansion project-level variability.

PCC Shortwave Absorptivity

Shortwave absorptivity data were collected as part of 2007 MEPDG calibration study 3) obtained from only three projects. The average value for shortwave absorptivity is 0.91 with a standard deviation of 0.02 and a median of 0.91. Figure A.19 shows the distribution of the average within-project PCC shortwave absorptivity. Figure A.20 shows that the cumulative distribution of PCC shortwave absorptivity has a 50th percentile (median) of 0.91. Figure A.21 shows the variability in PCC shortwave absorptivity within and between the projects. There were not many different unique measurements for albedo and, therefore, the cumulative distribution graph became a step-graph, shown in Figure A.20, as if it is drawn from discrete values.

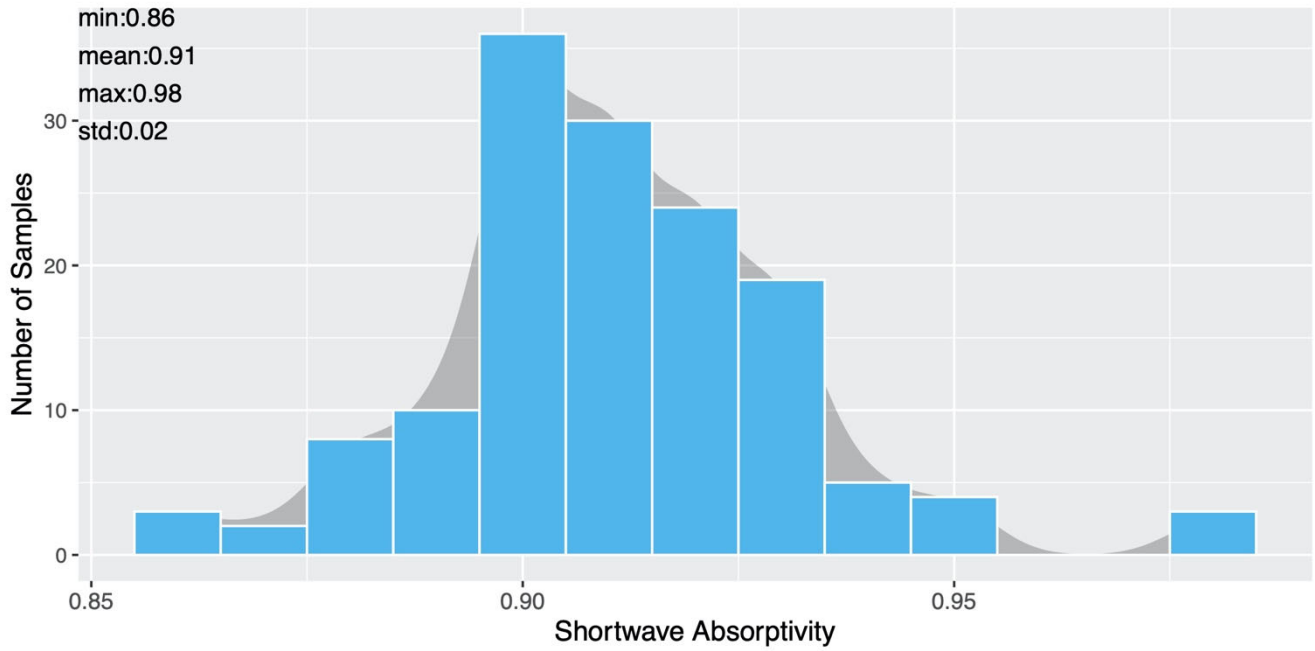


Figure A.19: PCC shortwave absorptivity distribution across all projects.

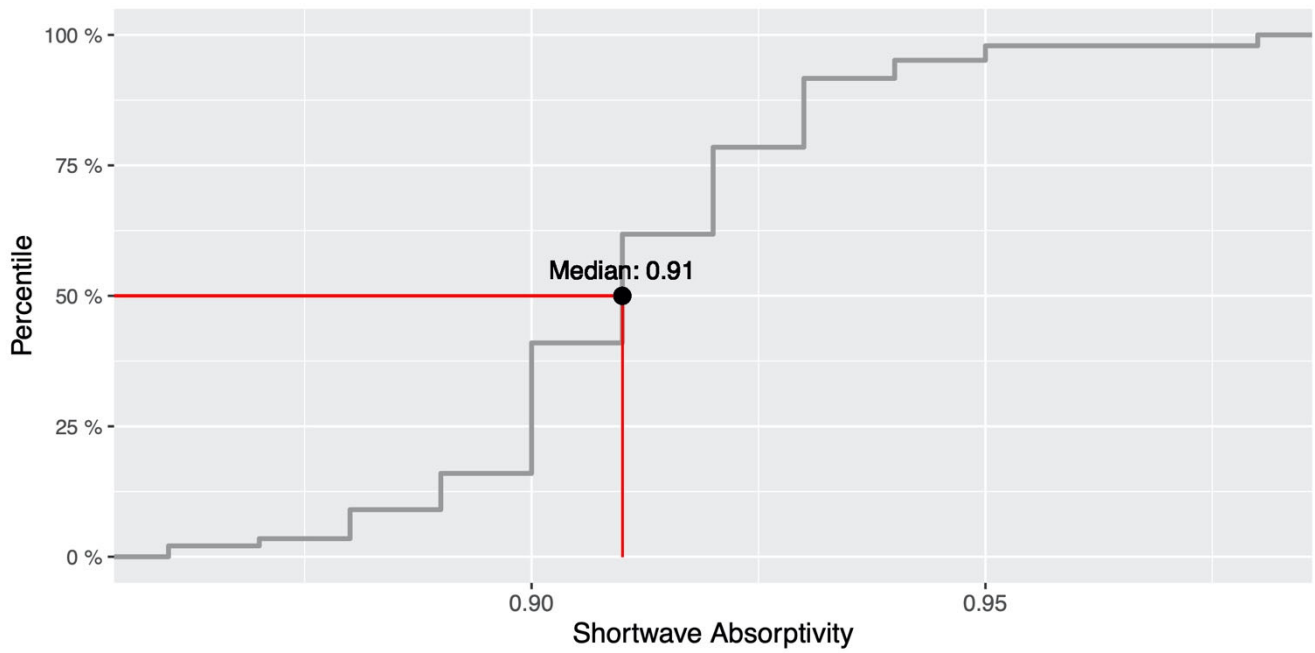


Figure A.20: PCC shortwave absorptivity cumulative distribution.

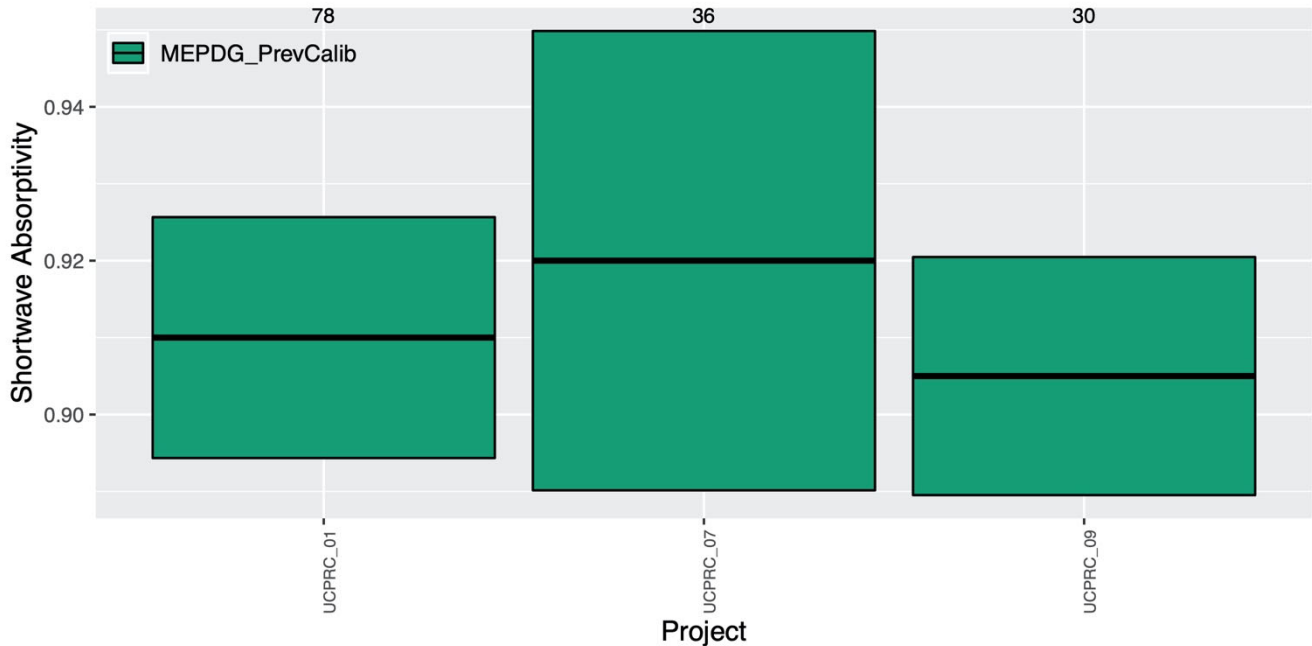


Figure A.21: PCC shortwave absorptivity project-level variability.

WIM Spectra

The following are the five weigh-in-motion (WIM) groups in California:

- Spectra 1 is the lightest *axle load distribution*, so-called because it has the highest load percentage (50 percent) of *single-counted axles*, that is, the sum of the number of single axles derived by adding up the number of single axles and each axle in a tandem axle between 20 and 30 kN.
- Spectra 2 is the second-lightest axle load distribution, with the largest percentage (about 65 percent) of single-counted axles concentrated between 20 and 40 kN.
- Spectra 3 is the medium axle load distribution, with its largest single-counted axle load proportion (70 percent) widely distributed between 20 and 50 kN, but with a light axle load proportion (20 kN) still slightly higher than the proportion of the heavy axle loads (60 kN).
- Spectra 4 is the second heaviest axle load distribution, with its single-counted axle loads fairly well distributed from 15 kN to 70 kN (between 10 and 20 percent); its proportion of single-counted axle loads at 20 kN is about the same as the proportion of single-counted axle loads at 50 kN.
- Spectra 5 is the heaviest axle load distribution, with its single-counted axle loads distributed more toward heavy axle loads (over 50 kN) than to light axle loads (under 40 kN).

Figure A.22 shows California’s five WIM spectra. The Single Equivalent Axle Load Frequency y-axis variable is the result of splitting tandem axles in two and tridem axles in three (e.g., one tandem becomes two singles with half the load each). The use of single equivalent axle loads is just a simplified way to determine the similarity between different WIM spectra. It does not impact the actual spectra being used in Pavement ME. Each WIM spectra (1 to 5) includes a detailed definition of truck types and axle weight distributions, similarly to the truck traffic class (TTC) classification in Pavement ME.

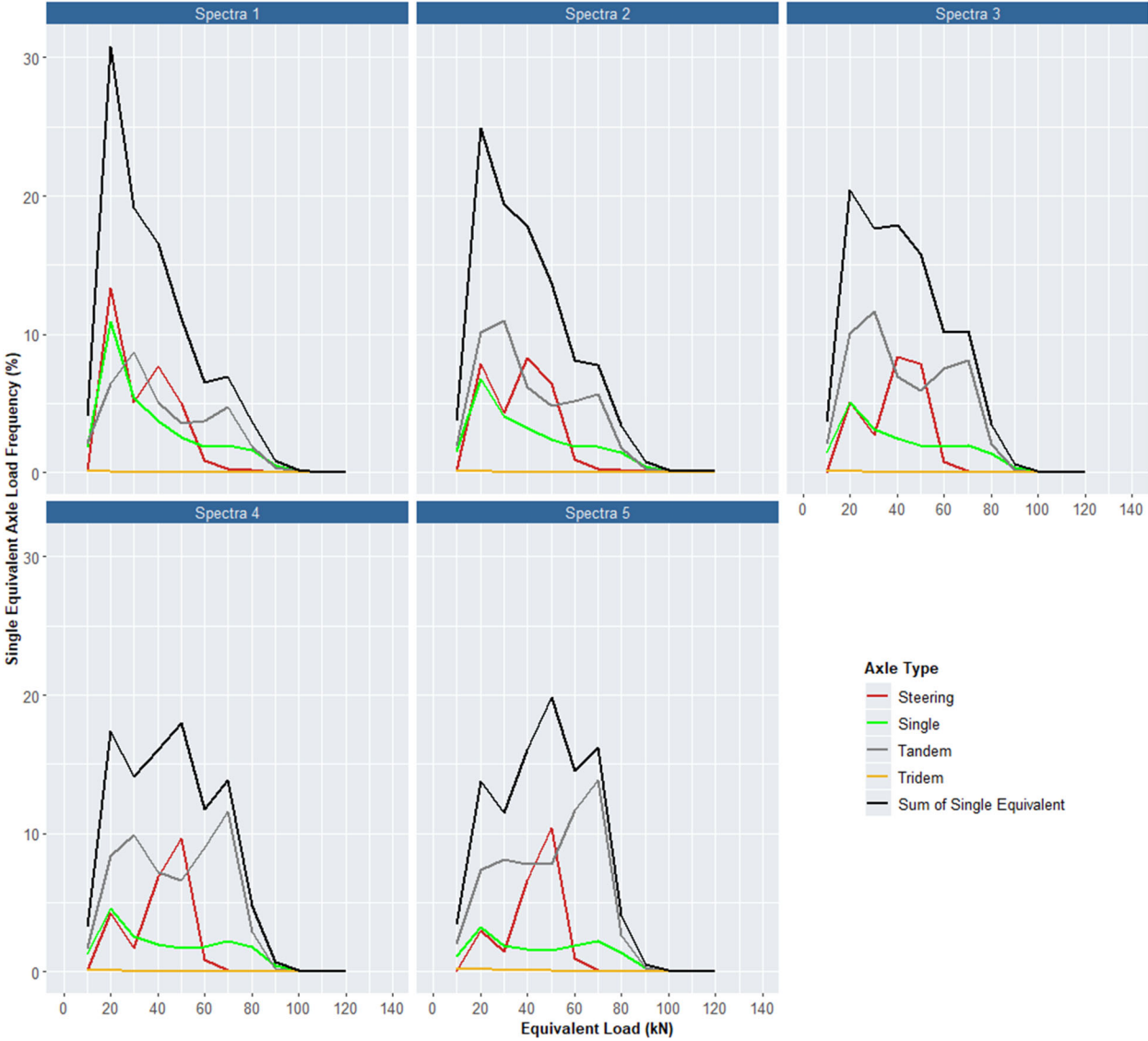


Figure A.22: Five WIM spectra in California.